Paleoecology and Taphonomy of Ediacaran macrofossils from the Khatyspyt Formation, Olenek Uplift, Siberia

Natalia Vladimirovna Bykova

Dissertation submitted to the faculty of the Virginia Polytechnic Institute and State University in partial fulfillment of the requirements for the degree of

Doctor of Philosophy
In
Geosciences

Shuhai Xiao
Benjamin C. Gill
Sterling Nesbitt
Brian Romans

August 30, 2017
Blacksburg, Virginia

Keywords: Geobiology, Paleobiology, Paleoecology, Taphonomy

Paleoecology and Taphonomy of Ediacaran macrofossils from the Khatyspyt Formation, Olenek Uplift, Siberia

Natalia Vladimirovna Bykova

ABSTRACT

The Ediacaran Period (635 – 541 Ma) is a critical transition in the history of the Earth and life. It is marked by the appearance of enigmatic Ediacara-like fossils and macroalgae, which had existed since the early Proterozoic, but started to diversify morphologically and ecologically during this geological period. Nevertheless, paleontologists have been studying Ediacaran fossils for more than a century, the key questions about these fossils remain unanswered, including their phylogenetic affinities, taphonomic history, ecology, and paleoenvironmental distribution. Thus, new ways of investigation need to be employed to unveil enigmas of Ediacaran organisms. As well as, scientists need to engage other representatives of Ediacaran assemblages, such as macroalgae, to fully understand how those communities operated in the past.

The chapters of this original research in this dissertation demonstrate innovative approaches and methods for studying the paleoecology and taphonomy of Ediacaran macrofossils. The second chapter presents the results of a geochemical analysis to resolve taphonomic and paleoecological questions about the Ediacara-like discoidal holdfast fossil *Aspidella*. Stable isotope data of organic carbon, carbonate carbon/oxygen, and pyrite sulfur were integrated with iron speciation data to reconstruct the taphonomy, paleoecology, and paleoenvironments of *Aspidella* fossils. The third chapter presents results from a comprehensive analysis of macroalgae from Proterozoic to early Paleozoic. In this study, a database of macroalgal fossil was updated and analyzed in order to gain insights into the big-picture evolutionary patterns of macroalgal morphology and ecology through time. These methods and approaches offer new opportunities to test major paleobiologic and geobiologic hypotheses, thus improving our understanding of the history of the biosphere and the Earth system.

ACKNOWLEDGEMENTS

I would like to thank everyone who has supported me on my way to a higher education; help me to develope as a scientist in the academic world; and played a role in my personal establishment. It is impossible to properly acknowledge all the people, who was helping me through all those years. Still, I want to take this opportunity to acknowledge and thank, in no particular order, the following exceptional people for their truthful support:

- My parents Anzhelika and Vladimir, who never limit my freedom of pursuing any of my new adventures or keep the old ones, no matter how dangerous or ambitious they were (and ironically, who probably will never be able to read these words)
- My sister, Olga and my brother-in-law Sergey, who basically my second parents and care for me more than I do
- My beautiful niece Anastasia and nephew Alex, who always keep me in the tonus and focus, as well as responsible for my change of perspective (have you ever played with 'Magformers'? or glue sequins on the paper Cinderella? – It is very relaxing)
- Hector, who laughs with me on my worst jokes, as well as challenge me and believe in my success as nobody even done before
- My fellow graduate students—particularly those in paleontology, including Mike Meyer, Andrew (Drew 1) Hawkins, Antony (Drew 2) Muscente Qing Tang, Jesse Broce, Ken O'Donnell, Jackie Wittmer, Caitlin Colleary, Candice Stefanic, Chris Griffin, Kiersten Formoso, Krista Koeller, Mitchell Riegler, as well as visiting scholars Zhen Dai, Zhou Wang, Wei Wang, Julia Arroy, Ke Pang, Qin Ye — for fun conversations, scientific and professional discussions, constructive feedback, and generally good and peaceful times
- My PhD committee: Ben Gill, Brian Romans and Sterling Nesbitt
- My co-authors and collaborators – Ben Gill, Vladimir Rogov, Steven Loduca, Dmitry Grazhdankin – who contributed to the work in this dissertation
- All the faculty and staff in the Virginia Tech Department of Geosciences, especially Connie Lowe, who keeps our sanity
- My labmates and friends from IPGG SB RAS – Dmitry Grazhdankin, Konstantin Nagovitsin, Vladimir Rogov, Vasiliy Marusin, Anton Kolesnikov, Boris Kochnev, Galina Karlova
- Anatoly Gibsher my first scientific mentor and Physical Geology professor, a person because of whom I fall in love with geology and especially Pre-Cambrian one. As well as Dmitry Grazhdankin, my bachelor and master advisor, whom I can truly call a life mentor.
- Last, but not least, my advisor Shuhai Xiao, who gave me an opportunity for one-of-a-lifetime experience of getting my PhD abroad, as well as has been extremely helpful and generous with his knowledge and time though all this time

ATTRIBUTIONS

Chapter Two or "A geochemical study of the Ediacaran discoidal fossil *Aspidella* preserved in limestones: Implications for its taphonomy and paleoecology" was published in *Geobiology*, 2017, volume 15, pages 572-587, by N. Bykova, B. C. Gill, D. Grazhdankin, V. Rogov and S. Xiao. N. Bykova and S. Xiao conceived the project. N. Bykova, B. Gill and V. Rogov collected all data. N. Bykova and S. Xiao developed the manuscript with contributions from D. Grazhdankin and B. Gill.

Chapter Three is in the final stages of preparation for submission to *Paleobiology* journal. The tentative title of the publication is "Seaweeds through time: Morphological and ecological analysis of Proterozoic and early Paleozoic benthic macroalgae with a focus on the Ediacaran Period" and my co-authors in the manuscript are S.T. LoDuca, M. Kowalewski, D. Grazhdankin, and S. Xiao. N. Bykova, D. Grazhdankin, S.T. LoDuca and S. Xiao conceived the project. N. Bykova and S. T. LoDuca collected data on Proterozoic and early Paleozoic macroalgal fossils respectively. N. Bykova conducted statistical analyses based on suggestions from M. Kowalewski. N. Bykova and S. Xiao developed the manuscript with contributions from S.T. LoDuca, M. Kowalewski, D. Grazhdankin.

TABLE OF CONTENTS

LIST OF FIGURES

Chapter 2

Chapter 3

LIST OF TABLES

Chapter 2

Chapter 3

GRANT INFORMATION

Chapter 2

This research was funded by the National Science Foundation (EAR-1528553), NASA Exobiology and Evolutionary Biology Program (NNX15AL27G), Russian Science Foundation (14–17–00409), National Geographic Society (8227-07, 8637-09, 9031-11), GSA Graduate Student Research Grant, and Virginia Tech Department of Geosciences.

Chapter 3

Financial support for this study was provided by the National Science Foundation (EAR 1250756, 1332320, 1528553), NASA Exobiology and Evolutionary Biology Program (NNX15AL27G), Russian Science Foundation (14–17–00409), National Geographic Society (8227-07, 8637-09, 9031-11), GSA Graduate Student Research Grant, and Charles J. Gose, Jr, Scholarship for Geological Sciences at Virginia Tech.

CHAPTER 1

Overview of Ediacaran paleoecology and taphonomy

N. BYKOVA

Department of Geosciences, Virginia Tech, Blacksburg, VA 24061, USA

1.1 Introduction

The Ediacaran Period (635 – 541 Ma) is a critical transition in the history of the Earth and life. The Ediacaran Period marked by the appearance of enigmatic Ediacara-like fossils (Narbonne 2005; Xiao and Laflamme 2009) and macroalgae, which had existed since the early Proterozoic, but started to diversify morphologically and ecologically during this geological period (Xiao and Dong 2006). Paleontologists have been studying Ediacaran fossils for more than a century (Billings 1872), but key questions about these fossils remain unanswered, including their phylogenetic affinities, taphonomic history, ecology, and paleoenvironmental distribution.

There are several hypotheses about the possible biological affinities of Ediacara-like fossils. Various Ediacara-like fossils have been interpreted as colonial prokaryotes (Steiner and Reitner 2001), microbial colonies (Grazhdankin and Gerdes 2007), unicellular protists (Zhuravlev 1993; Seilacher et al. 2003), lichens (Retallack 1994, 2007), fungi (Peterson et al. 2003), ancestral ctenophores (Dzik 2002, 2003), mollusks (Fedonkin and Waggoner 1997), and vendobionts (Seilacher 1989). The diverse opinions are partly a reflection of the diversity of Ediacara-like fossils, but they also indicate the uncertainty about the phylogenetic affinity of most Ediacara-like fossils (Seilacher 1989; Retallack 1994; Grazhdankin and Seilacher 2002; Narbonne 2004; Laflamme et al. 2013).

The paleoenvironments where Ediacaran organisms lived, as well as their ecology, are still an open question and a matter of considerable debate in the scientific community. A wide range of possible paleoenvironments have been proposed: from deep water ecosystems (up to 2 km) supporting chemotrophic organisms (Wood et al. 2003), to wave-influenced shallow waters (Gehling 2000), to terrestrial environments (Retallack 2013). Furthermore, Ediacara-like fossils as well as macroalgal fossils are preserved in both oxic and ferruginous (and even euxinic) environments around the world (e.g., Bowyer et al. 2017).

From above narrative, it is clear that we need to explore new ways to investigate Ediacaran organisms. To better understand the morphological constructions, biological affinities, life styles, ecologies, and paleoenvironments of Ediacara-like fossils, we need to focus on localities where there are abundant well-preserved fossils to allow analyses using several different techniques, including morphological and geochemical analyses. This is not an easy task, because most Ediacara-like organisms are commonly preserved in siliciclastic lithologies: sandstones and siltstones (White Sea, Russia) (Sokolov 1976), sandstones (Australia, Namibia) (Narbonne et al. 1997; Gehling 1999), or volcanic tuffs (Newfoundland, Canada) (Clapham et al. 2003). In addition, we need to explore the taphonomy of Ediacara-type fossils preserved in carbonate facies, which would offer opportunities for carbonate geochemical analyses. However, there are only two localities in the world where Ediacara-like fossils are preserved in carbonate rocks: the Dengying Formation in South China (Chen et al. 2014) and the Khatyspyt Formation in northern Siberia (Grazhdankin et al. 2008). To take advantage of the unique perspectives of these carbonate-hosted Ediacara-type assemblages afford, I investigated the taphonomy of *Aspidella*, which is a common element in the Ediacaran biota, preserved in the Khatyspyt Formation. I analyzed 14 three-dimensionally preserved *Aspidella* fossils using a variety of geochemical tools in order to test hypotheses about its taphonomy, paleoecology, and paleoenvironments. The results of this project are presented in Chapter 2.

Because of the taphonomic vagaries of Ediacaran fossils, case studies of individual Ediacaran assemblages are more prone to preservational and environmental biases, resulting in incomplete and biased snapshots of the Ediacaran biosphere. To complement the taphonomic investigation of the Ediacara-like fossils from the Khatyspyt Formation, I developed a project to analyze a database of Proterozoic-Paleozoic macroalgal fossils, in order to better understand the big-picture evolutionary patterns of this fossil group through

geological time. For this study, I assembled a morphological database of non-skeletal macroalgal fossils preserved as carbonaceous compressions. The database was analyzed using non-parametric multidimensional scaling technique (Huntley et al. 2006; Xiao and Dong 2006; Shen et al. 2008) and other statistical methods to quantify the evolutionary trends of Proterozoic-Paleozoic macroalgae. Because macroalgae play a crucial role in modern marine ecosystems, and they were likely important contributors to niche construction and primary bioproduction Proterozoic oceans (LoDuca et al. 2017), this study fills a knowledge gap of Proterozoic-Paleozoic macroalgae, which have been overlooked in previous paleoecological investigations. With the addition of macroalgal data, a more complete understanding of the Proterozoic-Paleozoic biosphere and of the Earth system as a whole is beginning to develop. Results of this project are presented in Chapter 3.

1.2 References

Billings, E. 1872. On some fossils from the Primordial rocks of Newfoundland. Canadian Naturalist and Geologist 6(4):465-479.

Bowyer, F., R. A. Wood, and S. W. Poulton. 2017. Controls on the evolution of Ediacaran metazoan ecosystems: a redox perspective. Geobiology 15(516-551).

Chen, Z., C. Zhou, S. Xiao, W. Wang, C. Guan, H. Hua, and X. Yuan. 2014. New Ediacara fossils preserved in marine limestone and their ecological implications. Scientific Reports 4(4180):1-10.

Clapham, M. E., G. M. Narbonne, and J. G. Gehling. 2003. Paleoecology of the oldest known animal communities: Ediacaran assemblages at Mistaken Point, Newfoundland. Paleobiology 29:527-544.

Dzik, J. 2002. Possible Ctenophoran affinities of the Precambrian "sea-pen" *Rangea*. Journal of Morphology 252:315-334.

Dzik, J. 2003. Anatomical information content in the Ediacaran fossils and their possible zoological affinities. Integrative and Comparative Biology 43:114-126.

Fedonkin, M. A., and B. M. Waggoner. 1997. The late Precambrian fossil *Kimberella* is a mollusc-like bilaterian organism. Nature 388:868-871.

Gehling, J. G. 1999. Microbial mats in terminal Proterozoic siliciclastics: Ediacaran death masks. Palaios 14:40-57.

Gehling, J. G. 2000. Environmental interpretation and a sequence stratigraphic framework for the terminal Proterozoic Ediacara Member within the Rawnsley Quartzite, South Australia. Precambrian Research 100:65-95.

Grazhdankin, D., and G. Gerdes. 2007. Ediacaran microbial colonies. Lethaia 40:201–210.

Grazhdankin, D., and A. Seilacher. 2002. Underground Vendobionta from Namibia. Palaeontology 45(1):57-78.

Grazhdankin, D. V., U. Balthasar, K. E. Nagovitsin, and B. B. Kochnev. 2008. Carbonate-hosted Avalon-type fossils in Arctic Siberia. Geology 36:803–806.

Huntley, J. W., S. Xiao, and M. Kowalewski. 2006. 1.3 billion years of acritarch history: An empirical morphospace approach. Precambrian Research 144:52-68.

Laflamme, M., S. A. F. Darroch, S. M. Tweedt, K. J. peterson, and D. H. Erwin. 2013. The end of the Ediacara biota: Extinction, biotic replacement, or Cheshire Cat? Gondvana Research 23:558-573.

LoDuca, S. T., N. Bykova, M. Wu, S. Xiao, and Y. Zhao. 2017. Seaweed morphology and ecology during the great animal diversification events of the early Paleozoic: A tale of two floras. Geobiology 15(4):588-616.

Narbonne, G. M. 2004. Modular construction of early Ediacaran complex life forms. Science 305:1141-1144.

Narbonne, G. M. 2005. The Ediacara Biota: Neoproterozoic origin of animals and their ecosystems. Annual Review of Earth and Planetary Sciences 33:421-442.

Narbonne, G. M., B. Z. Saylor, and J. P. Grotzinger. 1997. The youngest Ediacaran fossils from southern Africa. Journal of Paleontology 71(6):953-967.

Peterson, K. J., B. Waggoner, and J. W. Hagadorn. 2003. A fungal analog for Newfoundland Ediacaran fossils? Integrative and Comparative Biology 43:127-136.

Retallack, G. J. 1994. Were the Ediacaran fossils lichens? Paleobiology 20:523-544.

Retallack, G. J. 2007. Growth, decay and burial compaction of *Dickinsonia*, an iconic Ediacaran fossil. Alcheringa 31:215-240.

Retallack, G. J. 2013. Ediacaran life on land Nature 493:89-92.

Seilacher, A. 1989. Vendozoa: organismic construction in the Precambrian biosphere. Lethaia 22:229-239.

Seilacher, A., D. Grazhdankin, and A. Legouta. 2003. Ediacaran biota: The dawn of animal life in the shadow of giant protists. Paleontological Research 7(1):43-54.

Shen, B., L. Dong, S. Xiao, and M. Kowalewski. 2008. The Avalon explosion: Evolution of Ediacara morphospace. Science 319:81-84.

Sokolov, B. S. 1976. The Earth's organic world on the path toward Phanerozoic differentiation. Vestnik Akademiya Nauk SSSR 1:126-143.

Steiner, M., and J. Reitner. 2001. Evidence of organic structures in Ediacara-type fossils and associated microbial mats. Geology 29(12):1119-1122.

Wood, D. A., R. W. Dalrymple, and G. M. Narbonne. 2003. Paleoenviromental analysis of the late Neoproterozoic Mistaken Point and Trepassey formations, Southeastern Newfoundland. Canadian Journal of Earth Sciences 40:1375-1391.

Xiao, S., and L. Dong. 2006. On the morphological and ecological history of Proterozoic macroalgae. Pp. 57-90. *In* S. Xiao, and A. J. Kaufman, eds. Neoproterozoic Geobiology and Paleobiology. Springer, Dordrecht, the Netherlands.

Xiao, S., and M. Laflamme. 2009. On the eve of animal radiation: Phylogeny, ecology and evolution of the Ediacara biota. Trends in Ecology & Evolution 24:31-40.

Zhuravlev, A. Y. 1993. Were Ediacaran Vendobionta multicellulars? Neues Jahrbuch für Geologie und Paläontologie, Abhandlungen 190(2-3):299-314.

CHAPTER 2

A geochemical study of the Ediacaran discoidal fossil *Aspidella* preserved in limestones: Implications for its taphonomy and paleoecology

N. BYKOVA[1,2], B.C. GILL[1], D. GRAZHDANKIN[2,3], VLADIMIR ROGOV[2], S. XIAO[1]

[1]Department of Geosciences, Virginia Tech, Blacksburg, VA 24061, USA

[2]Trofimuk Institute of Petroleum Geology and Geophysics, Siberian Branch Russian Academy of Sciences, Novosibirsk 630090, Russia

[3]Department of Geology and Geophysics, Novosibirsk State University, Novosibirsk, 630090, Russia

2.1 Abstract

The Ediacara biota features the rise of macroscopic complex life immediately before the Cambrian explosion. One of the most abundant and widely distributed elements of the Ediacara biota is the discoidal fossil *Aspidella*, which is interpreted as a subsurface holdfast possibly anchoring a frondose epibenthic organism. It is a morphologically simple fossil preserved mainly in siliciclastic rocks, which are unsuitable for comprehensive stable isotope geochemical analyses to decipher its taphonomy and paleoecology. In this regard, three-dimensionally preserved *Aspidella* fossils from upper Ediacaran limestones of the Khatyspyt Formation in the Olenek Uplift of northern Siberia offer a rare opportunity to leverage geochemistry for insights into their taphonomy and paleoecology. To take advantage of this opportunity, we analyzed $\delta^{13}C_{carb}$, $\delta^{18}O_{carb}$, $\delta^{13}C_{org}$, $\delta^{34}S_{pyr}$, and iron speciation of the Khatyspyt *Aspidella* fossils and surrounding sediment matrix in order to investigate whether they hosted microbial symbionts, how they were fossilized, and the redox conditions of their ecological environments. *Aspidella* holdfasts and surrounding sediment matrix show indistinguishable $\delta^{13}C_{org}$ values, suggesting they did not host and derive significant amount of nutrients from microbial symbionts such as methanogens, methylotrophs, or sulfide-oxidizing bacteria. $\delta^{13}C_{carb}$, $\delta^{18}O_{carb}$, and $\delta^{34}S_{pyr}$ data, along with petrographic observations, suggest that microbial sulfate reduction facilitated the preservation of *Aspidella* by promoting early authigenic calcite cementation in the holdfasts before matrix cementation and sediment compaction. Iron speciation data are equivocal, largely because of the low total iron concentrations. However, consideration of published sulfur isotope and biomarker data suggests that *Aspidella* likely lived in non-euxinic waters. It is possible that *Aspidella* was an opportunistic organism, colonizing the seafloor in large numbers when paleoenvironments were favorable. This study demonstrates that geochemical data of Ediacaran fossils preserved

in limestones can offer important insights into the taphonomy and paleoecology of these enigmatic organisms living on the eve of the Cambrian explosion.

2.2 Introduction

The Ediacaran Period represents a critical transition in the history of life and surface environments (Xiao et al. 2016). During the Ediacaran Period our planet experienced major carbon cycle perturbations, at least transient oxygenation of the deep oceans, and transformative biological innovations (Erwin et al. 2011; Lenton et al. 2014). One of these key events was the radiation of macroscopic and complex eukaryotic life, which is evidenced by appearance of the Ediacara biota, represented by Ediacara-type soft-bodied fossils, in the late Ediacaran Period (Narbonne 2005; Xiao and Laflamme 2009).

Most macrofossils of the Ediacara biota are preserved as casts and molds in sandstones or siltstones (Wade 1968; Grazhdankin 2004; Narbonne 2005; Fedonkin et al. 2007), with their preservation facilitated by microbial masking and authigenic pyrite formation (Gehling 1999; Liu 2016), volcanic tuff sealing (Hofmann et al. 2008), authigenic clay mineral replication (Laflamme et al. 2011; Darroch et al. 2012; Meyer et al. 2014a), or perhaps early diagenetic silica cementation (Tarhan et al. 2016). Although these fossils are sometimes preserved with remarkable morphological details (Narbonne et al. 2009; Vickers-Rich et al. 2013), it remains a significant challenge to understand their taphonomy and paleoecology, in part because the hosting siltstones and sandstones offer limited opportunities for paleoenvironmental and taphonomic analyses using stable isotope geochemical tools.

In this regard, Ediacara-type macrofossils preserved in carbonate rocks, such as those hosted in bituminous limestones of the late Ediacaran Dengying Formation in South China (Xiao et al. 2005; Chen et al. 2014) and the Khatyspyt Formation in the Olenek Uplift of

northern Siberia (Grazhdankin et al. 2008), have the potential to offer valuable insights into and to broaden our perspectives of the taphonomy and paleoecology of the Ediacara biota. To take advantage of this opportunity, we chose to investigate the discoidal fossil *Aspidella* in the Khatyspyt Formation using geochemical tools. This formation was targeted because a complete set of chemostratigraphic data—including $\delta^{13}C_{carb}$, $\delta^{13}C_{org}$, $\delta^{34}S_{CAS}$, and $\delta^{34}S_{pyr}$ profiles of this stratigraphic unit—has been published (Knoll et al. 1995; Pelechaty et al. 1996; Cui et al. 2016a), thus providing a necessary context for a detailed geochemical analysis of *Aspidella* fossils. Importantly, Cui et al. (2016a) have published a detailed chemostratigraphic analysis of the Khatyspyt Formation from the same stratigraphic section (i.e., section 0601) where most *Aspidella* fossils were collected for the present study.

Among all Ediacara-type fossils in the Khatyspyt Formation, the discoidal fossil *Aspidella* is the most abundant. Indeed, it is one of the most abundant and widely distributed Ediacara-type fossils worldwide (Gehling et al. 2000), and it is also the first named Ediacaran body fossil (Billings 1872). However, the taxonomy, phylogenetic affinity, paleoecology, and taphonomy of *Aspidella* and other discoidal fossils have been debated for over a century. Dozens of taxonomic names have been proposed to describe Ediacaran discoidal fossils with or without concentric rims and radial ridges. Gehling, Narbonne, & Anderson (2000) regarded these forms as taphonomic variations and hence junior synonyms of *Aspidella terranovica*, but others have argued that Ediacaran discoidal fossils are heterogeneous and may represent a wide range of taxonomic groups (MacGabhann 2007). Indeed, *Aspidella* and broadly similar discoidal fossils have been variously interpreted as scratch marks or fluid escape structures (Jensen et al. 2002; Menon et al. 2016), microbial colonies (Grazhdankin and Gerdes 2007), giant protists (Seilacher et al. 2003), pelagic medusoidal cnidarians (Glaessner 1984), equilibrium trace fossils of benthic cnidarian polyps (Menon et al. 2013), subsurface holdfasts of benthic frondose organisms (Gehling et al. 2000; Tarhan et al. 2015), or fungus-like

organisms (Peterson et al. 2003). Additionally, it has been proposed that discoidal Ediacaran fossils such as *Aspidella* may have hosted photosymbionts or chemosymbionts such as sulfide-oxidizing bacteria (McMenamin 1986; Dzik 2003; Serezhnikova 2010; Dufour and McIlroy 2016). Furthermore, it was argued that *Aspidella* may have been filled with fluids during life (Seilacher 1992; Gehling et al. 2000; Tarhan et al. 2015) or partially contained sediments to enhance its structure stability as a holdfast (Laflamme et al. 2011). With regard to taphonomy, Retallack (1994) compared the three-dimensional preservation of Ediacara-type fossils to that of fossil logs, arguing for the compaction-resistant nature of Ediacara-type fossils, but this interpretation ignores the important role of early authigenic mineralization in the three-dimensional preservation of completely soft-bodied organisms and cellular structures (e.g., Xiao and Knoll 1999). A comprehensive geochemical investigation of *Aspidella* would complement the morphological analysis of this simple fossil and provide additional insights into its taphonomy and paleoecology.

In this study, we focus on a group of *Aspidella* fossils from the Khatyspyt Formation that are replicated by carbonate sediments and cements. The *Aspidella* discoidal structures are sometimes attached to a cylindrical or conical stalk, although the biological structure above the stalk has not been preserved. Hence, the analyzed fossils are most likely holdfasts and the genus name *Aspidella* is most appropriate (Billings 1872; Gehling et al. 2000; Bykova 2010). Our goal is to test several specific hypotheses about the taphonomy and paleoecology of *Aspidella* holdfasts, viz. (1) whether they hosted certain types of microbial symbionts, (2) what were the redox conditions of the environments in which they lived, and (3) how they were fossilized. The rationale of our analysis is as follows.

If *Aspidella* holdfasts hosted certain groups of microbial symbionts, then they may have distinct $\delta^{13}C_{org}$ values. Specifically, we would like to test whether *Aspidella* derived a significant amount of nutrients from symbiotic methanogens, methylotrophs, or sulfide-

oxidizing bacteria. Relative to carbon fixation through Rubisco, organic carbon produced by methanogens and methylotrophs has distinctively lower $\delta^{13}C_{org}$ values. In contrast, modern tube worms that depend on sulfide-oxidizing bacteria for nutrients have higher $\delta^{13}C_{org}$ values than organic carbon fixed through Rubisco (Robinson et al. 2003). Thus, organic carbon isotopes provide a useful tool to test whether *Aspidella* hosted and derived nutrients from such symbionts. If so, then $\delta^{13}C_{org}$ of the holdfasts would be distinct from that of the surrounding sediment matrix.

We use Fe speciation and stable isotopic data to understand the redox conditions of the water column where *Aspidella* organisms lived. Fe speciation has been used widely in paleoenvironmental and paleoredox studies of fine-grained siliciclastic sediments (Poulton and Canfield 2005). Recently, it has been demonstrated that Fe speciation can also be a useful tool to reconstruct the redox condition of carbonate sedimentary environments (Clarkson et al. 2014), and thus can be applied in the paleoenvironmental reconstruction of the Khatyspyt Formation.

The taphonomic history of Aspidella can be explored by comparing the $\delta^{13}C_{carb}$, $\delta^{18}O_{carb}$, and $\delta^{34}S_{pyr}$ values between *Aspidella* holdfasts and sediment matrix. Together with petrographic observations, these isotopic systems can help to determine the relative timing and source of alkalinity for calcite precipitation and hence preservation of *Aspidella* holdfasts. It should be emphasized, however, because fossils described in the literature as *Aspidella* are likely of heterogeneous origins, our interpretations are only applicable to *Aspidella* fossils representing holdfasts.

2.3 Geological setting

Ediacaran strata in the Olenek Uplift are represented by the Khorbusuonka Group, which crops out along the Khorbusuonka River, a tributary of the Olenek River in northern Siberia (Fig. 2.1a). It consists of the Maastakh, Khatyspyt, and Turkut formations in ascending order (Fig. 2.1b). The Turkut Formation contains small shelly fossils (SSFs) such as *Cambrotubulus decurvatus* that are interpreted by Russian paleontologists as early Cambrian fossils belonging to the *Anabarites trisulcatus* zone of the basal Fortunian Stage (Khomentovsky and Karlova 1993; Rogov et al. 2015). The Khatyspyt and Turkut formations are intruded by diatremes of tuff breccia with a U-Pb zircon age of 543.9 ± 0.2 Ma (Bowring et al. 1993; Rogov et al. 2015), which gives minimum age constraint on the Khorbusuonka Group. The Khorbusuonka Group is overlain by the Syhargalakh Formation of the Kessyusa Group, which contains the trace fossil *Treptichnus pedum* whose first appearance datum is used to define the Ediacaran–Cambrian boundary at its stratotype in Newfoundland (Brasier et al. 1994).

The Khatyspyt Formation consists of 190 m of finely-laminated, thin- to medium-bedded, calcitic and dolomitic carbonate mudstones and intraclastic wackestones with thin intercalations of volcanic tuff layers (Fig. 2.1b). It was deposited in the inner ramp of a carbonate basin (Knoll et al. 1995; Nagovitsin et al. 2015). Based on stratigraphic measurements of composite sections, the Khatyspyt Formation consists of four members (Nagovitsin et al. 2015). The first member has a thickness of ~ 25 m and it is composed of intraclastic limestones with interbeds of thick-bedded and finely laminated limestones. The second member is ~ 50 m thick and characterized by thin layers of limestones and shales interstratified with thick-bedded limestones. The third member is ~ 100 m thick, consisting of finely-laminated limestones with thick-bedded limestones and interbeds of shales. The fourth

member has a variable thickness up to 17 m at maximum, consisting of intraclastic limestones with finely laminated limestones and interbeds of shales (Fig. 2.1b).

The Khatyspyt Formation is exceptionally fossiliferous and has yielded abundant macrofossils preserved as casts/molds and carbonaceous compressions (Grazhdankin et al. 2008), as well as the problematic fossil *Nenoxites curvus* (Rogov et al. 2012; Brasier et al. 2013; Gamez-Vintaned and Zhuravlev 2013; Rogov et al. 2013a, b). Fossils preserved as carbonate casts/molds (Khatyspyt-type preservation) are found in thin- to medium-bedded bituminous limestones and include various discoidal forms (e.g., *Aspidella*, *Cyclomedusa*, *Ediacaria*, *Hiemalora*, *Nimbia*, *Paliella*, *Eoporpita*, and *Protodipleurosoma*), the frondose fossil *Khatyspytia grandis*, the rangeomorph *Charnia masoni*, and the serially chambered fossil *Palaeopascichnus delicatus* (Sokolov and Fedonkin 1984; Vodanjuk 1989; Grazhdankin et al. 2008). Among these, discoidal fossils are most abundant.

Fossils preserved as carbonaceous compressions [Miaohe-type preservation; (Xiao et al. 2002)] are hosted in silicified calcareous mudstones interbedded with bituminous limestones. They include *Mezenia kossovoyi*, *Beltanelloides sorichevae*, *Chuaria circularis*, *Liulingjitaenia alloplecta*, *Jiuqunaoella simplicis*, *Grypania spiralis*, *Glomulus filamentum*, *Longifuniculum dissolutum*, and several unnamed forms (Sokolov and Fedonkin 1984; Grazhdankin et al. 2008; Nagovitsin et al. 2015).

2.4 Materials and methods

All analyzed *Aspidella* specimens came from two fossiliferous intervals at two sections of the Khatyspyt Formation: a 6-m thick interval of thin-layered bituminous limestone in the upper part of the second member (~68 m from the base of the formation) in section 0601 (Cui et al. 2016a) and a 2-m thick interval at the top part of the third member in

section 0607 (Fig. 2.1). The specimens were collected by Sergey Vodanjuk in the late 1980s (Vodanjuk 1989) and are housed in the Central Siberian Geological Museum of Siberian Branch Russian Academy of Sciences (CSGM), in Novosibirsk, Russia, under the collection number 913.

A total of 14 unique *Aspidella* specimens (12 from section 0601 and 2 from section 0607) were selected for this study. These specimens were selected based on their three-dimensional preservation (to facilitate geochemical sampling), preservation with sediment matrix (to allow comparative analysis between fossils and sediment matrix), and fragmentary nature (to minimize the destruction of taxonomically valuable specimens). Some specimens show a biconvex discoidal structure connected to a cylindrical or conical stalk (Fig. 2.2a, c), and others show deformations (Fig. 2.2a) that are likely related to dragging and pulling (Gehling 1988; Gehling et al. 2000; Grazhdankin 2000; Tarhan et al. 2010), affirming that the analyzed *Aspidella* fossils represent subsurface holdfasts rather than microbial colonies or pelagic medusae.

Aspidella holdfasts analyzed in this study are all preserved as three-dimensional biconvex structures with positive relief on both the lower and upper surfaces of the holdfast (Grazhdankin et al. 2008). Because *Aspidella* holdfasts likely had a rather thin organic integument or membrane (Grazhdankin 2000), it is not always possible to determine whether the biconvex structure preserves the internal or external surface of the organic integument (Fig. 2.2b). Unlike shelly fossils where internal molds and casts can be easily distinguished (Fig. 2.2b), it is difficult to determine whether biconvex structures of *Aspidella* holdfasts are internal molds or casts. Thus, they are described as casts/molds to recognize this uncertainty.

Whenever possible, powders from the holdfast center, holdfast margin, stalk, and surrounding matrix were collected using a hand-held Dremel tool (Fig. 2.2a, d). Some

Aspidella holdfasts were attached to a thin piece of surrounding matrix sediments, which were physically removed using pliers and then powdered in a small shatterbox. Practically, no more than one powder sample was taken from the holdfast center, holdfast margin, stalk, and matrix sediments of each *Aspidella* specimen.

A total of 34 powder samples from the 14 *Aspidella* holdfast specimens were obtained, including 14 from holdfast center, 7 from holdfast margin, 3 from stalk, and 10 from sediment matrix (Tables 2.S1–4). These samples were used for the analysis of organic carbon ($\delta^{13}C_{org}$), carbonate carbon ($\delta^{13}C_{carb}$), carbonate oxygen ($\delta^{18}O_{carb}$), pyrite sulfur ($\delta^{34}S_{pyr}$) isotopic compositions, and iron speciation. To ensure the availability of material for geochemical analyses, which are the priorities of this study, thin sections were made for petrographic observation only after powder samples were taken. A total of 17 thin sections were made of six different *Aspidella* fossils and two sediment specimens.

All sample preparation and geochemical analyses were performed at the Department of Geosciences at the Department of Geosciences at Virginia Tech. To prepare for $\delta^{13}C_{org}$ and TOC analyses, ~200 mg of sample powder was acidified in 3N hydrochloric acid (HCl) for 3 days to remove carbonate minerals. The residue was rinsed with doubly deionized (18.2 MΩ) water until neutral pH was reached, and then dried at 40°C. Approximately 1 mg of dried residue was weighed and loaded in a tin cup for $\delta^{13}C_{org}$ and TOC analyses. $\delta^{13}C_{org}$ and TOC were determined on an Isoprime 100 isotope ratio mass spectrometer (IRMS) coupled with a vario ISOTOPE elemental analyzer (EA). $\delta^{13}C_{org}$ values are reported as ‰ deviation from the Vienna Pee Dee Belemnite (VPDB) and were calibrated to this scale using international (IAEA-CH-6, IAEA-CH-7) and commercial (Elemental Microanalysis wheat flour) standards. Analytical uncertainty (1σ) is better than 0.1‰ for $\delta^{13}C_{org}$ and 0.1% for TOC. To determine whether there was a significant difference in $\delta^{13}C_{org}$ between fossils and surrounding matrix, a paired two-tailed Student's t-test was carried out for all pairs of holdfast center and matrix

data. Because Student's t-test assumes normal distribution and our sample size is too small to allow for a normality test, a non-parametric test (i.e., Wilcoxon signed-rank test) was also carried out to verify the t-test.

To prepare for $\delta^{13}C_{carb}$ and $\delta^{18}O_{carb}$ analyses, an aliquot of 300–400 μg powder was weighed and placed in a septum vial. The vial was loaded in a MultiFlowGeo headspace sampler and flushed with helium. The powder was then allowed to react with orthophosphoric acid for 6 hours, and the evolved CO_2 was introduced to an Isoprime 100 IRMS for the determination of C and O isotopic compositions. $\delta^{13}C_{carb}$ and $\delta^{18}O_{carb}$ values are reported as ‰ deviation from the Vienna Pee Dee Belemnite (VPDB) and calibrated to this scale using international (IAEA-CO-1, IAEA-CO-9, and NBS-18) standards. Analytical uncertainty (1σ) is better than 0.1‰ for $\delta^{13}C_{carb}$ and 0.2‰ for $\delta^{18}O_{carb}$. To determine whether there was a significant difference in $\delta^{13}C_{carb}$ and $\delta^{18}C_{carb}$ between fossils and surrounding matrix, paired Student's t-test and Wilcoxon signed-rank test were applied to all pairs of holdfast center and matrix data.

Sample preparation for $\delta^{34}S_{pyr}$ analysis was conducted using the chromium reduction method (Canfield et al. 1986). Approximately 1–2 g powder was reacted with acidified chromium chloride ($CrCl_2$) solution and heated for 2 hours on a specialized distillation line. Evolved hydrogen sulfide (H_2S) was trapped by zinc acetate solution that formed zinc sulfide (ZnS) and was then converted to silver sulfide (Ag_2S) by adding 0.1 M silver nitrate ($AgNO_3$) to the solution. The Ag_2S precipitates were dried and pyrite sulfur contents were calculated as weight percentage of sample powders, and pyrite Fe contents were then calculated stoichiometrically. The Ag_2S was then loaded into tin capsules with vanadium pentoxide (V_2O_5) and combusted in a vario ISOTOPE Cube EA coupled to an Isoprime 100 IRMS for determination of $\delta^{34}S_{pyr}$. $\delta^{34}S_{pyr}$ values are reported as ‰ deviation from the Vienna Canyon Diablo Troilite (V-CDT) and calibrated to this scale using the international IAEA-S-1, IAEA-

S-2, and IAEA-S-3 standards. Analytical uncertainty (1σ) is better than 0.2‰ for $\delta^{34}S_{pyr}$. To determine whether there was a significant difference in $\delta^{34}S_{pyr}$ between fossils and surrounding matrix, paired Student's t-test and Wilcoxon signed-rank test were applied to all pairs of holdfast center and matrix data.

Fe speciation analysis was performed following a sequential extraction procedure modified from Poulton and Canfield (2005). Briefly, iron from carbonate minerals (Fe_{carb}) was extracted using a Na-acetate solution at 60°C for 48 hours, iron present in iron oxides minerals (Fe_{ox}) was extracted using Na-dithionite solution at room temperature for 2 hours, and magnetite bound iron (Fe_{mag}) was extracted using an ammonium oxalate solution at room temperature for 6 hours. Sequential extraction of Fe_{carb}, Fe_{ox}, and Fe_{mag} were rerun for 33 of the 34 samples that had sufficient powders for duplicate analyses. This time Fe_{carb} was extracted at 50°C as described in Poulton and Canfield (2005), and the duplicate analyses gave results similar to those run at 60°C (Table 2.S4). Measurement of aqueous iron extracted from each treatment was performed using the ferrozine method (Stookey 1970; Viollier et al. 2000) on a Thermo GENESYS 10S UV-Vis spectrophotometer. Total iron (Fe_T) was extracted from ashed samples (heated 8 h in furnace at 900 °C) by reacting them with a boiling 12 N HCl for 2 days.

2.5 Results

Petrographic thin sections showed that the host rock mainly consists of thin-bedded to microlaminated micrite and peloidal micrite with remnants of organic-rich microbial mats (Fig. 2.2e, j–k) and relatively small amount of calcitic cements (upper part of Fig. 2.2e). In contrast, *Aspidella* holdfasts and their surroundings consist of peloidal and micritic sediments with a much greater amount of calcitic cements, diffuse kerogen, and small patches or organic

carbon (Fig. 2.2d, f–h, l). As a result, the *Aspidella* holdfasts always appear lighter in color than surrounding matrix in transmitted light microscopy (Fig. 2.2d, f–h, l vs. Fig. 2.2e, j–k). Sedimentary microlaminae warp around biconvex *Aspidella* holdfasts (Fig. 2.2d, j–k), although they sometimes extend into the margin of the holdfasts. This observation suggests that cementation in the holdfasts must have occurred earlier than in the matrix.

$\delta^{13}C_{org}$ of *Aspidella* fossils and sediment matrix ranges from –34.1‰ to –31.5‰ (Fig. 2.3; Table 2.S1). Eight specimens have $\delta^{13}C_{org}$ values for both holdfast center and sediment matrix. To test the null hypothesis (H_o) that there is no difference in $\delta^{13}C_{org}$ between holdfast center and sediment matrix, two statistical analyses were carried out, which revealed no significant differences (paired two-tailed Student's t-test, $p = 0.39$, $n = 8$ pairs of analyses for 8 unique *Aspidella* specimens; two-tailed Wilcoxon signed-rank test, $W = 15$, $W_{critical} = 3$, H_o not rejected at $\alpha = 0.05$, $n = 8$). Similarly, there is no significant difference in $\delta^{13}C_{org}$ between holdfast margin and sediment matrix, between the stalk and sediment matrix, or among different parts of the *Aspidella* fossil; however, the number of paired comparisons is limited ($n = 8$) and hence the statistical power is low. TOC contents for all samples are below 1% (Tables 2.S1, 2.S4) and there is no significant difference in TOC content between any parts of the fossil and the matrix.

$\delta^{13}C_{carb}$ values range from –0.7‰ to +3‰, and $\delta^{18}O_{carb}$ values from –9.5‰ to –6.4‰. Overall, the data do not show a significant correlation between $\delta^{13}C_{carb}$ and $\delta^{18}O_{carb}$ (Fig. 2.4). Ten of the 14 unique *Aspidella* specimens have $\delta^{13}C_{carb}$ and $\delta^{18}O_{carb}$ data for both holdfast center and sediment matrix, and statistical tests showed that $\delta^{13}C_{carb}$ values of holdfast center are significantly lower than those of respective sediment matrix (average $\delta^{13}C_{carb}$ of holdfast center = 0.7‰; average $\delta^{13}C_{carb}$ of matrix = 1.4‰; paired one-tailed Student's t-test, $p < 0.01$, $n = 10$; one-tailed Wilcoxon signed-rank test, $W = 2$, $W_{critical} = 5$, H_o rejected at $\alpha = 0.05$, $n = 8$ because pairs with identical holdfast center and matrix values were excluded from the

analysis) (Fig. 2.5a, c; Table 2.S2). Similarly, $\delta^{18}O_{carb}$ values of the holdfast center are also significantly lower than those of respective sediment matrix (average $\delta^{18}O_{carb}$ of holdfast center = –7.6‰; average $\delta^{18}O_{carb}$ of matrix = –7.1‰; paired one-tailed Student's t-test, p = 0.03, n = 10; one-tailed Wilcoxon signed-rank test, W = 7, $W_{critical}$ = 8, H_o rejected at $\alpha = 0.05$, n = 9) (Fig. 2.5b, d; Table 2.S2).

$\delta^{34}S_{pyr}$ values are highly positive, ranging from 34.5‰ to 41.9‰ for samples from section 0601, although one sample from section 0607 gives a lower value of about 14.0‰ (Fig. 2.6a, b; Table 2.S3). Eight *Aspidella* specimens have $\delta^{34}S_{pyr}$ values for both holdfast center and sediment matrix. Paired comparisons show that the $\delta^{34}S_{pyr}$ values of holdfast center are significantly lower than those of respective sediment matrix (average $\delta^{34}S_{pyr}$ of holdfast center = 34.6‰; average $\delta^{34}S_{pyr}$ of matrix = 36.5‰; paired one-tailed Student's t-test, p = 0.01, n = 8; one-tailed Wilcoxon signed-rank test, W = 2, $W_{critical}$ = 5, H_o rejected at $\alpha = 0.05$, n = 8; Fig. 2.6a-b). Indeed, the average difference of these paired comparison is 2.0‰, suggesting that the $\delta^{34}S_{pyr}$ values of the holdfast center are notably lower than those of respective sediment matrix.

Fe speciation data are presented in Fig. 2.7 and Table 2.S4. Total iron concentration (Fe_T) ranges from 0.14 to 0.60 wt%. Among the 34 powder samples, only six (from 5 *Aspidella* samples) yielded Fe_T values ≥ 0.50 wt% (highlighted in bold in Table 2.S4), the threshold for Fe speciation data from carbonate rocks to be a reliable proxy for the reconstruction of water-column redox conditions (Clarkson et al. 2014). Also, nine analyses of 6 *Aspidella* specimens yielded both low Fe_T and TOC contents (both < 0.50 wt%; pale blue in Table 2.S4); it has been shown that oxic carbonate-rich sediments with such low Fe_T and TOC contents often give spuriously high Fe_{HR}/Fe_T ratios (Clarkson et al. 2014). Based on the first batch of reactive Fe analyses, the ratio of Fe_{HR} (= Fe_{pyr} + Fe_{carb} + Fe_{ox} + Fe_{mag}) to Fe_T ranges from 0.37 to 1.00, with a median = 0.75, whereas Fe_{pyr}/Fe_{HR} varies from 0.06 to 0.65,

with median of 0.24. Thus, none of the measurements are plotted in the euxinic field defined by $Fe_{HR}/Fe_T > 0.38$ and $Fe_{pyr}/Fe_{HR} > 0.80$. Among all reactive Fe species, Fe_{carb} is the most dominant, representing 6–81% of Fe_{HR}, with median of 50%. The duplicate analyses of reactive Fe show similar results.

2.6 Discussion

2.6.1 Did *Aspidella* holdfast host microbial symbionts?

Several authors have proposed that various Ediacara-type organisms may have hosted photosymbionts (Seilacher 1984; McMenamin 1986). Others suggested that Ediacara-type organisms, some of which inhabited in deep-water aphotic environments (Wood et al. 2003), may have hosted sulfide-oxidizing bacteria (Dzik 2003; Brasier 2012; Dufour and McIlroy 2016). To our knowledge, however, tests of the symbiosis hypothesis using geochemistry have not been attempted.

If A*spidella* hosted photosymbionts, then these symbionts would likely reside in the fronds rather than the subsurface holdfast. On the other hand, chemosymbionts would likely explore redox boundaries and be hosted in the holdfasts. If these chemosymbionts involved methanogens, methylotrophs, or sulfide-oxidizing bacteria, and if *Aspidella* derived a significant portion of nutrients from these symbionts, then *Aspidella* holdfasts would have a $\delta^{13}C_{org}$ signature distinct from the sediment matrix. Specifically, methanogens and methylotrophs would produce organic carbon with distinctly lower $\delta^{13}C_{org}$ values, and sulfide-oxidizing bacteria with high $\delta^{13}C_{org}$ values relative to organic carbon in the sediment matrix which was presumably derived mostly from oxygenic photoautotrophs. Such $\delta^{13}C_{org}$ signatures could be preserved in the *Aspidella* fossils and sediment matrix, given the exceptional preservation of indigenous biomarkers in the Khatyspyt Formation (Duda et al.

2016). Thus, certain forms of the symbiosis hypothesis can be tested with $\delta^{13}C_{org}$ data. Our observation that the different parts of *Aspidella* fossils and the surrounding sediment matrix have indistinguishable $\delta^{13}C_{org}$ values does not support the hypothesis that *Aspidella* holdfasts hosted microbial consortia (e.g., methanogens, methylotrophs, or sulfide-oxidizing bacteria) that would impart a distinct $\delta^{13}C_{org}$ signature.

Of course, we cannot exclude the possibility that *Aspidella* in the Khatyspyt Formation may have hosted photosybionts that used the Rubisco enzyme for carbon fixation, because these photosymbionts would produce organic carbon with $\delta^{13}C_{org}$ indistinguishable from that of the primary production (and of organic carbon in the matrix sediments). Neither can we exclude the possibility that microbial consortia with similar metabolic pathways might have inhabited *Aspidella*, the water column, and surrounding sediments. Another caveat relates to diagenetic alteration and migration of organic compounds, particularly given that bitumens are prevalent in the overlying Turkut Formation although biomarkers in the Khatyspyt Formation seem to be indigenous (Duda et al. 2016). The currently available data do not allow us to thoroughly address these concerns. SIMS $\delta^{13}C_{org}$ analysis and careful biomarker analysis of the Khatyspyt *Aspidella* holdfasts (e.g., Duda et al. 2016) could potentially provide further geochemical data to further test whether and what kind of symbionts *Aspidella* holdfasts might have hosted.

2.6.2 The taphonomy of *Aspidella*

Like most other Ediacara-type fossils, *Aspidella* holdfasts are preserved with certain degree of three dimensionality despite the lack of biomineralized skeletons. This style of preservation prompted some paleontologists to compare the preservation of Ediacara fossils with fossil logs, arguing that Ediacara organisms were compaction-resistant lichens (Retallack

1994). However, recent studies have shown that early authigenic mineralization (i.e., in-situ mineral precipitation and crystallization within enclosing sediments during or shortly after deposition), rather than compaction-resistant tissues, is responsible for the three-dimensional preservation of non-skeletal Ediacara macrofossils (Gehling 1999; Schiffbauer et al. 2014; Liu 2016; Tarhan et al. 2016) and microfossils (Xiao and Knoll 1999).

Petrographic observations of and geochemical data from *Aspidella* fossils further reinforce the importance of early authigenic mineralization in the exceptional preservation of soft-bodied Ediacara fossils. The three-dimensional cast preservation has been previously recognized in *Aspidella* holdfasts of the Khatyspyt Formation, which were sometimes described as carbonate "nodules" (Vodanjuk 1989; Grazhdankin et al. 2008). Similar to early diagenetic nodules from the Ediacaran Doushantuo Formation (Xiao et al. 2010), *Aspidella* holdfasts are often preserved as biconvex casts or molds (Fig. 2.2b–d, i), with microbial and sedimentary laminae warping around the fossils (Fig. 2.2j–k). Furthermore, there is petrographic evidence suggesting that *Aspidella* holdfasts consist of proportionally more calcite cements than surrounding matrix (Fig. 2.2f–h), suggesting that *Aspidella* holdfasts were lithified by early authigenic calcite cementation before the sediment compaction (Fig. 2.2d). This interpretation is further supported by geochemical data obtained in this study.

The $\delta^{13}C_{carb}$ and $\delta^{18}O_{carb}$ data suggest that, although seawater alkalinity was a major contributor to carbonate contents in *Aspidella* holdfasts (particularly if *Aspidella* holdfasts may have been infilled with carbonate sediments from the ambient environment, e.g., Laflamme *et al.*, 2011), authigenic calcite cements may have also played an important role in the preservation of *Aspidella* holdfasts. Cross-plot of pooled $\delta^{13}C_{carb}$ and $\delta^{18}O_{carb}$ data shows that C and O isotope values of *Aspidella* holdfasts largely overlap with those of matrix sediments (Fig. 2.4), and that the Khatyspyt $\delta^{13}C_{carb}$ data are broadly similar to those of late Ediacaran marine sediments in other sedimentary basins (e.g., Macdonald et al. 2013; Cui et

al. 2016a; Cui et al. 2016b; Xiao et al. 2016). This observation suggests that seawater alkalinity was the major contributors to carbonate minerals in *Aspidella* holdfasts. However, a paired comparison of *Aspidella* holdfasts and surrounding sediments shows that $\delta^{13}C_{carb}$ and $\delta^{18}O_{carb}$ values of *Aspidella* holdfasts are slightly lower than those of matrix sediments, and the differences are statistically significant (Fig. 2.5). The differences are best interpreted as evidence that the holdfasts contain a proportionally greater amount of authigenic cements, which typically have lower $\delta^{13}C_{carb}$ and $\delta^{18}O_{carb}$ values than those of carbonates precipitated solely from marine waters. This is consistent with petrographic observation that cementation of holdfasts predates sediment compaction, hence proportionally more pore space was filled with authigenic calcite cements in the holdfasts than in surrounding sediment matrix. Indeed, a similar interpretation has been proposed for the three-dimensional preservation of the Ediacaran trace fossil *Lamonte trevallis* in limestone of the Dengying Formation (Meyer et al. 2014b). This interpretation, however, begs the question of what was the source of ^{13}C-depleted alkalinity that drove pre-compaction calcite cementation in the holdfasts.

We believe that the $\delta^{34}S_{pyr}$ data can shed light on the source of ^{13}C-depleted alkalinity that drove pre-compaction calcite cementation in *Aspidella* holdfasts. Sedimentary pyrite is an archive of microbial sulfate reduction (generalized reaction: $2CH_2O + SO_4^{2-} \rightarrow HS^- + H^+ + 2HCO_3^-$), which generates H_2S (supporting pyrite precipitation if reactive Fe is available, $HS^- + Fe^{2+} \rightarrow FeS + H^+$; $FeS + S^0 \rightarrow FeS_2$) and HCO_3^- (supporting calcite precipitation if supersaturation level is high, $2HCO_3^- + Ca^{2+} \rightarrow CaCO_3 + H_2O + CO_2$). As HCO_3^- is derived from organic carbon, it is expected to be ^{13}C-depleted relative to seawater alkalinity. Also, because microbial sulfate reduction discriminates against ^{34}S, H_2S and hence pyrite has lower $\delta^{34}S$ values relative to sulfate, unless the reaction is quantitative or occurs as a distillation process in a semi-closed system. Factors affecting the magnitude of isotopic fractionation during microbial sulfate reduction include the availability of sulfate and metabolizable

organic compounds, sulfate reduction rates, and oxic recycling of H_2S (Bourdeau and Westrich 1984; Canfield et al. 2010; Xiao et al. 2010; Leavitt et al. 2013; Gomes and Hurtgen 2015; Bradley et al. 2016). In a typical sediment column in marine environments, pore-water SO_4^{2-} concentration drops as microbial sulfate reduction proceeds, and in the meantime, $\delta^{34}S_{sulfide}$ and $\delta^{34}S_{sulfate}$ increase because of diffusion-related sulfate limitation and distillation (Fig. 2.6c) (Jorgensen et al. 2004). As such, it is anticipated that pyrite precipitated in the upper sediment column would be isotopically lighter than in the lower sediment column. In other words, if *Aspidella* holdfasts were lithified before sediment compaction, pyrite in the holdfasts would be formed mostly in the upper sediment column and thus have lower $\delta^{34}S_{pyr}$ values than sediment matrix.

This is indeed the case. Although overall $\delta^{34}S_{pyr}$ values are high and comparable to bulk-sample $\delta^{34}S_{CAS}$ values of the fossiliferous stratigraphic interval (Cui et al. 2016a), $\delta^{34}S_{pyr}$ of *Aspidella* holdfasts is appreciably and significantly lower than that of sediment matrix (Fig. 2.6a–b). Previous studies have shown that the fossiliferous interval was deposited in non-euxinic environments and pyrite was formed in sediments (Cui et al. 2016a; Duda et al. 2016). Thus, the high $\delta^{34}S_{pyr}$ values resulted from a combination of lower-than-modern levels of marine sulfate concentrations, obstruction of seawater-porewater communication by microbial mats, and diffusion-related sulfate limitation (Fike et al. 2015; Cui et al. 2016a). Along the same line of reasoning, we further hypothesize that microbial sulfate reduction in post-mortem *Aspidella* holdfasts occurred before sediment compaction, supplying ^{13}C-depleted alkalinity to support calcite cementation and holdfast preservation (Fig. 2.8). Thus, alkalinity for pre-compaction calcite cementation in *Aspidella* holdfasts was partly derived from microbial sulfate reduction. And because *Aspidella* holdfasts contain proportionally more calcite cements, they have slightly lower $\delta^{13}C_{carb}$ and $\delta^{18}O_{carb}$ values than sediment matrix (Fig. 2.8).

This hypothesis begs additional questions: why was early authigenic calcite cementation focused on *Aspidella* holdfasts and why is $\delta^{13}C_{org}$ of *Aspidella* holdfasts indistinguishable from that of matrix sediments? We speculate that microbial sulfate reduction initially targeted post-mortem *Aspidella* holdfasts because they provided a local abundance of highly metabolizable organic matter for anaerobic microbes in shallow sediment depths. In other words, *Aspidella* holdfasts are functionally analogous to the organic-rich nuclei that fueled microbial sulfate reduction and subsequent growth of chert nodules in the Ediacaran Doushantuo Formation (Xiao et al. 2010). As to the indistinguishable $\delta^{13}C_{org}$ values between *Aspidella* holdfasts and matrix sediments, we note that heterotrophic sulfate reducers have limited impact on the carbon isotopic composition of their organic substrates and that their biomass is isotopically similar to the organic substrates (Londry and Des Marais 2003).

2.6.3 Water column redox conditions

Whereas a better understanding of pore-water geochemistry is important to reconstructing the taphonomic history of *Aspidella* holdfasts, constraining the water column redox conditions is critical to interpreting the paleoecology of the *Aspidella* organism. Iron speciation data have been used extensively for the reconstruction of water column redox conditions (Canfield et al. 2008; Li et al. 2010; Johnston et al. 2013; Sperling et al. 2015; Sahoo et al. 2016). Originally, this proxy was established for fine-grained siliciclastic sediments and sedimentary rocks (Raiswell and Canfield 1998) and it has been proposed that $Fe_{HR}/Fe_T < 0.38$ (or 0.20 depending on depositional settings) represents oxic settings, whereas $Fe_{HR}/Fe_T > 0.38$ represents anoxic settings. Anoxic settings can be further parsed into ferruginous ($Fe_{pyr}/Fe_{HR} < 0.8$) and euxinic ($Fe_{pyr}/Fe_{HR} > 0.8$) conditions (Raiswell and Canfield 1998; Poulton and Canfield 2005; Canfield et al. 2008). In carbonate-rich sediments,

however, Fe speciation data have been suggested to provide a reliable proxy for water column redox conditions only when Fe_T is greater than 0.5 wt% (Clarkson et al. 2014). When Fe_T is less than 0.5 wt%, because of enrichment of the highly reactive pool of iron during early diagenetic recrystallization of carbonates, Fe_{HR}/Fe_T is elevated regardless of water column redox conditions. Indeed, oxic carbonate-rich samples with low Fe_T (<0.5 wt%) and low TOC (< 0.5 wt%) often give spuriously elevated $Fe_{HR}/Fe_T > 0.38$ (Clarkson et al. 2014).

In our analysis, only six of the 34 powder samples (5 of the 14 *Aspidella* specimens) have Fe_T concentrations ≥ 0.5 wt%, and they all fall in the ferruginous field (Fig. 2.7; Table 2.S4). Most powder samples (28 out of 34) have Fe_T concentrations < 0.5 wt%, and their Fe speciation data cannot be used as a reliable redox proxy. Among these samples, nine (representing six of 14 *Aspidella* specimens) exhibit both low Fe_T (<0.5 wt%) and low TOC (< 0.5 wt%), and potentially represent oxic conditions. Despite this uncertainty, it is safe to conclude that the *Aspidella* organism, which was elevated above the substrate in the water column, probably lived in a non-euxinic water column, given the toxicity of hydrogen sulfide.

This interpretation is consistent with Cui *et al.'s* (2016a) conclusion, based on chemostratigraphic profiles of $\delta^{34}S_{pyr}$, $\delta^{34}S_{CAS}$, and Ce/Ce* from section 0601, that the stratigraphic appearance of *Aspidella* and other Ediacara-type fossils in the Khatyspyt Formation coincides with a transition from euxinic to ferruginous or weakly oxic conditions. Also, preliminary biomarker analysis of a fossiliferous Khatyspyt sample, collected from middle of Member 3 of the Khatyspyt Formation, found no evidence for photic zone anoxia (Duda et al. 2016). Whereas currently available data are not sufficient to determine whether *Aspidella* organisms lived in a ferruginous or oxic water column, it is useful to note that Ediacara-type fossils (including *Aspidella*) are often preserved in oxic sediments in Newfoundland (Canfield et al. 2007), East European Platform (Johnston et al. 2012), and Namibia (Darroch et al. 2015; Wood et al. 2015). Therefore, although Fe speciation data were

ambiguous, we hypothesize that *Aspidella* organisms in the Khatyspyt Formation may have also lived in oxic environments.

In some Ediacaran successions, Ediacara-type macrofossils and macroalgae are found in sediments deposited under ferruginous or even euxinic conditions, e.g., in the June Bed and Blueflower Formation at Sekwi Brook of the Mackenzie Mountains (Sperling et al. 2016), the Lantian Formation in southern Anhui Province of South China (Yuan et al. 2011; Guan et al. 2014; Wang et al. 2017), and the uppermost Doushantuo Formation at Miaohe of South China (Xiao et al. 2002; Li et al. 2015). However, in these Ediacaran succession, it has been proposed that frequent interruption of anoxic conditions by brief (ecological time-scale) episodes of oxic conditions may have allowed the opportunistic colonization by aerobic macro-organisms (Yuan et al. 2011), and such redox changes at ecological time scale cannot be captured by present geochemical sampling protocols (Sperling et al. 2016; Wang et al. 2017). Such dynamic changes in ocean redox conditions preserved in Ediacaran successions are analogous to the paleontological and geochemical signals for intermittent anoxia and euxinia recorded in younger Phanerozoic successions (Kenig et al. 2004; Boyer et al. 2011). In light of the possible dynamic nature of Ediacaran ocean redox conditions, we favor the hypothesis that *Aspidella* fossils represent opportunistic organisms that capitalized upon intermittent oxic conditions to rapidly colonize favorable environments, resulting in the occurrence of remarkably dense populations of holdfasts (Gehling et al. 2000). This hypothesis needs to be further investigated in future paleoecological and geochemical investigations of *Aspidella*.

2.7 Conclusions

To our knowledge, this study is the first comprehensive geochemical analysis of Ediacara-type fossils. We present $\delta^{13}C_{carb}$, $\delta^{18}O_{carb}$, $\delta^{13}C_{org}$, $\delta^{34}S_{pyr}$, and Fe speciation data for the discoidal holdfast fossil *Aspidella* from the late Ediacaran Khatyspyt Formation in the Olenek Uplift of northern Siberia, in order to contribute to our knowledge about the taphonomy and paleoecology of *Aspidella*. Specifically, the research was designed to address the following questions: whether *Aspidella* holdfasts host microbial symbionts, how *Aspidella* was preserved, and what were the redox conditions of the water column where *Aspidella* organisms lived.

The geochemical data show that there is no significant difference in $\delta^{13}C_{org}$ among *Aspidella* holdfast, stalk, and sediment matrix, suggesting that *Aspidella* holdfasts did not host a consortium of symbiotic microbes that would impart a distinct $\delta^{13}C_{org}$ signature. $\delta^{13}C_{carb}$, $\delta^{18}O_{carb}$, and $\delta^{34}S_{pyr}$ values of *Aspidella* holdfasts are significantly lower than those of sediment matrix. Together with petrographic observations, these geochemical data indicate that *Aspidella* holdfasts were mineralized and preserved through early authigenic and pre-compaction calcite cementation in likely shallow depths of the sediment column. Microbial sulfate reduction targeting *Aspidella* holdfasts led to the precipitation of pyrite with lower $\delta^{34}S_{pyr}$ values (relative to the matrix, which incorporated pyrite formed at a later stage and probably at greater sediment depths), and also contributed ^{13}C-depleted alkalinity to calcite cementation of *Aspidella* holdfasts. Finally, although iron speciation data are equivocal because of the low Fe_T concentrations, sulfur isotope systematics and biomarker data from previous studies suggest that *Aspidella* organisms likely inhabited non-euxinic and perhaps oxic environments. We hypothesize that *Aspidella* was an opportunistic taxon that relatively rapidly capitalized upon brief oxic intervals to produce dense populations of individuals.

These hypotheses need to be further tested in the future with additional paleoecological, geochemical, and biomarker data.

2.8 Acknowledgments

We would like to thank Theodore Them, Mathew Petroff, Matthew Leroy, and Esther Schwarzenbach for laboratory assistance; Alan J. Kaufman and Huan Cui for sharing chemostratigraphic data of the Khatyspyt Formation; and Alan J. Kaufman, Konstantin Nagovitsin, Sara Peek, and Vladimir Rogov for field assistance. This research was funded by the National Science Foundation (EAR-1528553), NASA Exobiology and Evolutionary Biology Program (NNX15AL27G), Russian Science Foundation (14–17–00409), National Geographic Society (8227-07, 8637-09, 9031-11), and GSA Graduate Student Research Grant. The authors declare no conflict of interest.

2.9 Tables and table captions

Table 2.S1. $\delta^{13}C_{org}$ and TOC content data. Gray-shaded cells indicate cases where it was not possible to collect powder samples. Cells with "x" indicate that powder samples were collected but did not yield enough material for an analysis.

Sample horizon & section	Sample number	$\delta^{13}C_{org}$				TOC %			
		center	**margin**	**stalk**	**matrix**	**center**	**margin**	**stalk**	**matrix**
Second member, section 0601	CSGM #913-600	-33.5		-33.6	-33.6	0.4		0.4	0.6
	CSGM #913-601	-33.8			-34.0	0.7			0.5
	CSGM #913-602	-31.9		-32.5	-32.1	1.0		0.7	0.7
	CSGM #913-603	x	-33.5		-31.9	x	0.1		0.8
	CSGM #913-604	-31.8	-31.8		-31.6	x	0.9		0.7
	CSGM #913-605	-31.9	-32.2		-31.8	0.8	0.7		0.7
	CSGM #913-606	-32.0		-32.0		0.7		0.3	
	CSGM #913-607	x	-31.5		-31.8	x	0.0		0.3
	CSGM #913-608	-32.4	-32.5			0.8	0.7		
	CSGM #913-609	-32.3			-31.9	0.9			0.7
	CSGM #913-610	x	-31.9			x	0.6		
	CSGM #913-611	-33.8	x			x	x		
Third member, section 0607	CSGM #913-612	-33.7			-33.8	0.2			0.3
	CSGM #913-613	-31.9			-34.1	0.1			0.2

Table 2.S2. $\delta^{13}C_{carb}$ and $\delta^{18}O_{carb}$ data. Gray-shaded cells indicate cases where it was not possible to collect powder samples.

Sample horizon & section	Sample number	$\delta^{13}C_{carb}$				$\delta^{18}O_{carb}$			
		center	**margin**	**stalk**	**matrix**	**center**	**margin**	**stalk**	**matrix**
Second member, section 0601	CSGM #913-600	2.2		2.6	3.0	-6.5		-6.8	-6.9
	CSGM #913-601	2.6			2.4	-7.2			-6.9
	CSGM #913-602	0.0		0.3	1.3	-7.7		-7.4	-6.6
	CSGM #913-603	-0.1	-0.2		1.2	-7.6	-7.6		-6.4
	CSGM #913-604	0.2	-0.3		1.4	-7.7	-6.6		-6.4
	CSGM #913-605	-0.7	0.6		1.1	-7.0	-7.0		-6.5
	CSGM #913-606	1.2		1.2		-7.3		-7.3	
	CSGM #913-607	-0.2	0.7		0.4	-7.2	-7.5		-7.6
	CSGM #913-608	0.9	1.4			-7.8	-7.6		
	CSGM #913-609	1.0			1.1	-7.3			-6.7
	CSGM #913-610	0.0	0.2			-7.7	-7.6		
	CSGM #913-611	0.4	0.3			-7.7	-7.8		
Third member, section 0607	CSGM #913-612	0.9			0.9	-9.5			-9.5
	CSGM #913-613	1.0			1.0	-8.2			-8.1

Table 2.S3. $\delta^{34}S_{pry}$ data. Gray-shaded cells indicate cases where it was not possible to collect powder samples. Cells with "x" indicate that powder samples were collected but did not yield enough material for an analysis.

Sample horizon & section	Sample number	$\delta^{34}S_{pyr}$			
		center	**margin**	**stalk**	**matrix**
Second member, section 0601	CSGM #913-600	37.8		38.4	37.6
	CSGM #913-601	37.9			40.1
	CSGM #913-602	39.0		39.2	40.5
	CSGM #913-603	36.3	36.9		40.6
	CSGM #913-604	35.2	38.4		39.9
	CSGM #913-605	39.0	40.5		41.9
	CSGM #913-606	40.0		38.7	
	CSGM #913-607	37.3	x		37.4
	CSGM #913-608	36.8	37.5		
	CSGM #913-609	36.8			x
	CSGM #913-610	39.5	36.7		
	CSGM #913-611	36.1	34.5		
Third member, section 0607	CSGM #913-612	x			x
	CSGM #913-613	14.0			14.2

Table 2.S4. Iron speciation data. Bold numbers in Fe_T column represent samples with Fe_T ≥0.5 wt% for iron speciation data to be used to infer redox conditions according to Clarkson et al. (2014). Cells shaded in pale blue indicate samples with both low Fe_T and low TOC contents (both < 0.5 wt%). Cells with "x" indicate no sufficient powder for an analysis.

First batch of measurements (with carbonate Fe extracted at 60°C)											
Sample horizon & section	Sample number	**Part**	**TOC %**	**Fe_T (wt%)**	**Fe_{carb} (wt%)**	**Fe_{ox} (wt%)**	**Fe_{mag} (wt%)**	**Fe_{pyr} (wt%)**	**Fe_{HR} (wt%)**	**Fe_{HR}/ Fe_T**	**Fe_{pyr}/ Fe_{HR}**
Second member, section 0601	CSGM #913-600	**center**	0.35	0.14	0.04	0.00	0.00	0.08	0.13	0.91	0.65
		stalk	0.42	0.42	0.08	0.03	0.01	0.04	0.15	0.37	0.24
		matrix	0.59	0.41	0.11	0.08	0.01	0.06	0.25	0.62	0.23
	CSGM #913-601	**center**	0.71	0.41	0.01	0.12	0.01	0.02	0.16	0.39	0.12
		matrix	0.49	0.48	0.04	0.12	0.01	0.02	0.19	0.39	0.11
	CSGM #913-602	**center**	0.95	0.45	0.35	0.01	0.00	0.10	0.45	1.00	0.22
		stalk	0.67	0.46	0.27	0.04	0.01	0.14	0.45	0.99	0.30
		matrix	0.73	**0.53**	0.09	0.07	0.01	0.12	0.28	0.53	0.43
	CSGM #913-603	**center**	x	0.42	0.30	0.02	0.00	0.10	0.42	1.00	0.24
		margin	0.95	0.45	0.29	0.03	0.00	0.04	0.36	0.80	0.11
		matrix	0.82	0.29	0.07	0.06	0.01	0.04	0.18	0.60	0.25
	CSGM #913-604	**center**	x	0.43	0.26	0.04	0.01	0.10	0.40	0.95	0.25
		margin	0.88	**0.55**	0.14	0.16	0.01	0.08	0.39	0.72	0.21
		matrix	0.69	0.30	0.09	0.05	0.01	0.05	0.19	0.65	0.24
	CSGM #913-605	**center**	0.83	0.34	0.10	0.04	0.01	0.07	0.22	0.64	0.33
		margin	0.66	0.42	0.20	0.06	0.01	0.10	0.36	0.87	0.27
		matrix	0.74	0.35	0.11	0.07	0.01	0.05	0.23	0.64	0.20
	CSGM #913-606	**center**	0.65	0.32	0.12	0.05	0.00	0.05	0.23	0.70	0.21
		stalk	0.31	0.40	0.13	0.06	0.01	0.08	0.28	0.69	0.28
	CSGM #913-607	**center**	x	**0.51**	0.20	0.08	0.01	0.10	0.38	0.75	0.25
		margin	0.03	0.47	0.29	0.10	0.00	0.03	0.42	0.90	0.06
		matrix	0.29	**0.60**	0.31	0.10	0.01	0.11	0.52	0.86	0.21
	CSGM #913-608	**center**	0.75	0.48	0.25	0.05	0.00	0.12	0.42	0.87	0.28
		margin	0.68	0.44	0.21	0.05	0.01	0.10	0.36	0.81	0.27
	CSGM #913-609	**center**	0.86	0.37	0.17	0.06	0.00	0.12	0.35	0.96	0.33
		matrix	0.65	0.33	0.07	0.08	0.01	0.09	0.25	0.75	0.36
	CSGM #913-610	**center**	x	0.49	0.24	0.02	0.00	0.09	0.36	0.73	0.26
		margin	0.56	**0.59**	0.34	0.06	0.01	0.11	0.52	0.88	0.21
	CSGM #913-611	**center**	x	0.44	0.31	0.04	0.00	0.08	0.43	0.97	0.18
		margin	x	**0.50**	0.30	0.04	0.00	0.09	0.44	0.87	0.20
Third member, section 0607	CSGM #913-612	**center**	0.23	0.43	0.11	0.08	0.01	0.15	0.36	0.84	0.42
		matrix	0.29	0.49	0.10	0.16	0.01	0.04	0.32	0.66	0.14
	CSGM #913-613	**center**	0.09	0.22	0.05	0.06	0.01	0.04	0.15	0.65	0.24
		matrix	0.22	0.28	0.06	0.07	0.01	0.02	0.15	0.55	0.10

Duplicate measurements (with carbonate Fe extracted at 50°C)											
Sample horizon & section	Sample number	**Part**	**TOC %**	**Fe_T (wt%)**	**Fe_{carb} (wt%)**	**Fe_{ox} (wt%)**	**Fe_{mag} (wt%)**	**Fe_{pyr} (wt%)**	**Fe_{HR} (wt%)**	**Fe_{HR}/Fe_T**	**Fe_{pyr}/Fe_{HR}**
Second member, section 0601	CSGM #913-600	**center**	0.35	0.14	0.02	0.02	0.00	0.08	0.12	0.86	0.67
		stalk	0.42	0.42	0.08	0.03	0.01	0.04	0.16	0.38	0.25
		matrix	0.59	0.41	0.12	0.08	0.01	0.06	0.27	0.66	0.22
	CSGM #913-601	**center**	0.71	0.41	0.01	0.13	0.00	0.02	0.16	0.39	0.13
		matrix	0.49	0.48	0.03	0.15	0.00	0.02	0.20	0.42	0.10
	CSGM #913-602	**center**	0.95	0.45	0.34	0.01	0.00	0.10	0.45	1.00	0.22
		stalk	0.67	0.46	0.27	0.04	0.00	0.14	0.45	0.98	0.31
		matrix	0.73	**0.53**	0.08	0.08	0.01	0.12	0.29	0.55	0.41
	CSGM #913-603	**center**	x	0.42	0.29	0.03	0.00	0.10	0.42	1.00	0.24
		margin	0.95	0.45	0.29	0.05	0.00	0.04	0.38	0.84	0.11
		matrix	0.82	0.29	0.06	0.08	0.00	0.04	0.18	0.62	0.22
	CSGM #913-604	**center**	x	0.43	0.25	0.05	0.00	0.10	0.40	0.93	0.25
		margin	0.88	**0.55**	0.11	0.20	0.00	0.08	0.39	0.71	0.21
		matrix	0.69	0.30	0.07	0.07	0.00	0.05	0.19	0.63	0.26
	CSGM #913-605	**center**	0.83	0.34	0.11	0.04	0.00	0.07	0.22	0.65	0.32
		margin	0.66	0.42	0.19	0.06	0.01	0.10	0.36	0.86	0.28
		matrix	0.74	0.35	0.10	0.08	0.01	0.05	0.24	0.69	0.21
	CSGM #913-606	**center**	0.65	0.32	0.12	0.05	0.00	0.05	0.22	0.69	0.23
		stalk	0.31	0.40	0.14	0.06	0.01	0.08	0.29	0.73	0.28
	CSGM #913-607	**center**	x	**0.51**	0.20	0.08	0.00	0.10	0.38	0.75	0.26
		margin	0.03	0.47	0.28	0.09	0.00	0.03	0.40	0.85	0.08
		matrix	0.29	**0.60**	0.30	0.09	0.01	0.11	0.51	0.85	0.22
	CSGM #913-608	**center**	0.75	0.48	0.24	0.05	0.00	0.12	0.41	0.85	0.29
		margin	0.68	0.44	0.20	0.06	0.01	0.10	0.37	0.84	0.27
	CSGM #913-609	**center**	0.86	0.37	0.15	0.08	0.00	0.12	0.35	0.95	0.34
		matrix	0.65	0.33	0.06	0.09	0.00	0.09	0.24	0.73	0.38
	CSGM #913-610	**center**	x	0.49	0.24	0.03	0.00	0.09	0.36	0.73	0.25
		margin	0.56	**0.59**	0.33	0.05	0.01	0.11	0.50	0.85	0.22
	CSGM #913-611	**center**	x	0.44	0.30	0.05	0.00	0.08	0.43	0.98	0.19
		margin	x	**0.50**	x	x	x	0.09	x	x	x
Third member, section 0607	CSGM #913-612	**center**	0.23	0.43	0.10	0.09	0.01	0.15	0.35	0.81	0.43
		matrix	0.29	0.49	0.16	0.09	0.01	0.04	0.30	0.61	0.13
	CSGM #913-613	**center**	0.09	0.22	0.07	0.04	0.01	0.04	0.16	0.73	0.25
		matrix	0.22	0.28	0.08	0.05	0.01	0.02	0.16	0.57	0.13

Comparison between the first batch of analyses and duplicate analyses										
Sample horizon & section	Sample number	Part	TOC %	Fe_T (wt%)	50°C			60°C		
					Fe_{HR} (wt%)	Fe_{HR}/Fe_T	Fe_{pyr}/Fe_{HR}	Fe_{HR} (wt%)	Fe_{HR}/Fe_T	Fe_{pyr}/Fe_{HR}
Second member, section 0601	CSGM #913-600	**center**	0.35	0.14	0.12	0.86	0.67	0.13	0.91	0.65
		stalk	0.42	0.42	0.16	0.38	0.25	0.15	0.37	0.24
		matrix	0.59	0.41	0.27	0.66	0.22	0.25	0.62	0.23
	CSGM #913-601	**center**	0.71	0.41	0.16	0.39	0.13	0.16	0.39	0.12
		matrix	0.49	0.48	0.20	0.42	0.10	0.19	0.39	0.11
	CSGM #913-602	**center**	0.95	0.45	0.45	1.00	0.22	0.45	1.00	0.22
		stalk	0.67	0.46	0.45	0.98	0.31	0.45	0.99	0.30
		matrix	0.73	**0.53**	0.29	0.55	0.41	0.28	0.53	0.43
	CSGM #913-603	**center**	x	0.42	0.42	1.00	0.24	0.42	1.00	0.24
		margin	0.95	0.45	0.38	0.84	0.11	0.36	0.80	0.11
		matrix	0.82	0.29	0.18	0.62	0.22	0.18	0.60	0.25
	CSGM #913-604	**center**	x	0.43	0.40	0.93	0.25	0.40	0.95	0.25
		margin	0.88	**0.55**	0.39	0.71	0.21	0.39	0.72	0.21
		matrix	0.69	0.30	0.19	0.63	0.26	0.19	0.65	0.24
	CSGM #913-605	**center**	0.83	0.34	0.22	0.65	0.32	0.22	0.64	0.33
		margin	0.66	0.42	0.36	0.86	0.28	0.36	0.87	0.27
		matrix	0.74	0.35	0.24	0.69	0.21	0.23	0.64	0.20
	CSGM #913-606	**center**	0.65	0.32	0.22	0.69	0.23	0.23	0.70	0.21
		stalk	0.31	0.40	0.29	0.73	0.28	0.28	0.69	0.28
	CSGM #913-607	**center**	x	**0.51**	0.38	0.75	0.26	0.38	0.75	0.25
		margin	0.03	0.47	0.40	0.85	0.08	0.42	0.90	0.06
		matrix	0.29	**0.60**	0.51	0.85	0.22	0.52	0.86	0.21
	CSGM #913-608	**center**	0.75	0.48	0.41	0.85	0.29	0.42	0.87	0.28
		margin	0.68	0.44	0.37	0.84	0.27	0.36	0.81	0.27
	CSGM #913-609	**center**	0.86	0.37	0.35	0.95	0.34	0.35	0.96	0.33
		matrix	0.65	0.33	0.24	0.73	0.38	0.25	0.75	0.36
	CSGM #913-610	**center**	x	0.49	0.36	0.73	0.25	0.36	0.73	0.26
		margin	0.56	**0.59**	0.50	0.85	0.22	0.52	0.88	0.21
	CSGM #913-611	**center**	x	0.44	0.43	0.98	0.19	0.43	0.97	0.18
		margin	x	**0.50**	x	x	x	0.44	0.87	0.20
Third member, section 0607	CSGM #913-612	**center**	0.23	0.43	0.35	0.81	0.43	0.36	0.84	0.42
		matrix	0.29	0.49	0.30	0.61	0.13	0.32	0.66	0.14
	CSGM #913-613	**center**	0.09	0.22	0.16	0.73	0.25	0.15	0.65	0.24
		matrix	0.22	0.28	0.16	0.57	0.13	0.15	0.55	0.10

2.10 Figures and figure captions

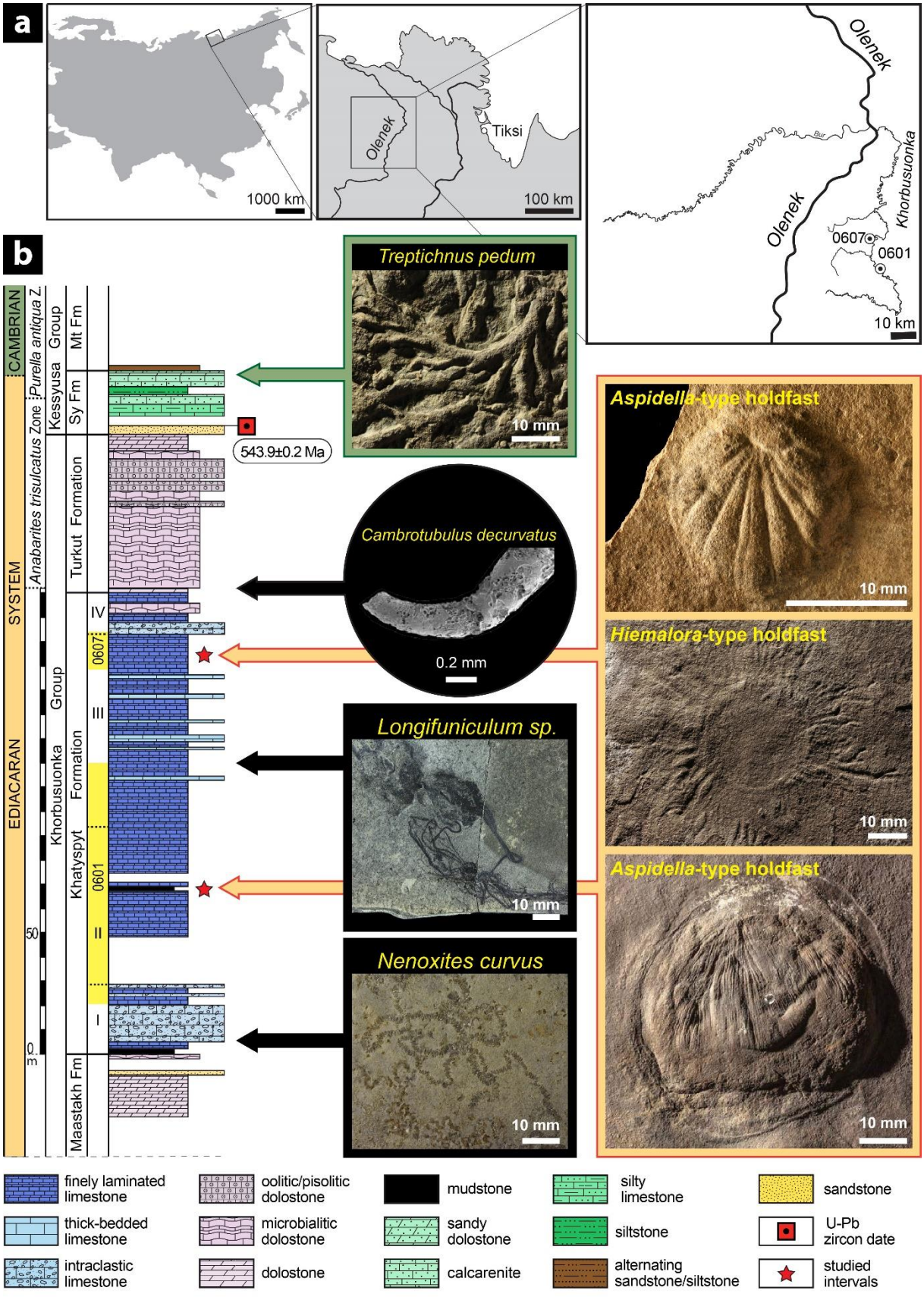

Figure 2.1. Geographic location of the Khorbusuonka River and composite stratigraphic column of the Khorbusuonka and lowermost Kessyusa groups. (a) Location of the sections 0601 and 0607 from which all studied material was collected. (b) Litho-, bio-, and chronostratigraphy of the Khorbusuonka and lower part of Kessyusa groups (Rogov et al. 2015; Cui et al. 2016a). Stars mark approximate stratigraphic horizons from which Aspidella fossils in this study were collected. Lithostratigraphic column and stratigraphic meterage are based on composite sections that are correlated using marker beds (Nagovitsin et al. 2015). The lowest occurrence of Nenoxites curvus is in the first member of the Khatyspyt Formation. There are two levels with typical Ediacara-type fossils, including Aspidella, in the second and uppermost third members. Miaohe-type preservation of carbonaceous compressions (e.g., Longifuniculum) occurs in the lower part of the third member (Nagovitsin et al. 2015; Rogov et al. 2015). The conotubular shelly fossil Cambrotubulus decurvatus first occurs in the Turkut Formation (Nagovitsin et al. 2015), and the trace fossil Treptichnus pedum first occurs in the Syhargalakh Formation (Sy Fm) of the Kessyusa Group. The Turkut Formation is penetrated by diatremes that yield a U–Pb age of 543.9±0.2 Ma (Bowring et al. 1993; Rogov et al. 2015). Mt Fm = Mattaia Formation.

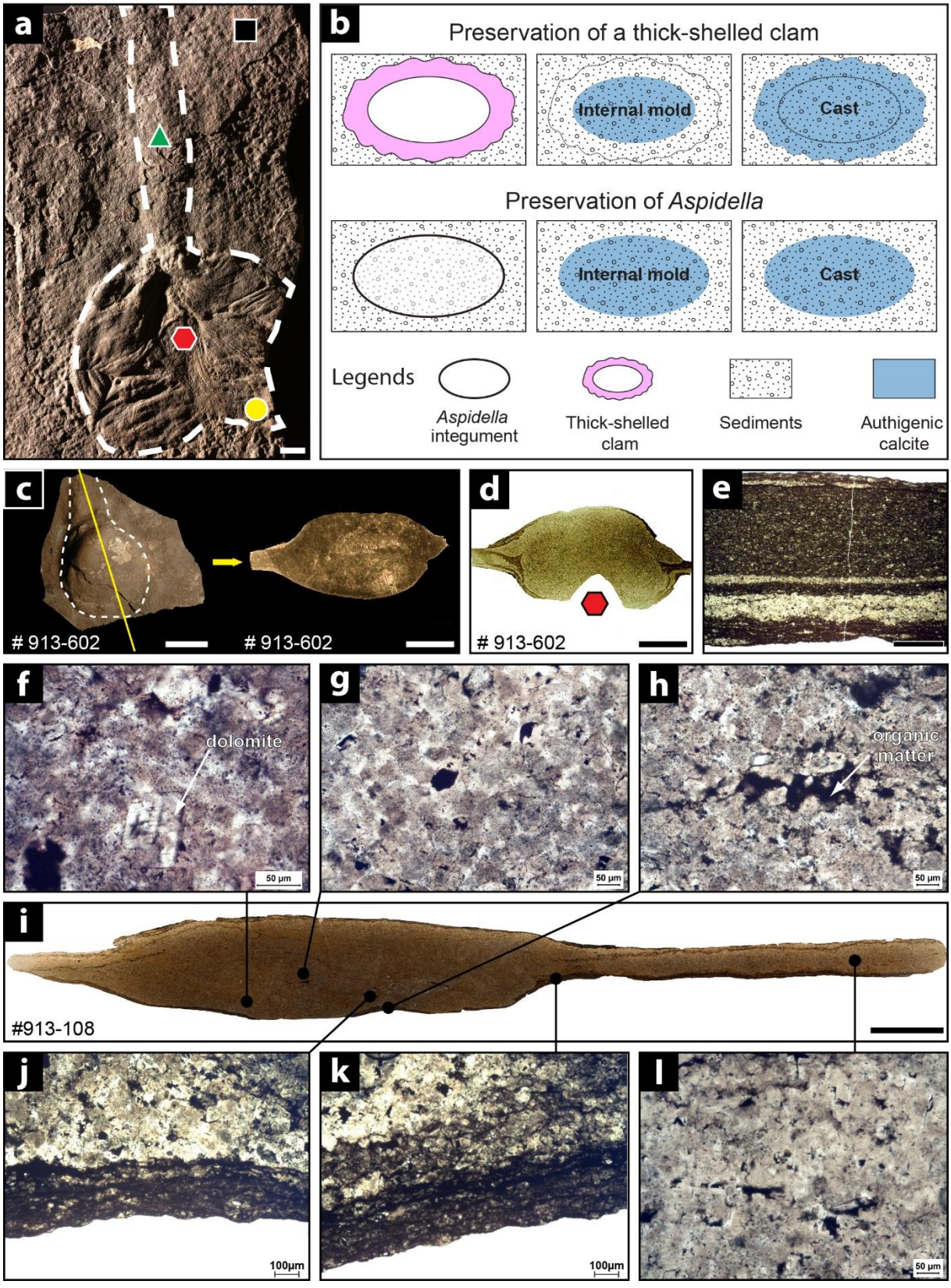

Figure 2.2. Taphonomy of *Aspidella* fossils from the Khatyspyt Formation. Color coding in this and all subsequent figures identifies the different parts of *Aspidella* fossils and matrix

sediments sampled for geochemical analyses: red (hexagon), yellow (circle), green (triangle), and black (square) symbols represent holdfast center, holdfast margin, stalk, and carbonate matrix, respectively. (a) CSGM #913-14, an example of an *Aspidella* holdfast with an attached stalk. (b) Diagram showing taphonomic modes and processes of Khatyspyt *Aspidella* holdfasts compared with those of skeletal fossils such as thick-shelled clams. Note that it is not always possible to differentiate casts and internal molds of *Aspidella* holdfasts which likely had a very thin organic integument or membrane, because it is difficult to determine whether the internal or external surface of the integument is replicated. (c) CSGM #913-602, A representative *Aspidella* specimen analyzed in this study, shown in bedding surface view (left) and vertical cross sectional view cut along solid yellow line (right; reflected light image). Note the conical stalk and the three-dimensional biconvex preservation of the holdfast (white dashed line). (d) Transmitted light photomicrograph of a vertical thin section cut through the holdfast shown in (c) after a powder sample was take from holdfast center (red hexagon). Note that the holdfast is more transparent and contains proportionally more authigenic calcite compared with small slivers of darker matrix sediments attached to the holdfast. (e) Transmitted light photomicrograph of a vertical thin section, showing typical matrix sediments in the fossiliferous Khatyspyt Formation. (f–l) Plane-polarized transmitted light microphotographs of a holdfast (i) and magnifications showing relict peloids, calcite cements, diffuse kerogen, patches of organic carbon, and rare dolomite crystals in *Aspidella* holdfast (f–h, l), and microbial laminae warping around *Aspidella* holdfast (j–k). Scale bars in a = 10 mm; c, d, i = 5 mm; e = 1 mm; f–h, l = 50 μm; j, k = 100 μm. Figure 2.2d, 2.2e-l are placed in stratigraphic position (i.e., stratigraphic up direction on top).

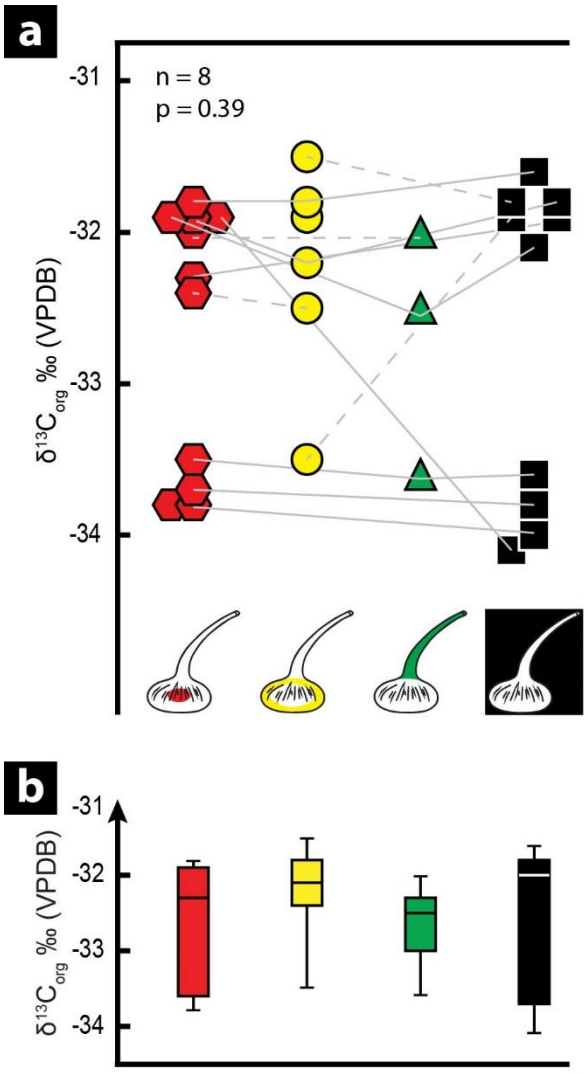

Figure 2.3. $\delta^{13}C_{org}$ of *Aspidella* fossils and matrix sediments. (a) $\delta^{13}C_{org}$ values of different parts of the same *Aspidella* fossil and corresponding matrix are linked by solid or dashed lines, with schematic diagram showing the sampling position of holdfast center, holdfast margin, stalk, and matrix sediment. Solid lines depict the 8 pairs of $\delta^{13}C_{org}$ data used in statistical analyses, which showed no significant difference between the holdfast center and matrix (paired two-tailed Student's t-test, p = 0.39, n = 8 pairs of measurements of 8 unique *Aspidella* specimens; Table 2.S1). Overall, $\delta^{13}C_{org}$ values from our analysis are similar to bulk-sample $\delta^{13}C_{org}$ values reported by Cui et al. (2016a) from the same stratigraphic interval at section 0601. (b) Boxplot of $\delta^{13}C_{org}$ of different parts of *Aspidella* fossils and matrix,

showing the median, the first and third quartiles, and the range of each category. Color coding follows that of Figure 2.2.

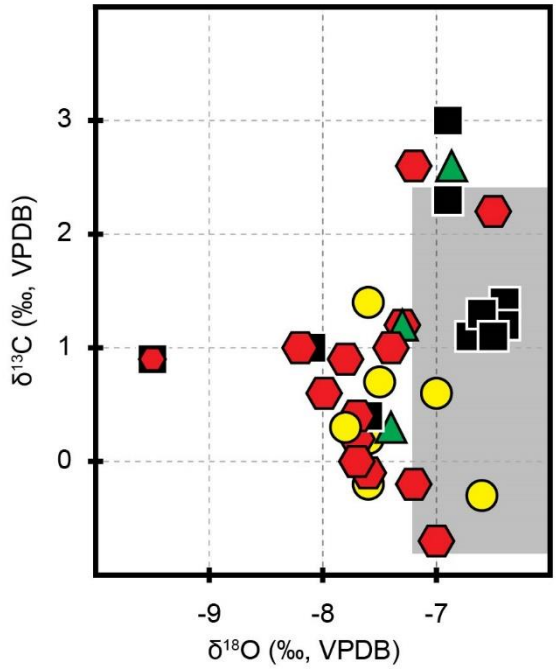

Figure 2.4. Cross-plot of $\delta^{13}C_{carb}$ and $\delta^{18}O_{carb}$ of different parts of *Aspidella* fossils and matrix sediments. Gray box represents ranges of $\delta^{13}C_{carb}$ and $\delta^{18}O_{carb}$ values of sediments in the same stratigraphic interval at section 0601 (Cui et al. 2016a). $\delta^{13}C_{carb}$ data are generally comparable to other upper Ediacaran carbonate successions (Macdonald et al. 2013; Cui et al. 2016a; Cui et al. 2016b; Xiao et al. 2016). Color coding follows that of Figure 2.2.

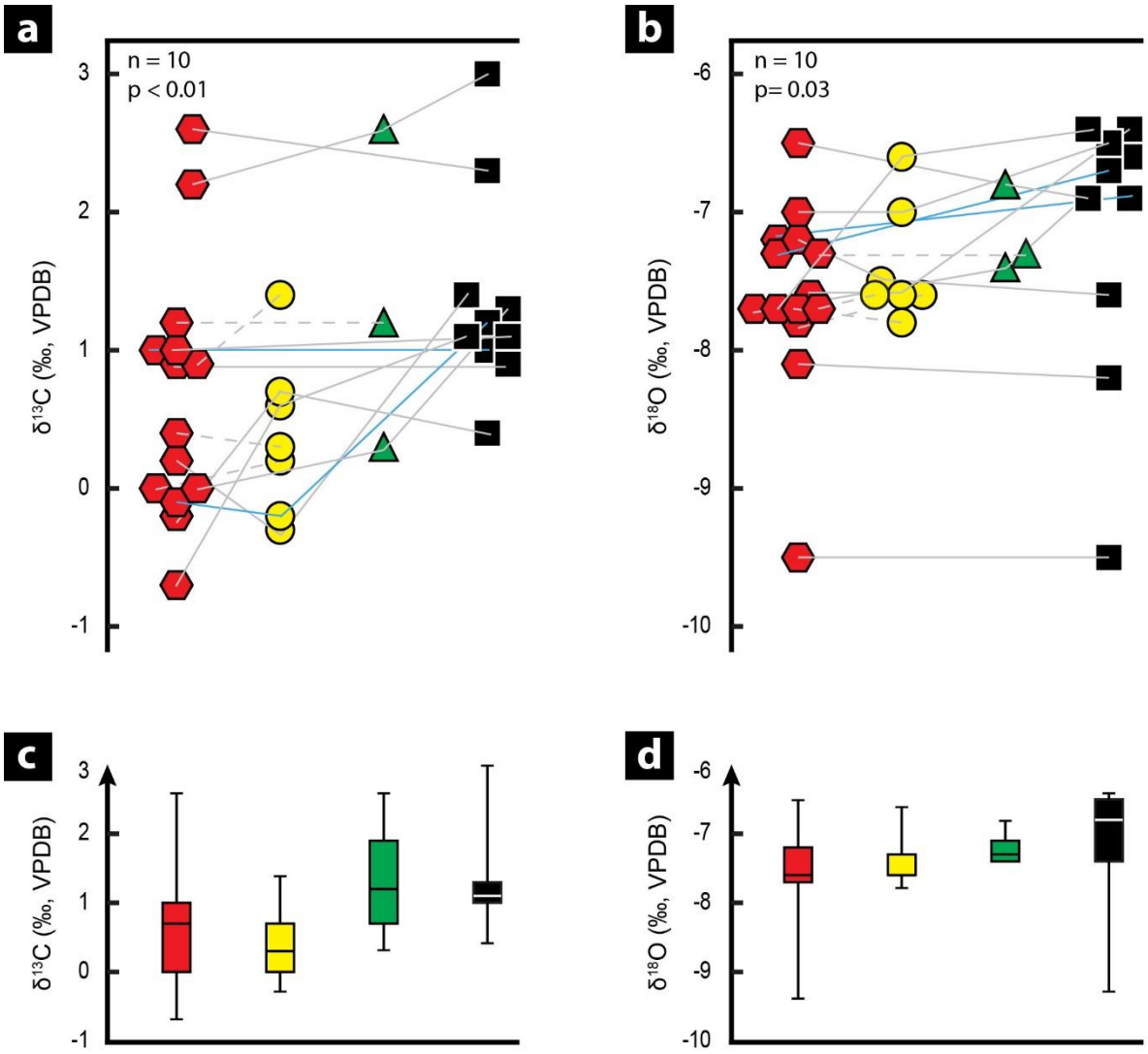

Figure 2.5. $\delta^{13}C_{carb}$ and $\delta^{18}O_{carb}$ of *Aspidella* fossils and matrix sediments. (a–b) $\delta^{13}C_{carb}$ and $\delta^{18}O_{carb}$ values of different parts of the same *Aspidella* fossil and corresponding matrix are linked by solid or dashed lines. Two solid lines are colored in blue to improve clarity. Solid lines depict the 10 pairs of $\delta^{13}C_{carb}$ or $\delta^{18}O_{carb}$ data used in statistical analyses, which showed that holdfast centers yielded lower $\delta^{13}C_{carb}$ and $\delta^{18}O_{carb}$ values than carbonate matrix (paired one-tailed Student's t-test, $p < 0.01$ for $\delta^{13}C_{carb}$ and $p = 0.03$ for $\delta^{18}O_{carb}$, n = 10 pairs of measurements of 10 unique *Aspidella* specimens; Table 2.S2). (c–d) Boxplots of $\delta^{13}C_{carb}$ and $\delta^{18}O_{carb}$ values of different parts of *Aspidella* fossils and carbonate matrix, showing the

median, the first and third quartiles, and the range of each category. Color coding follows that of Figure 2.2.

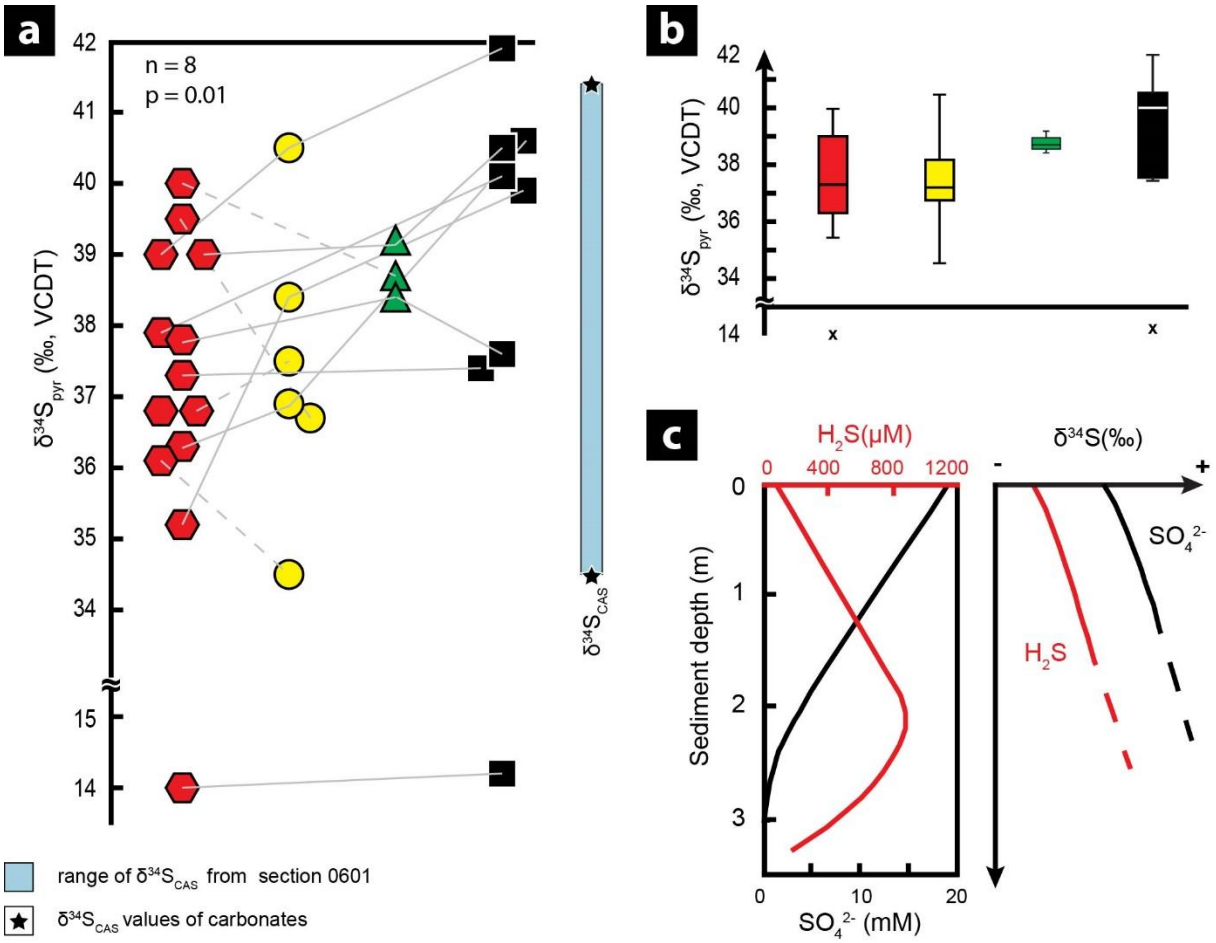

Figure 2.6. $\delta^{34}S_{pyr}$ of *Aspidella* fossils and matrix sediments. (a) $\delta^{34}S_{pyr}$ values of different parts of the same *Aspidella* fossil and corresponding matrix are linked by solid or dashed lines. Solid lines depict the 8 pairs of $\delta^{34}S_{pyr}$ data used in statistical analyses, which showed that holdfast centers yielded significantly lower $\delta^{34}S_{pyr}$ values than carbonate matrix (paired one-tailed Student's t-test, p = 0.01, n = 8 pairs of measurements of 8 unique *Aspidella* specimens; Table 2.S3). For comparison, bulk-sample $\delta^{34}S_{CAS}$ values (stars) from the same stratigraphic interval at section 0601 (Cui et al. 2016a) are also shown to the right (in blue shade). Except for a single specimen with $\delta^{34}S_{pyr}$ values of about 14.0%, all other specimens analyzed in this study were collected from section 0601. (b) Boxplots of $\delta^{34}S_{pyr}$ values of different parts of *Aspidella* fossils and carbonate matrix, showing the median, the first and third quartiles, and the range of each category. Outliers are marked by "x" (less than the first quartile minus 1.5× interquartile range). Color coding in (a–b) follows that of Figure 2.2. (c)

Schematic diagram showing representative profiles [H_2S], [SO_4^{2-}], $\delta^{34}S_{H2S}$, and $\delta^{34}S_{SO4}$ of modern marine sediments (Jorgensen et al. 2004). Vertical axis represents sediment depth below the water-sediment interface.

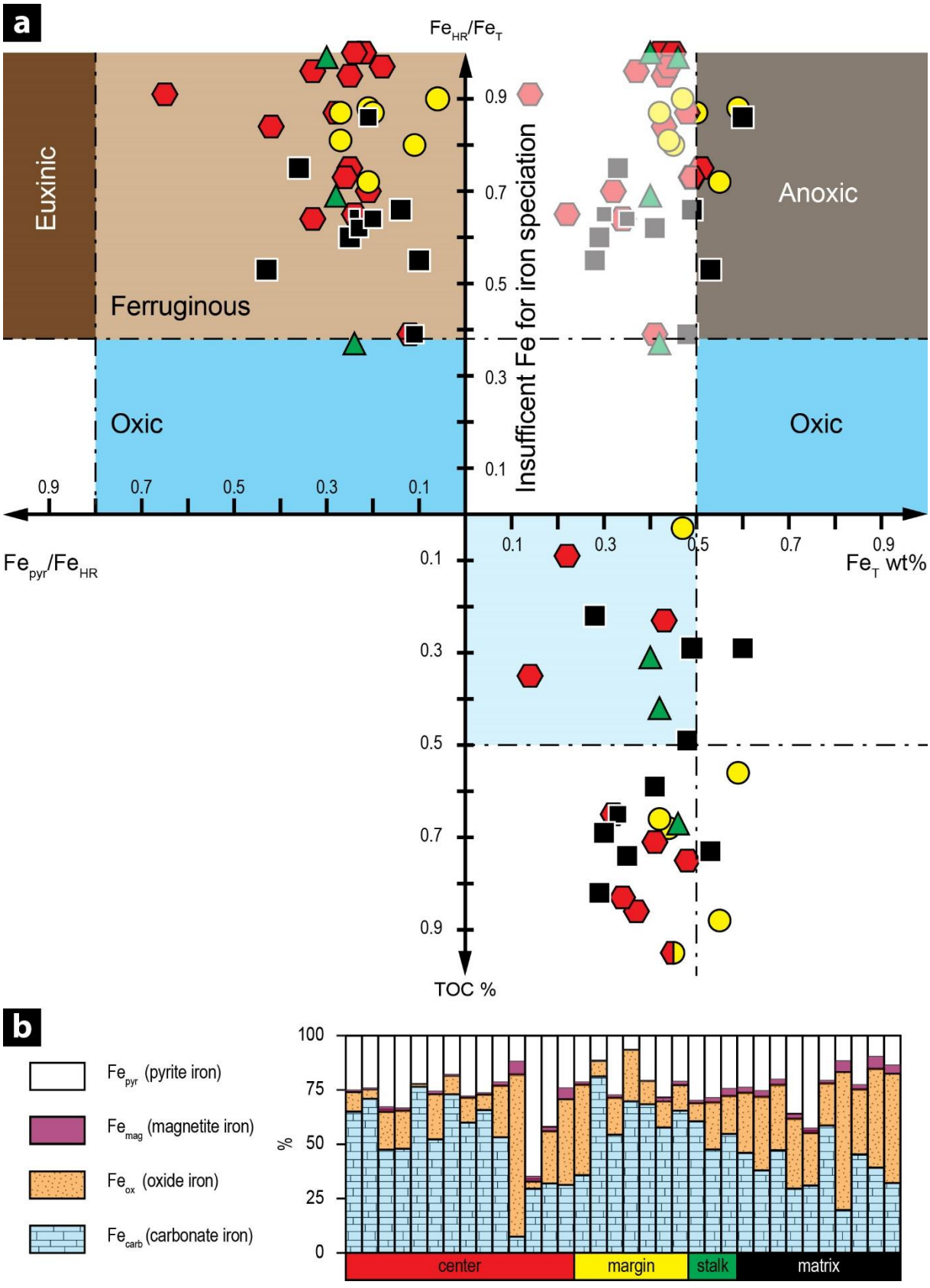

Figure 2.7. Iron speciation data of different parts of *Aspidella* fossils and carbonate matrix. Only the first batch of measurements (with carbonate Fe extracted at 60°C) are plotted in this

figure. Duplicate measurements (with carbonate Fe extracted at 50°C) are similar but not plotted in this figure. See Table 2.S4 for data. (a) Cross-plots of Fe_{HR}/Fe_T vs. Fe_{pyr}/Fe_{HR}, Fe_{HR}/Fe_T vs. Fe_T, and Fe_T vs. TOC. In the Fe_{HR}/Fe_T vs. Fe_{pyr}/Fe_{HR} cross-plot, most data points fall in the ferruginous field. However, as shown in the Fe_{HR}/Fe_T vs. Fe_T cross-plot, most samples have low Fe_T (<0.5 wt%) so that Fe speciation data do not provide a reliable redox proxy for carbonate rocks (Clarkson et al. 2014). Samples with both low Fe_T and low TOC contents (shaded in light blue in the Fe_T vs. TOC cross-plot) could represent an oxic water column. (b) Distribution of highly reactive iron species ($Fe_{HR} = Fe_{pyr} + Fe_{carb} + Fe_{ox} + Fe_{mag}$) in each powder sample. Carbonate Fe represents 6–81% (median = 50%), pyrite Fe 7–62% (median = 25%), and Fe oxides 2–75% (median = 21%), but magnetite Fe is negligible (<7%, median = 3%). Color coding follows that of Figure 2.2.

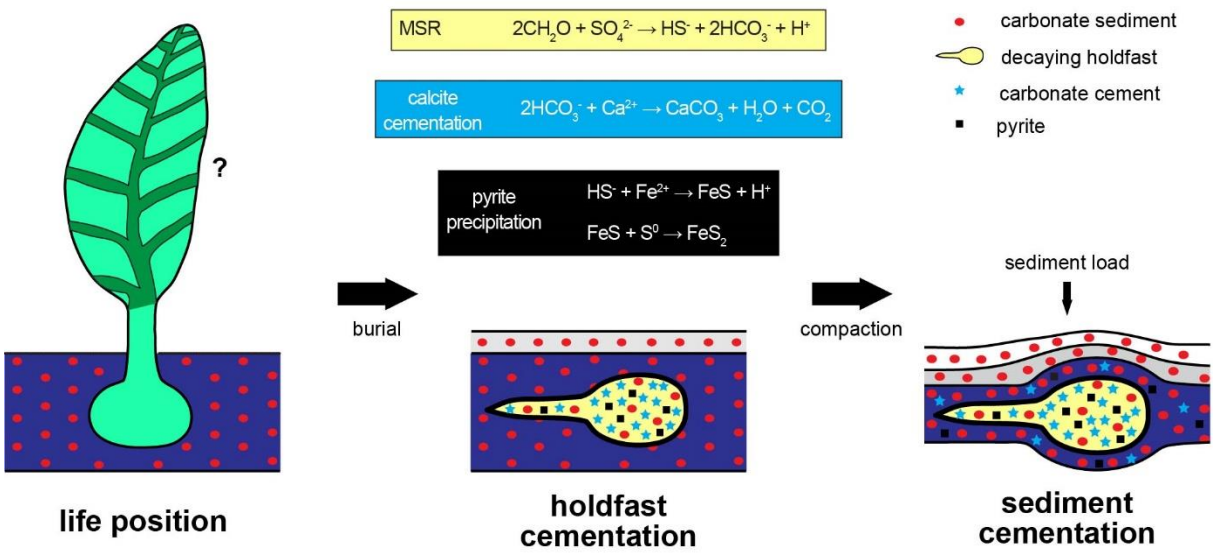

Figure 2.8. Schematic diagram showing the taphonomic processes that led to the three-dimensional preservation of Khatyspyt *Aspidella* holdfasts.

2.11 References

Billings, E. 1872. On some fossils from the Primordial rocks of Newfoundland. Canadian Naturalist and Geologist 6(4):465-479.

Bourdeau, B. P., and J. T. Westrich. 1984. The dependence of bacterial sulfate reduction on sulfate concentration in marine sediments. Geochimica et Cosmochimica Acta 48:2503-2516.

Bowring, S. A., J. P. Grotzinger, C. E. Isachsen, A. H. Knoll, S. M. Pelechaty, and P. Kolosov. 1993. Calibrating rates of Early Cambrian evolution. Science 261:1293-1298.

Boyer, D. L., J. D. Owens, T. W. Lyons, and M. L. Droser. 2011. Joining forces: combined biological and geochemical proxies reveal a complex but refined high-resolution palaeo-oxygen history in Devonian epeiric seas. Palaeogeography, Plaeoclimatology, Palaeoecology 306:134-146.

Bradley, A. S., W. D. Leavitt, M. Schmidt, A. H. Knoll, P. R. Girguis, and D. T. Johnston. 2016. Patterns of sulfur isotope fractionation during microbial sulfate reduction. Geobiology 14:91–101.

Brasier, M., J. Cowie, and M. Taylor. 1994. Decision on the Precambrian-Cambrian boundary stratotype. Episodes 17:3-8.

Brasier, M. D. 2012. Exploring a major role for sulphur symbioses in Ediacaran ecosystems. The 2012 Fermor Meeting of the Geological Society (The Neoproterozoic Era: Evolution, Glaciation, Oxygenation):71-72.

Brasier, M. D., D. McIlroy, A. G. Liu, J. B. Antcliffe, and L. R. Menon. 2013. The oldest evidence of bioturbation on Earth: Comment. Geology 41:e289.

Bykova, N. V. 2010. Ediacaran holdfasts and their systematics. Journal of Earth Science: Special Issue 21:1-3.

Canfield, D. E., J. Farquhar, and A. L. Zerkle. 2010. High isotope fractionations during sulfate reduction in a low-sulfate euxinic ocean analog. Geology 38:415–418.

Canfield, D. E., S. W. Poulton, A. H. Knoll, G. M. Narbonne, G. Ross, T. Goldberg, and H. Strauss. 2008. Ferruginous conditions dominated later Neoproterozoic deep-water chemistry. Science 321:949-952.

Canfield, D. E., S. W. Poulton, and G. M. Narbonne. 2007. Late Neoproterozoic deep-ocean oxygenation and the rise of animal life. Science 315:92-95.

Canfield, D. E., R. Raiswell, J. T. Westrich, C. M. Reaves, and R. A. Berner. 1986. The use of chromium reduction in the analysis of reduced inorganic sulfur in sediments and shale. Chemical Geology 54:149-155.

Chen, Z., C. Zhou, S. Xiao, W. Wang, C. Guan, H. Hua, and X. Yuan. 2014. New Ediacara fossils preserved in marine limestone and their ecological implications. Scientific Reports 4(4180):1-10.

Clarkson, M. O., S. W. Poulton, R. Guilbaud, and R. A. Wood. 2014. Assessing the utility of Fe/Al and Fe-speciation to record water column redox conditions in carbonate-rich sediments. Chemical Geology 382:111-122.

Cui, H., D. V. Grazhdankin, S. Xiao, S. Peek, V. I. Rogov, N. V. Bykova, N. Sievers, X.-M. Liu, and A. J. Kaufman. 2016a. Redox-dependent distribution of early macro-organisms: Evidence from the terminal Ediacaran Khatyspyt Formation in Arctic Siberia. Palaeogeography Palaeoclimatology Palaeoecology 461:122–139.

Cui, H., A. J. Kaufman, S. Xiao, S. Peek, H. Cao, X. Min, Y. Cai, Z. Siegel, X.-M. Liu, Y. Peng, J. D. Schiffbauer, and A. J. Martin. 2016b. Environmental context for the terminal Ediacaran biomineralization of animals. Geobiology 14:344-363.

Darroch, S. A. F., M. Laflamme, J. D. Schiffbauer, and D. E. G. Briggs. 2012. Experimental formation of a microbial death mask. Palaios 27:293–303.

Darroch, S. A. F., E. A. Sperling, T. H. Boag, R. A. Racicot, S. J. Mason, A. S. Morgan, S. Tweedt, P. Myrow, D. T. Johnston, D. H. Erwin, and M. Laflamme. 2015. Biotic replacement and mass extinction of the Ediacara biota. Proceedings of the Royal Society of London B: Biological Sciences 282:20151003.

Duda, J.-P., V. Thiel, J. Reitner, and D. Grazhdankin. 2016. Openening up a window into ecosystems with Ediacara-type organisms: preservation of molecular fossils in the Khatyspyt Lagerstätte (Arctic Siberia). Paläontologische Zeitschrift 10.1007/s12542-12016-10317-12545.

Dufour, S. C., and D. McIlroy. 2016. Ediacaran pre-placozoan diploblasts in the Avalonian biota: the role of chemosynthesis in the evolution of early animal life. Geological Society London Special Publications 448:doi: 10.1144/SP448.5.

Dzik, J. 2003. Anatomical information content in the Ediacaran fossils and their possible zoological affinities. Integrative and Comparative Biology 43:114-126.

Erwin, D. H., M. Laflamme, S. M. Tweedt, E. A. Sperling, D. Pisani, and K. J. Peterson. 2011. The Cambrian conundrum: Early divergence and later ecological success in the early history of animals. Science 334:1091-1097.

Fedonkin, M. A., J. G. Gehling, K. Grey, G. M. Narbonne, and P. Vickers-Rich. 2007. The Rise of Animals: Evolution and Diversification of the Kingdom Animalia. Johns Hopkins University Press, Baltimore.

Fike, D. A., A. S. Bradley, and C. V. Rose. 2015. Rethinking the ancient sulfur cycle. Annual Review of Earth and Planetary Sciences 43:593-622.

Gamez-Vintaned, J. A., and A. Y. Zhuravlev. 2013. The oldest evidence of bioturbation on Earth: Comment. Geology 41:e299.

Gehling, J. G. 1988. A cnidarian of actinian-grade from the Ediacaran Pound Subgroup, South Australia. Alcheringia 12:299-314.

Gehling, J. G. 1999. Microbial mats in terminal Proterozoic siliciclastics: Ediacaran death masks. Palaios 14:40-57.

Gehling, J. G., G. M. Narbonne, and M. M. Anderson. 2000. The first named Ediacaran body fossil, *Aspidella terranovica*. Palaeontology 43(3):427-456.

Glaessner, M. F. 1984. The Dawn of Animal Life: A Biohistorical Study. Cambridge Univ. Press, Cambridge, UK.

Gomes, M. L., and M. T. Hurtgen. 2015. Sulfur isotope fractionation in modern euxinic systems: Implications for paleoenvironmental reconstructions of paired sulfate-sulfide isotope records. Geochimica et Cosmochimica Acta 157:39-55.

Grazhdankin, D. 2000. The Ediacaran genus *Inaria*: a taphonomic/morphodynamic analysis. Neues Jahrbuch fuer Geologie und Palaeontologie. Abhandlungen 216(1):1-34.

Grazhdankin, D. 2004. Patterns of distribution in the Ediacaran biotas: facies versus biogeography and evolution. Paleobiology 30(2):203–221.

Grazhdankin, D., and G. Gerdes. 2007. Ediacaran microbial colonies. Lethaia 40:201–210.

Grazhdankin, D. V., U. Balthasar, K. E. Nagovitsin, and B. B. Kochnev. 2008. Carbonate-hosted Avalon-type fossils in Arctic Siberia. Geology 36:803–806.

Guan, C., C. Zhou, W. Wang, B. Wan, X. Yuan, and Z. Chen. 2014. Fluctuation of shelf basin redox conditions in the early Ediacaran: Evidence from Lantian Formation black shales in South China. Precambrian Research 245:1-12.

Hofmann, H. J., S. J. O'Brien, and A. F. King. 2008. Ediacaran biota on Bonavista Peninsula, Newfoundland, Canada. Journal of Paleontology 82:1-36.

Jensen, S., J. G. Gehling, M. L. Droser, and S. W. F. Grant. 2002. A scratch circle origin for the medusoid fossil *Kullingia*. Lethaia 35:291-299.

Johnston, D. T., S. W. Poulton, T. Goldberg, V. N. Sergeev, V. Podkovyrov, N. G. Vorob'eva, A. Bekker, and A. H. Knoll. 2012. Late Edicaran redox stability and metazoan evolution. Earth and Planetary Science Letters 335-336:25-35.

Johnston, D. T., S. W. Poulton, N. J. Tosca, T. O'Brien, G. P. Halverson, D. P. Schrag, and F. A. Macdonald. 2013. Searching for an oxygenation event in the fossiliferous Ediacaran of northwestern Canada. Chemical Geology 362:273-286.

Jorgensen, B. B., M. E. Bottcher, H. Luschen, L. N. Neretin, and I. I. Volkov. 2004. Anaerobic methane oxidation and a deep H_2S sink generate isotopically heavy sulfides in Black Sea sediments. Geochimica et Cosmochimica Acta 68(9):2095-2118.

Kenig, F., J. D. Hudson, J. S. S. Damste, and B. N. Popp. 2004. Intermittent euxinia: reconciliation of a Jurassic black shale with its biofacies. Geology 32(5):421-424.

Khomentovsky, V. V., and G. A. Karlova. 1993. Biostratigraphy of the Vendian-Cambrian beds and the Lower Cambrian boundary in Siberia. Geological Magazine 130(1):29-45.

Knoll, A. H., J. P. Grotzinger, A. J. Kaufman, and P. Kolosov. 1995. Integrated approaches to terminal Proterozoic stratigraphy: An example from the Olenek Uplift, northeastern Siberia. Precambrian Research 73:251-270.

Laflamme, M., J. D. Schiffbauer, G. M. Narbonne, and D. E. G. Briggs. 2011. Microbial biofilms and the preservation of the Ediacara biota. Lethaia 44:203–213.

Leavitt, W. D., I. Halevy, A. S. Bradley, and D. T. Johnston. 2013. Influence of sulfate reduction rates on the Phanerozoic sulfur isotope record. Proceedings of the National Academy of Sciences of the United State of America 110(28):11244-11249.

Lenton, T. M., R. A. Boyle, S. W. Poulton, G. A. Shields-Zhou, and N. J. Butterfield. 2014. Co-evolution of eukaryotes and ocean oxygenation in the Neoproterozoic era. Nature Geosciences 7(257-265).

Li, C., G. D. Love, T. W. Lyons, D. A. Fike, A. L. Sessions, and X. Chu. 2010. A stratified redox model for the Ediacaran ocean. Science 328:80-83.

Li, C., N. J. Planavsky, W. Shi, Z. Zhang, C. Zhou, M. Cheng, L. G. Tarhan, G. Luo, and S. Xie. 2015. Ediacaran marine redox heterogeneity and early animal ecosystems. Scientific Reports 5:17097.

Liu, A. G. 2016. Framboidal pyrite shroud confirms the 'death mask' model for moldic preservation of Ediacaran soft-bodied organisms. Palaios 31:259-274.

Londry, K. L., and D. J. Des Marais. 2003. Stable carbon isotope fractionation by sulfate-reducing bacteria. Applied and Environmental Microbiology 69:2942-2949.

Macdonald, F. A., J. V. Strauss, E. A. Sperling, G. P. Halverson, G. M. Narbonne, D. T. Johnston, M. Kunzmann, D. P. Schrag, and J. A. Higgins. 2013. The stratigraphic relationship between the Shuram carbon isotope excursion, the oxygenation of Neoproterozoic oceans, and the first appearance of the Ediacara biota and bilaterian trace fossils in northwestern Canada. Chemical Geology 362:250-272.

MacGabhann, B. A. 2007. Discoidal fossils of the Ediacaran Biota: a review of current understanding. Pp. 297-313. *In* P. Vickers-Rich, and P. Komarower, eds. The Rise and Fall of the Ediacaran Biota (Geological Society of London Special Publications 286).

McMenamin, M. A. S. 1986. The Garden of Ediacara. Palaios 1:178-182.

Menon, L. R., D. McIlroy, and M. D. Brasier. 2013. Evidence for Cnidaria-like behavior in ca. 560 Ma Ediacaran *Aspidella*. Geology 41(8):895-898.

Menon, L. R., D. McIlroy, A. G. Liu, and M. D. Brasier. 2016. The dynamic influence of microbial mats on sediments: fluid escape and pseudofossil formation in the Ediacaran Longmyndian Supergroup, UK. Journal of the Geological Society 173(1):177-185.

Meyer, M., D. Elliott, J. D. Schiffbauer, M. Hall, K. H. Hoffman, G. Schneider, P. Vickers-Rich, and S. Xiao. 2014a. Taphonomy of the Ediacaran fossil *Pteridinium simplex*

preserved three-dimensionally in mass flow deposits, Nama Group, Namibia. Journal of Paleontology 88:240-252.

Meyer, M., S. Xiao, B. C. Gill, J. D. Schiffbauer, Z. Chen, C. Zhou, and X. Yuan. 2014b. Interactions between Ediacaran animals and microbial mats: insights from *Lamonte trevallis*, a new trace fossil from the Dengying Formation of South China. Palaeogeography Palaeoclimatology Palaeoecology 396:62-74.

Nagovitsin, K. E., V. I. Rogov, V. V. Marusin, G. A. Karlova, A. V. Kolesnikov, N. V. Bykova, and D. V. Grazhdankin. 2015. Revised Neoproterozoic and Terreneuvian stratigraphy of the Lena-Anabar Basin and north-western slope of the Olenek Uplift, Siberian Platform. Precambrian Research 270:226-245.

Narbonne, G. M. 2005. The Ediacara Biota: Neoproterozoic origin of animals and their ecosystems. Annual Review of Earth and Planetary Sciences 33:421-442.

Narbonne, G. M., M. Laflamme, C. Greentree, and P. Trusler. 2009. Reconstructing a lost world: Ediacaran rangeomorphs from Spaniard's Bay, Newfoundland. Journal of Paleontology 83:503-523.

Pelechaty, S. M., A. J. Kaufman, and J. P. Grotzinger. 1996. Evaluation of $\delta^{13}C$ chemostratigraphy for intrabasinal correlation; Vendian strata of Northeast Siberia. Geological Society of America Bulletin 108(8):992-1003.

Peterson, K. J., B. Waggoner, and J. W. Hagadorn. 2003. A fungal analog for Newfoundland Ediacaran fossils? Integrative and Comparative Biology 43:127-136.

Poulton, S. W., and D. E. Canfield. 2005. Development of a sequential extraction procedure for iron: implications for iron partitioning on contitentally derived particulates. Chemical Geology 214:209-221.

Raiswell, R., and D. E. Canfield. 1998. Sources of iron for pyrite formation in marine sediments. American Journal of Science 298:219-245.

Retallack, G. J. 1994. Were the Ediacaran fossils lichens? Paleobiology 20:523-544.

Robinson, J., K. M. Scott, S. T. Swanson, M. H. O'Leary, K. Horken, F. R. Tabita, and C. M. Cavanaugh. 2003. Kinetic isotope effect and characterization of form II Rubisco from the chemoautotrophic endosymbionts of the hydrothermal vent tubeworm *Riftia pachyptila*. Limnology and Oceanography 48:48-54.

Rogov, V., V. Marusin, N. Bykova, Y. Goy, K. Nagovitsin, B. Kochnev, G. Karlova, and D. Grazhdankin. 2012. The oldest evidence of bioturbation on Earth. Geology 40:395-398.

Rogov, V., V. Marusin, N. Bykova, Y. Goy, K. Nagovitsin, B. Kochnev, G. Karlova, and D. Grazhdankin. 2013a. The oldest evidence of bioturbation on Earth: REPLY. Geology 41:e290.

Rogov, V., V. Marusin, N. Bykova, Y. Goy, K. Nagovitsin, B. Kochnev, G. Karlova, and D. Grazhdankin. 2013b. The oldest evidence of bioturbation on Earth: REPLY. Geology 41(9):e300.

Rogov, V. I., G. A. Karlova, V. V. Marusin, B. B. Kochnev, K. E. Nagovitsin, and D. V. Grazhdankin. 2015. Duration of the first biozone in the Siberian hypostratotype of the Vendian. Russian Geology and Geophysics 56:573-583.

Sahoo, S. K., N. J. Planavsky, B. Kendall, J. D. Owens, X. Wang, X. Shi, A. D. Anbar, and T. W. Lyons. 2016. Oceanic oxygenation events in the anoxic Ediacaran ocean. Geobiology 14(5):457-468.

Schiffbauer, J. D., S. Xiao, Y. Cai, A. F. Wallace, H. Hua, J. Hunter, H. Xu, Y. Peng, and A. J. Kaufman. 2014. A unifying model for Neoproterozoic–Palaeozoic exceptional fossil preservation through pyritization and carbonaceous compression. Nature Communications 5:5754.

Seilacher, A. 1984. Late Precambrian and Early Cambrian Metazoa: preservational or real extinctions? Pp. 159-168. *In* H. D. Holland, and A. F. Trendall, eds. Patterns of Change in Earth Evolution. Springer-Verlag, Berlin.

Seilacher, A. 1992. Vendobionta and Psammocorallia: lost constructions of Precambrian evolution. Journal of the Geological Society, London 149:607-613.

Seilacher, A., D. Grazhdankin, and A. Legouta. 2003. Ediacaran biota: The dawn of animal life in the shadow of giant protists. Paleontological Research 7(1):43-54.

Serezhnikova, E. A. 2010. Colonization of substrates: Vendian sedentary benthos. Paleontological Journal 44(12):1560-1569.

Sokolov, B. S., and M. A. Fedonkin. 1984. The Vendian as the Terminal System of Precambrian. Episodes 7(1):12-19.

Sperling, E. A., C. Carbone, J. V. Strauss, D. T. Johnston, G. M. Narbonne, and F. A. Macdonald. 2016. Oxygen, facies, and secular controls on the appearance of Cryogenian and Ediacaran body and trace fossils in the Mackenzie Mountains of northwestern Canada. GSA Bulletin 128(3/4):558-575.

Sperling, E. A., C. J. Wolock, A. S. Morgan, B. C. Gill, M. Kunzmann, G. P. Halverson, F. A. Macdonald, A. H. Knoll, and D. T. Johnston. 2015. Statistical analysis of iron geochemical data suggests limited late Proterozoic oxygenation. Nature 523(7561):451-454.

Stookey, L. L. 1970. Ferrozine - A new spectrophotometric reagent for iron. Analytical Chemistry 42(7):779-781.

Tarhan, L. G., M. L. Droser, and J. G. Gehling. 2010. Taphonomic controls on Ediacaran diversity: uncovering the holdfast origin of morphologically variable enigmatic structures. Palaios 25:823-830.

Tarhan, L. G., M. L. Droser, J. G. Gehling, and M. P. Dzaugis. 2015. Taphonomy and morphology of the Ediacara form genus *Aspidella*. Precambrian Research 257:124-136.

Tarhan, L. G., A. v. S. Hood, M. L. Droser, J. G. Gehling, and D. E. G. Briggs. 2016. Exceptional preservation of soft-bodied Ediacara Biota promoted by silica-rich oceans. Geology 44:951-954.

Vickers-Rich, P., A. Y. Ivantsov, P. W. Trusler, G. M. Narbonne, M. Hall, S. A. Wilson, C. Greentree, M. A. Fedonkin, D. A. Elliott, K. H. Hoffmann, and G. I. C. Schneider. 2013. Reconstructing *Rangea*: new discoveries from the Ediacaran of southern Namibia. Journal of Paleontology 87:1-15.

Viollier, E., P. W. Inglett, K. Hunter, and A. N. Roychoudhury. 2000. The ferrozine method revisited: Fe(II)/Fe(III) determination in natural waters. Applied Geochemistry 15(6):785-790.

Vodanjuk, S. A. 1989. Ostatki besskeletnykh Metazoa iz khatyspytskoi svity Olenekskogo podniatia. Pp. 61-74. *In* V. V. Khomentovsky, and Y. K. Sovetov, eds. Pozdnii dokembrii i rannii paleozoi Sibiri, Aktualnye voprosy stratigrafii. Institut geologii i geofiziki Sibirskogo otdelenia Akademii Nauk SSSR, Novosibirsk.

Wade, M. 1968. Preservation of soft-bodied animals in Precambrian sandstones at Ediacara, South Australia. Lethaia 1(3):238-267.

Wang, W., C. Guan, C. Zhou, Y. Peng, L. M. Pratt, X. Chen, L. Chen, Z. Chen, X. Yuan, and S. Xiao. 2017. Integrated carbon, sulfur, and nitrogen isotope chemostratigraphy of the Ediacaran Lantian Formation in South China: spatial gradient, ocean redox oscillation, and fossil distribution. Geobiology DOI: 10.1111/gbi.12226.

Wood, D. A., R. W. Dalrymple, and G. M. Narbonne. 2003. Paleoenviromental analysis of the late Neoproterozoic Mistaken Point and Trepassey formations, Southeastern Newfoundland. Canadian Journal of Earth Sciences 40:1375-1391.

Wood, R. A., S. W. Poulton, A. R. Prave, K.-H. Hoffmann, M. O. Clarkson, R. Guilbaud, J. W. Lyne, R. Tostevin, F. Bowyer, A. M. Penny, A. Curtis, and S. A. Kasemann. 2015. Dynamic redox conditions control late Ediacaran metazoan ecosystems in the Nama Group, Namibia. Precambrian Research 261:252-271.

Xiao, S., and A. H. Knoll. 1999. Fossil preservation in the Neoproterozoic Doushantuo phosphorite Lagerstätte, South China. Lethaia 32:219-240.

Xiao, S., and M. Laflamme. 2009. On the eve of animal radiation: Phylogeny, ecology and evolution of the Ediacara biota. Trends in Ecology & Evolution 24:31-40.

Xiao, S., G. M. Narbonne, C. Zhou, M. Laflamme, D. V. Grazhdankin, M. Moczydłowska-Vidal, and H. Cui. 2016. Toward an Ediacaran time scale: problems, protocols, and prospects. Episodes 39:540–555.

Xiao, S., J. D. Schiffbauer, K. A. McFadden, and J. Hunter. 2010. Petrographic and SIMS pyrite sulfur isotope analyses of Ediacaran chert nodules: Implications for microbial processes in pyrite rim formation, silicification, and exceptional fossil preservation. Earth and Planetary Science Letters 297:481–495.

Xiao, S., B. Shen, C. Zhou, G. Xie, and X. Yuan. 2005. A uniquely preserved Ediacaran fossil with direct evidence for a quilted bodyplan. Proceedings of the National Academy of Sciences, USA 102:10227-10232.

Xiao, S., X. Yuan, M. Steiner, and A. H. Knoll. 2002. Macroscopic carbonaceous compressions in a terminal Proterozoic shale: A systematic reassessment of the Miaohe biota, South China. Journal of Paleontology 76:347-376.

Yuan, X., Z. Chen, S. Xiao, C. Zhou, and H. Hua. 2011. An early Ediacaran assemblage of macroscopic and morphologically differentiated eukaryotes. Nature 470:390-393.

CHAPTER 3

Seaweeds through time: Morphological and ecological analysis of Proterozoic and early Paleozoic benthic macroalgae with a focus on the Ediacaran Period

NATALIA BYKOVA[1,2], STEVEN T. LODUCA[3], MICHAŁ KOWALEWSKI[4], DMITRY GRAZHDANKIN[2,5], AND SHUHAI XIAO[1]

[1]Department of Geosciences, Virginia Tech, Blacksburg, VA 24061, USA

[2]Trofimuk Institute of Petroleum Geology and Geophysics, Siberian Branch Russian Academy of Sciences, Novosibirsk 630090, Russia

[3]Department of Geography and Geology, Eastern Michigan University, Ypsilanti, MI 48197, USA

[4]Division of Invertebrate Paleontology, Florida Museum of Natural History, University of Florida, Gainesville, FL 32611, USA

[5]Novosibirsk State University, ulitsa Pirogova 2, Novosibirsk 630090, Russia

3.1 Abstract

Benthic marine macroalgae or seaweeds are key ecological players in oceans today and have been since the Proterozoic. However, their fossil record and evolutionary patterns are poorly documented. To address this knowledge gap, we updated a dataset of Proterozoic to early Paleozoic noncalcified macroalgae fossils preserved as macroscopic carbonaceous compressions. The data were analyzed using non-parametric multidimensional scaling (NMDS) and functional-form group (FFG) approaches, in order to characterize morphological and ecological evolutionary patterns of these macroalgae. The results show a progressive increase in thallus size, morphospace range, and aspects of ecological complexity such as canopy heights, surface area/volume ratios, and functional-form groups through time. These increases, however, is not monotonous. One of the most significant increases in macroalgal morphological and ecological diversity appears to have occurred in the Ediacaran Period. Analysis of Ediacaran macroalgal assemblages show that macroalgae have greater morphospace range, taxonomic diversity, thallus size, and ecological diversity during the early portion of that period (635–550 Ma), and experienced a significant drop in these metrics at the termination of the period (~ 550–540 Ma). The latter event occurs during the Kotlinian crisis experienced by Ediacara-type macro-organisms, highlighting the possibility that this extinction event during the Ediacaran-Cambrian transition affected both macroalgae and Ediacara-type macro-organisms.

3.2 Introduction

Marine macroalgae or seaweeds are macroscopic photosynthetic eukaryotes, including many green, red, and brown algae. Most are multicellular/coenocytic, benthic organisms that are visible to naked eye. Although not a monophyletic clade, they are an important ecological group in modern marine ecosystems. Not only are they important contributors to primary and

export productivity, particularly in coastal environments, they also create new niches for animals and other organisms (Christie et al. 2009), thus shaping the marine ecosystems through ecological engineering. It has been argued that they may have played an even greater ecological role in the geological past, particularly in the early Paleozoic when epeiric seas were widespread (more seafloor in the photic zone) and other types of marine benthic macrophytes (e.g., seagrasses) were absent (LoDuca et al. 2017). A similar argument can be made for Proterozoic seaweeds. However, due to the limited fossil material of seaweeds and the greater interest in animal evolution (e.g., Bambach 1993), the evolutionary patterns and ecological impacts of seaweeds have been largely overlooked, resulting in an incomplete understanding of ancient marine ecosystems.

According to molecular clock estimates, the Archaeplastida—the clade to which green and red algae belong—diverged from its living sister group in the Paleoproterozoic Era (Parfrey et al. 2011) (although brown algae diverged much later in the Mesozoic (Brown and Sorhannus 2010; Silberfeld et al. 2010)). However fossil record of macroalgae, particularly non-calcified macroalgae, is rather poor as they are commonly preserved as macroscopic carbonaceous compressions (Hofmann 1994; Xiao and Dong 2006). The taxonomic assignment of carbonaceous compressions as macroalgal fossils is not straightforward, because key features such as pigments and cellular structures are often not preserved. Nonetheless, the oldest purported macroalgae are from the Paleoproterozoic Era (2500–1600 Ma), as represented by *Grypania* from the 1874±9 Ma Negaunee Iron Formation (Han and Runnegar 1992; Schneider et al. 2002) although this fossil has been alternatively interpreted as giant cyanobacteria (Sharma and Shukla 2009). More conclusive macroalgal fossils have been reported from the Mesoproterozoic Era (1600–1000 Ma) (e.g., Zhu et al. 2016b) and by the Neoproterozoic Era (1000–540 Ma), particularly in the Ediacaran Period (635–540 Ma), definitive macroalgae with holdfasts and dichotomously branching patterns are common

(Xiao et al. 2002). Few studies have provided a quantitative analysis of the Proterozoic macroalgal fossil record. The only such quantitative analysis was published more than ten years ago (Xiao and Dong 2006)and in the past decade, there have been additional studies that have added to the known Proterozoic macroalgal fossil diversity and improved geochronological constraints of this record. Therefore, it is possible to build upon the analysis Xiao and Dong (2006) with this new data.

In this contribution, we expand on the Xiao and Dong (2006) dataset by adding recently published and unpublished data on Proterozoic macroalgal fossils. This database is also augmented with the early Paleozoic macroalgal fossils reported by LoDuca et al. (2017). The dataset was then analyzed to characterize the morphological and ecological evolution of macroalgae in the Proterozoic and early Paleozoic eras, with special focus on the Ediacaran Period.

3.3 Material and methods

All the non-calcified macroalgae fossils in our dataset are preserved as carbonaceous compressions. The vast majority of fossils in our dataset are >1 mm in overall size (Figs. 3.1, 3.2), although some have branches or filaments that are as thin as 0.1 mm (e.g., Fig. 3.1G). This size limit is somewhat arbitrary, but it ensures that most fossils in our database represent benthic organisms, as most modern macroalgae do. It is possible that a small number of fossils in the database may not be photosynthetic or eukaryotic organisms (e.g., cyanobacteria colonies or even animals (e.g., Wan et al. 2016)), but the vast majority of them are likely macroalgae with diagnostic macroalgal structures such as a holdfast with a branching system (Xiao et al. 2002; Xiao and Dong 2006).

We coded the presence/absence (coded as 1/0) of 30 morphological characters for a total of 1458 Proterozoic to early Paleozoic carbonaceous compression fossils (Tables 3.1–2). The database consists of 578 specimens from the Xiao and Dong (2006) study, as well as 880 new specimens from the published literature and unpublished material housed in the Central Siberian Geological Museum of the Siberian Branch of the Russian Academy of Sciences (CSGM) in Novosibirsk, Russia. The unpublished material includes collections № 2025 from the Perevalok Formation of the Urals Mountains and № 2026 from the Khatyspyt Formation, Olenek Uplift, Siberia. We also included in our database the early Paleozoic macroalgal fossils from LoDuca et al. (2017). To accommodate the early Paleozoic fossils and to improve the description of macroalgal morphologies, we also expanded the list of morphological characters from 19 in Xiao and Dong (2006) to 30 in the current study.

It is important to point out that the Proterozoic data were coded at the level of specimen occurrence (i.e., each entry represents a specimen), whereas the Paleozoic data were coded at the level of species occurrence (i.e., each entry represents a species, often the holotype specimen). This difference is in part driven by the taxonomic assignment (or lack thereof) of Proterozoic macroalgal fossils: a number of specimens are unnamed (e.g., those in CSGM) or placed in open nomenclatures (e.g., Yuan et al. 1999); specimens described under the same species may have different morphologies [e.g., specimens described under *Vendotaenia antiqua* can be either tubular or ribbonlike fossils (Sun 1986; Cohen et al. 2009); and specimens described under different species may have similar morphologies (i.e., synonyms). A result of this methodological difference is that there are a number of duplicate entries in the Proterozoic portion of the database, with the exception of the Cryogenian database, which consists of only 12 specimens (Ye et al. 2015). While these duplicate entries do not affect the range of occupied morphospace, they do affect the calculation of variance.

Thus, the variance of Proterozoic geochronological bins, particularly the Ediacaran where the level of duplicate coding is high, is underestimated relative to those in the early Paleozoic.

The presence/absence data were analyzed using non-parametric multidimensional scaling (NMDS) method to evaluate the morphological evolution of macroalgae through time. NMDS is a ordination technique that simplifies multidimensional data matrices (Schiffman et al. 1981; Huntley et al. 2006). Unlike Principal Component Analysis (PCA), NMDS can handle binary data (e.g., presence/absence data) and missing values. Thus, it is the most appropriate method to analyze the database. All ordination procedures were performed in *R*, using the function "metaMDS" from the 'vegan' package (Oksanen et al. 2016). We used Euclidean distance with 20 trials for plotting NMDS results. First, NMDS was used to ordinate our data in two-dimensional space (Figs. 3.3–4). To verify our results, three- and four-dimensional ordinations were run and they gave results similar to those of two-dimensional ordination; therefore, these results are not presented here. NMDS calculated two scores (NMDS 1 and NMDS 2) for each specimen or species occurrence, which were then allocated to eight geochronological time bins (P: Paleoproterozoic, 1800–1600 Ma; M: Mesoproterozoic, 1600-1000 Ma; T: Tonian, 1000–720 Ma; Cr: Cryogenian, 720–635 Ma; E: Ediacaran, 635–540 Ma; C: Cambrian, 540–485 Ma; O: Ordovician, 485–444 Ma; S: Silurian, 444–419 Ma; Table 3.2). The NMDS 1 and NMDS 2 scores are plotted in a two-dimensional space and the morphospace range for each geochronological bin is visualized by a convex hull (Fig. 3.3). In addition, the sum variance of the NMDS 1 and NMDS 2 scores was calculated to quantify morphological disparity in each geochronological bin (Fig. 3.3I). Because the Cryogenian dataset consists of only 12 entries representing 7 different morphotypes (Ye et al. 2015), we repeated the analyses with and without the Cryogenian data to investigate how the low sampling intensity and low duplicate coding levels of the Cryogenian data would affect

the results, particularly NMDS variances. Analytical results without the Cryogenian data are shown in Figure 3.3, and those with the Cryogenian data in Supplementary Figure (Fig. 3.S1).

To test whether there is a significant difference in NMDS variance among different geochronological bins, Permutational Multivariate Analysis of Variance (PERMANOVA) and Multivariate Analysis of Variance (MANOVA; with Bonferroni correction to account for multiple comparisons) were applied (Table 3.4, 3.S1). MANOVA assumes normal distribution while PERMANOVA assumes homogeneous multivariate dispersion. Our data are neither normally distributed nor have a homogenous multivariate dispersion within group. Thus, we applied both tests, and only consider the test result valid when both tests agree with each other. The null hypothesis H_0 for the PERMANOVA is that the centroids of the tested groups are indistinguishable from each other. The null hypothesis H_0 for the MANOVA is that the mean vectors of the tested groups are indistinguishable from each other.

To complement NMDS analysis, the functional-form group (FFG) approach was also implemented. The concept of functional-form group was proposed by Littler and Littler (1980) and has been widely used in the ecological analysis of modern seaweed communities. Following Littler and Arnold (1982), Steneck and Dethier (1994), and LoDuca et al. (2017), we used the following FFGs (Table 3.3): (1) sheet and thin tubular forms; (2) delicately branched forms with branches thinner than 2 mm; (2.5) similar to FFG 2 but with some branches thicker than 2 mm; (3) coarsely branched forms with branches thicker than 2 mm; (4) thick (leathery) blades. The macroalgal fossils were first classified into various morphogroups and then to certain FFGs based on a scheme developed by LoDuca et al. (2017) (Table 3.3). Each Proterozoic specimen or early Paleozoic species occurrence was assigned to a FFG. Because Proterozoic fossils were coded at the specimen level, we counted the number of morphotypes as a proxy of species-level occurrences in each FFG for each geochronological bin. For instance, if a geochronological bin consists of two assemblages,

which respectively have 2 and 3 species or morphotypes belonging to FFG-1, then the total number of species-level occurrences of FFG-1 for this geochronological bin is 5, regardless how many FFG-1 species these two assemblages share. This exercise was repeated for all FFGs, and the percentage of species-level occurrences in each FFG was calculated for each geochronological bin (Fig. 3.5A).

The Ediacaran portion of the database contains a large number of occurrences and assemblages that permits a more detailed analysis. In order to further characterize morphological and ecological variations within the Ediacaran Period, NMDS, PERMANOVA/MANOVA, and FFG analyses were performed on the different Ediacaran assemblages (Figs. 3.4, 3.5B; Table 3.5). For these analyses, the categorization bins are Ediacaran assemblages rather than time bins. Only assemblages with ≥3 different morphotypes were included in these analyses. These assemblages are listed below in approximate geochronological order: DS – lower Doushantuo Formation, Sandouping, Hubei Province, China; LN – lower Lantian Formation, Anhui Province, China; DG – upper Doushantuo Formation at Wenghui, Guizhou Province, China; DM – Miaohe Member of upper Doushantuo Formation, Miaohe village, Hubei province, China; PV – Perevalok Formation, Ural Mountains, Russia; KH – Khatyspyt Formation, Arctic Siberia; YJ –Jiucheng Member of the Dengying Formation, Yunnan Province, China; DK –Kliphoek Member of the Dabis Formation of the Kuibis Subgroup, Namibia; LP – Liuchapo Formation, Hunan Province, China (Tables 3.2, 3.5; Figs. 3.4, 3.5B).

Finally, morphometric data, such as maximum dimension (as an approximation for canopy height) (LoDuca et al. 2017) and surface area/volume (SA/V) ratio, were collected by measuring specimens or images using ImageJ (Figs. 3.6-7, 3S1E). To estimate SA/V ratios, we modeled the three-dimensional morphology of macroalgal fossils based on current estimates of their geometrical shape. For example, *Chuaria* (Fig. 3.1C) is considered as a

spherical organism, therefore the arithmetical average of the maximum and minimum diameters of compressed *Chuaria* specimens was used to calculate their SA/V ratios. SA/V ratios were calculated as 3/radius for spheres, 4/width for cylinders, and 1/thickness for sheets. For more complex forms, such as *Lonfgengshania* (Fig. 3.1J), the surface area and volume were calculated for individual components of the fossil, and were summed from each component to yield an estimated SA/V ratios for the whole organism. Both maximum dimensions and SA/V ratios were tested for significance by pairwise comparison of adjacent geochronological bins using the Mann-Whitney (U) test. This test was chosen because it is a nonparametric test that does not assume a normal distribution. The null hypothesis (H_0) is that the distribution of both populations of data is indistinguishable.

Finally, the number of taxa or morphotypes were counted for each assemblage and for each geochronological bin to estimate the alpha (α) and gamma (γ) diversities, respectively (Fig. 3.8). To test the sensitivity of diversity patterns with respected to taxonomic uncertainties, alpha and gamma diversities were calculated at both the species/morphotype and genus/morphotype levels. The species/morphotype-level diversity was also calculated with or without unnamed taxa.

3.4 Results

Regardless whether Cryogenian data were included or excluded from the analysis, NMDS results show that the morphospace range, as represented by convex hulls, expands from the Paleoproterozoic to the Silurian (Figs. 3.3, 3.S1B). This is particularly true for the Proterozoic, where the convex hulls are nested inside successively younger ones. Ordovician and Silurian convex hulls expand into the top right and bottom left corners in the NMDS plot (Fig. 3.3A–H). These expansions are driven by the rise of coarsely branched and thick blade

forms, which plot in the top right corner, and the cortex-forming and monopodial branched forms, which plot in the bottom left corner. These morphotypes are not common in the Proterozoic, and are only sporadically represented in the Cryogenian and Ediacaran periods, e.g., by cortex-forming forms such as *Elainabella* (Rowland and Rodriguez 2014) and monopodially branched forms such as *Anomalophyton* (Xiao et al. 2002) (Table 3.1).

With the Cryogenian data excluded, sum variances of NMDS 1 and NMDS 2 (as an approximation of disparity) illustrate two stepwise increases in the Ediacaran and Ordovician periods (Fig. 3.3I). PERMANOVA and MANOVA tests resulted in p-values of > 0.05 (hence insignificant differences) for the Paleoproterozoic-Mesoproterozoic, Mesoproterozoic-Tonian, and Ordovician-Silurian comparisons, but p-values of < 0.05 (hence significant differences) for the Tonian-Ediacaran, Ediacaran-Cambrian, and Cambrian-Ordovician comparisons (Table 3.4). Of the significant results, the Tonian-Ediacaran and Cambrian-Ordovician comparisons show an increase in disparity, whereas the Ediacaran-Cambrian comparison shows a decrease. The stepwise increases in disparity in the Ediacaran and Ordovician periods co-occur with the expansion in morphospace range (Fig. 3.3C–D, F–G, H) and evolution of novel morphological characters (Table 3.1) in these two periods.

With Cryogenian data included, the first increase in variance shifts to the Cryogenian Period (Fig. 3.S1C). PERMANOVA and MANOVA tests show significant differences (p-values <0.05) in the Tonian-Cryogenian and Ediacaran-Cambrian comparisons (Table 3.S1), with the former showing an increase and the latter showing a decrease. It is possible that the Cryogenian increase in disparity is an artifact driven by the low number of sample and low duplicate coding in this period, because this increase occurs without an increase in morphospace range (Fig. 3.S1B) and the evolution of novel morphological characters (Table 3.1). Also, notably, the Cryogenian variance is artificially elevated, due to fewer duplicate codings, relative to the Ediacaran Period, which has many duplicate codings (Fig. 3.S1A).

NMDS analysis of Ediacaran assemblages does not show any clear trends in the morphospace occupation (Fig. 3.4). Most of the assemblages have considerable overlap. However, older Ediacaran assemblages (635–550 Ma), such as the Lantian, Doushantuo, Perevalok, and Khatyspyt assemblages, appear to demonstrate a greater morphospace range than younger Ediacaran ones (550–540 Ma) such as the Yuhucun, Dabis, and Liuchapo assemblages. These older assemblages are responsible for the full morphospace range of the entire Ediacaran Period (Fig. 3.4A–F). Among the older assemblages, the Khatyspyt assemblage is dominated by filamentous, bundled filamentous, and ovoid forms, whereas the Doushantuo and Lantian assemblages by various branching forms. Sum NMDS variances, on the other hand, vary widely among Ediacaran assemblages and do not show any systematic differences between older and younger assemblages (Fig. 3.4L). PERMANOVA and MANOVA results do not show consistent support for any significant differences in NMDS variance among assemblages (Table 3.5), indicating appreciable geographic or environmental variations in macroalgal morphological disparity.

Functional-form group (FFG) data show trends similar to the NMDS results (Fig. 3.5A), with significant increase in the number of FFGs at the Tonian/Cryogenian-Ediacaran and Cambrian-Ordovician transitions (Figs. 3.5A, 3.S1C). Paleoproterozoic and Mesoproterozoic macroalgae are exclusively dominated by FFG-1 (spherical, tubiform and ribbon-like forms), with FFG-2 appearing in the Tonian, and FFG-2.5 and FFG-3 in the Ediacaran. Interestingly, FFG-2.5 and FFG-3 are not represented in the Cambrian but become dominant later in the Ordovician. The Silurian Period has the highest number of FFGs, with all FFGs represented.

FFG analysis of Ediacaran assemblages shows that the older assemblages in the Doushantuo and Lantian formations are represented by FFG-1, 2, and 2.5, with the latter two accounting for approximately 20% of species-level occurrences (Fig. 3.5B). Among older

Ediacaran assemblages, the ~558 Ma Perevalok assemblage is the only one not hosting any distinct branching forms. Younger Ediacaran assemblages have smaller sample size and, with exception of Dabis assemblage, consist predominantly of FFG-1 (tubifrom and ribbon-like forms).

The maximum dimension analysis did not include the Cryogenian data because only a few specimens from this period are completely preserved (Ye et al. 2015). The results show an overall increase in macroalgal size through time, with two significant increases in the Ediacaran and Silurian according to the Mann-Whitney significance test (p-values < 0.05) (Fig. 3.6A-B). Among Ediacaran assemblages, there is a significant decrease in maximum dimension from the older Ediacaran (635–550 Ma) to younger Ediacaran (550–541 Ma) assemblages (Fig. 3.6C–D).

SA/V ratios also show an overall increasing trend through time (Fig. 3.7A-B). All except the Cambrian-Ordovician neighborhood comparisons show significant differences according to the Mann-Whitney test (p-value < 0.05). Among these comparisons with significant differences, all except the Mesoproterozoic-Tonian comparison are characterized by a significant increase in SA/V ratios. Among Ediacaran assemblages, there are no consistent trends in SA/V ratios (Fig. 3.7C–D).

To summarize, the morphospace range (as defined by convex hulls), morphological disparity (as measured by NMDS variances), canopy height (as measured by maximum dimensions), and SA/V ratios all increase in parallel through time. Indeed, there is a positive correlation among these metrics (e.g., maximum dimension vs. NMDS variance, $r^2 = 91.4\%$; SA/V ratio vs. NMDS variance, $r^2 = 75.6\%$). Our analysis also shows that early Ediacaran assemblages exhibit greater morphospace range, taxonomic diversity, canopy height, and functional-form complexity than terminal Ediacaran assemblages.

3.5 Discussion

A significant challenge in the study of the evolutionary history of non-calcified marine macroalgae is the dearth of fossils and potential taphonomic biases. Since these organisms have no skeletons and their preservation in the fossil record critically depends on the availability of Lagerstätten (sedimentary deposits with exceptionally preserved fossils), which in turn depends on environmental factors such as anoxia and bioturbation (Muscente et al. 2017). For much of the geological periods covered in this study (particularly Proterozoic to Cambrian), however, deep marine environments were commonly dominated by anoxia (Sperling et al. 2015) and bioturbation was relatively mild (Tarhan et al. 2015). Furthermore, although the secular changes in taphonomic conditions may affect the abundance of macroalgal fossils, they would unlikely introduce systematic megabiases (e.g., Kowalewski and Flessa 1996) in macroalgal morphology. At the current stage, the pressing need is to more thoroughly investigate the geological record in order to fill critical gaps in the fossil record of macroalgae, for example, in the Paleoproterozoic-Mesoproterozoic (e.g., Zhu et al. 2016b), Tonian (e.g., Nagovitsin et al. 2015), and Cryogenian (e.g., Ye et al. 2015). Only after the macroalgal database reaches a certain critical size can more rigorous analyses be applied to detect systematic taphonomic and sampling biases (e.g., Alroy et al. 2001).

A second challenge relates to the interpretation of carbonaceous compression fossils. We emphasize that, although most carbonaceous compression fossils in our database can be plausibly interpreted as macroalgae, some may in fact be microbial colonies or even non-skeletal metazoans. The morphologically simple form *Chuaria circularis*, for example, has been variously interpreted as colonial cyanobacteria, single-celled eukaryotes, or multicellular macroalgae; the latter interpretation has been recently suggested using novel observation using back-scattered electron microscopy (Tang et al. 2017). That said, there are no particular

reasons to think that the morphological history of macroalgal fossils would be systematically and pervasively biased because of misclassifications of the fossils.

Despite these challenges, the available data allow us to gain important insights into the large-scale patterns of macroalgal evolution (e.g., Knoll and Nowak 2017). Our analysis confirms the findings of previous studies (Xiao and Dong 2006; LoDuca et al. 2017) that concluded that the morphospace range, morphological disparity, FFG, maximum dimension, and SA/V ratio broadly increase from the Proterozoic through the early Paleozoic. Superimposed on this trajectory are two stepwise increases, one in the Ediacaran and the other in the Ordovician. The former is consistent with the previous analysis by Xiao and Dong (2006) and is supported by the congruent increase in number of coded characters (Table 3.1), convex hull, NMDS variance, number of FFGs, maximum dimension, and SA/V ratio. The latter has been discussed extensively in LoDuca et al. (2017) and will not be consider here.

The apparent Cryogenian peak in NMDS variance (Fig. 3.S1C) is likely exaggerated due to the sparse data and relatively few duplicate codings relative to the Ediacaran Period. The Cryogenian dataset consists of only 12 specimens, 7 described species/morphotypes (Table 3.2), 5 morphogroups (ribbon-like, spherical, delicately dichotomously branched, stoloniform, and frondose; Table 3.3), and 11 coded characters (Table 3.1). For comparison, the Ediacaran dataset consists of 712 specimens, 70 described species/morphotypes (Table 3.2), 9 morphogroups (all but the complex monopodial morphogroup listed in Table 3.3), and 25 coded characters (Table 3.1).

The observation that older Ediacaran macroalgal assemblages (635–550 Ma) show greater morphospace range and taxonomic diversity than younger ones (550–540 Ma) is intriguing. In particular, it is important to note that terminal Ediacaran macroalgal assemblages show a decline in morphospace range (Fig. 3.4), canopy height (Fig. 3.6C-D),

and alpha diversity (Fig. 3.8B). We cannot completely rule out the possibility that this decline may have been driven in part by the lower sampling intensity in younger vs. older Ediacaran assemblages. Indeed, all younger Ediacaran assemblages have relatively low sampling intensity and low number of species- or morphotype-level occurrences (Figs. 3.4-5), and this may be part of the reason that they have spuriously high NMDS variances (Fig. 3.4L). However, it is possible that the database reflects genuinely low taxonomic and morphological diversity in the late Ediacaran Period. In fact, a late Ediacaran decline in morphological diversity of macroalgae echoes the decrease in Ediacara-type macrofossils (Xiao and Laflamme 2009; Laflamme et al. 2013; Darroch et al. 2015; Boag et al. 2016; Smith et al. 2016).

The terminal Ediacaran decline has been long recognized and dubbed as "the Kotlinian crisis" (Brasier 1992; Kolesnikov et al. 2015), which appears to have occurred concurrent with the rise of bioturbating, skeletal, and reef-building metazoans (Grazhdankin 2014; Meyer et al. 2014; Penny et al. 2014; Darroch et al. 2015). The coupled decline in macroalgae and Ediacara-type macro-organisms seems to be protracted and occurs over the terminal Ediacaran Period. This decline may have been driven by ecological impacts of mobile, predatory, or grazing metazoans [e.g., biotic replacement hypothesis of Laflamme et al. (2013) and Darroch et al. (2015)], or by continuous environmental deterioration during the terminal Ediacaran Period [e.g., expanding oceanic anoxia; (Kimura et al. 1997; Schröder and Grotzinger 2007; Smith et al. 2016)] that affected both macroalgae and Ediacara-type macro-organisms.

Our study confirms the absence of a Cambrian explosion of macroalgae (LoDuca et al. 2017). If anything, there is a decline in taxonomic diversity, morphospace range, and morphological disparity of macroalgae during the Cambrian (Fig. 3.3), and this decline may be a continuation of the terminal Ediacaran Kotlinian crisis. Thus, if animal evolution had an

impact on macroalgae through top-down ecological interactions, such interactions must have been negative in nature, rather than positive ecological feedbacks as suggested by the cropping hypothesis (Stanley 1973). In contrast, the Great Ordovician Biodiversification Event (GOBE) seems to have had a positive impact on the morphological diversification of macroalgae (LoDuca et al. 2017), as indicated by the Ordovician increase in macroalgal diversity, morphospace range, morphological disparity, and FFGs (Figs. 3.3, 3.5A).

The progressive increase in FFGs, maximum dimension, and SA/V ratio of Proterozoic and early Paleozoic macroalgae have important ecological and geobiological implications. The FFG approach is effective in addressing ecosystem-level questions about macroalgae (Littler and Littler 1980; Littler and Arnold 1982; Hanisak et al. 1988; Steneck and Dethier 1994), particularly when specific functions (e.g. nutrient uptake rates, photosynthesis rates, herbivore resistance, and disturbance resistance) are taken into consideration (Padilla and Allen 2000). In this regard, the single most important increase in FFGs seems to have occurred in the Ordovician, probably driven by ecological response to increasing grazing levels associated with the GOBE (LoDuca et al. 2017).

The increasing trajectory of maximum dimension and SA/V ratio of Proterozoic and early Paleozoic macroalgae seem to be smoother than that of morphological disparity and FFGs. As a first-order approximation, these metrics can be taken as estimates of canopy heights and primary production (Xiao and Dong 2006). As most macroalgae are epibenthic, their maximum size provides a robust approximation of canopy heights and thus tiering heights of macroalgal communities. Similarly, there is a robust positive relationship between SA/V ratio and mass-specific growth rate (hence primary production) of photosynthetic organisms (Nielsen and Sand-Jensen 1990). Thus, the progressive increase in maximum dimension and SA/V ratio of Proterozoic and early Paleozoic macroalgae—mostly driven by the evolution of erect, epibenthic, and branching macroalgae—likely created more ecological

niches for other organisms and resulted in greater bioproduction in coastal environments. Through these ecological and geobiological processes, macroalgae made greater impacts on ecological feedbacks and global carbon cycles.

Although it is clear that macroalgae experienced a significant taxonomic, morphological, and ecological diversification in the Ediacaran Period (e.g., Xiao and Dong 2006 and this study), there are still a number of unresolved questions that warrant further investigation. Of primary importance are questions related to the precise time line of macroalgal evolution in the Ediacaran Period, the complex ecological feedbacks involving Ediacaran macroalgae, and the taxonomic and morphological diversity of macroalgae preceding the Ediacaran Period. To address these questions, a solid stratigraphic framework and better geochronological constraints are needed for reliable and high-resolution correlation of Ediacaran strata (Xiao et al. 2016). Quantitative ecological modeling would help us to better understand the geobiological role of macroalgae in the Earth-life system during the Ediacaran Period. Investigation of pre-Ediacaran macroalgae assemblages has already led to promising results, including the discovery of Cryogenian macroalgal fossils (Ye et al. 2015) and dichotomously branching macroalgae in the Tonian Period (Nagovitsin et al. 2015). With coordinated multidisciplinary efforts, a more nuanced picture of macroalgal evolution in the Neoproterozoic Eon is within reach in the next decade.

3.6 Conclusions

Our analysis using simple morphometric, NMDS, and functional-form group (FFG) approaches shows an overall increasing trajectory in morphospace range, morphological disparity, FFGs, maximum dimension, and surface area/volume (SA/V) ratio of macroalgae from Proterozoic to early Paleozoic. This trend is superimposed by two stepwise increases in

taxonomic diversity, morphospace range, morphological disparity, and FFGs during the Ediacaran and Ordovician periods. A Cryogenian peak in morphological disparity is probably an artifact of low sampling intensity and low number of duplicate codings, but this warrant further analysis as more Cryogenian data become available. We found no Cambrian explosion of macroalgae; indeed, Cambrian macroalgae have lower taxonomic diversity, morphospace range, morphological disparity, and FFGs than their Ediacaran counterparts. These results suggest that the Cambrian explosion of animals had little impact on macroalgae. Instead, the initial diversification of macroalgae appear to have occurred in the Ediacaran Period prior to the main episode of Cambrian explosion.

NMDS analysis of Ediacaran macroalgal assemblages shows that morphospace range is greater in older Ediacaran assemblages (635–550 Ma), and that younger Ediacaran assemblages (550–540 Ma) exhibit a decline in morphospace range, taxonomic diversity, and FFGs. Together with data of Ediacara-type fossils published by other researchers, these results suggest that there is an extinction event in the last ~10 Myr prior to the Ediacaran-Cambrian boundary, and this extinction affected both macroalgae and Ediacara-type macro-organisms. The pattern of this extinction is consistent with the biotic replacement model or the environmental perturbation model.

Measurements of maximum dimension and surface area/volume ratio reveal a long-term increase in these metrics from the Proterozoic to early Paleozoic. This pattern is interpreted as evidence for a long-term increase in macroalgal canopy height and mass-specific growth rate. Macroalgae therefore may have become increasingly important in ecological tiering and carbon cycling in coastal environments from the Proterozoic to early Paleozoic.

3.7 Acknowledgments

We would like to thank Vasiliy Marusin for providing access to unpublished carbonaceous compression fossils from the Perevalok Formation in the Ural Mountains; Qin Ye for providing photographs of macroalgal fossils from the Nantuo Formation, South China; Benjamin Gill for fruitful discussion; LISA (Laboratory for Interdisciplinary Statistical Analysis) at Virginia Tech for providing help with statistical analyses. This research was funded by the National Science Foundation (EAR 1250756, 1332320, 1528553), NASA Exobiology and Evolutionary Biology Program (NNX15AL27G), Russian Science Foundation (14–17–00409), National Geographic Society (8227-07, 8637-09, 9031-11), and a GSA Graduate Student Research Grant.

3.8 Tables and table captions

Table 3.1. List of macroalgal characters and their temporal distribution. Abbreviations: P – Paleoproterozoic (2500 – 1600 Ma); M – Mesoproterozoic (1600 – 1000 Ma); T – Tonian (1000 – 750 Ma); Cr – Cryogenian (750 – 635 Ma); E – Ediacaran (635 – 541 Ma); C – Cambrian (541 – 485 Ma); O – Ordovician (485 – 444 Ma); S – Silurian (444 – 419 Ma). Star (*) indicates characters represented by a single species or morphotype. For example, an unnamed form from the Burskaya-3410 borehole is the only known representative of delicately and dichotomously branching macroalgae in the Tonian Period (Nagovitsin et al. 2015), and *Anomalophyton zhangzhongyingi* is the only representative of monopodially branching macroalgae (Xiao et al. 2002) and *Elainabella* the only possible representative of macroalgae with cortex differentiation in the Ediacaran Period (Rowland and Rodriguez 2014).

	Morphological features	**P**	**M**	**Neoproterozoic**			**Early Paleozoic**		
				T	**Cr**	**E**	**C**	**O**	**S**
	Thallus Morphologies								
1	Conical				+	+			
2	Tomaculate	+	+	+		+			
3	Thin tubular			+	+	+	+	+	+
4	Filamentous	+	+	+		+	+		+
5	Fan-like					+	+	+	
6	Sheet-like					+			
7	Thin blade or ribbon				+	+	+	+	+
8	Thick blade	?			+	+	?	+	+
9	Leathery								+
10	Spherical	+	+	+	+	+	+	+	+
11	Ellipsoidal	+	+	+		+			
12	Ovoid			+		+			
	Thallus differentiation								
13	Discoidal holdfast		+	+		+	+	+	+
14	Rhizoidal holdfast				+	+	+	+	+
15	Hook-like holdfast							+	+
16	Inferred holdfast	?		+	+	+	+	+	+
17	Stipe	?		+	+	+	+	+	+
	Other features								
18	Monopodial branching				+	+*	+	+	+

19	Pseudomonopodial branching					+	+		
20	Dichotomous branching			+*	+	+	+	+	+
21	Delicately branching			+*	+	+	+	+	+
22	Coarsely branching					+	+	+	+
23	Colonial					+			
24	Bundled filaments					+	+	+	+
25	Cortex differentiation					+*		+	+
26	Serial segmentation								+
27	Longitudinal striation					+			
28	Transverse annulation			+		+			
29	Verticils							+	+
30	Heterocladous								+

Table 3.2. List of geochronological bins and source data. CSGM – Central Siberian Geological Museum, Siberian Branch of the Russian Academy of Sciences, Novosibirsk, Russia.

Paleoproterozoic (1800 – 1700 Ma): 29 (19) specimens, 4 described species	
Changzhougou Fm., 1800 – 1625 Ma	(Zhu et al. 2000)
Tuanshanzi Fm., 1800 – 1625 Ma	(Du and Tian 1986; Zhu and Chen 1995, 10 specimens not included in further analysis)
Mesoproterozoic (1600 – 1000 Ma): 52 specimens, 4 described species	
Hongshuizhuang Fm., ~1400 Ma	(Du and Tian 1986; Walter et al. 1990)
Rohtas Fm., 1600 – 1000 Ma	(Kumar 1995)
Suket Shale, 1600 – 1000 Ma	(Kumar 2001)
Greyson Shale, ~1400 Ma	(Walter et al. 1990)
Gaoyuzhuang Fm., ~1560 Ma	(Du and Tian 1986; Zhu et al. 2016a)
Tonian (1000 – 720 Ma): 472 specimens, 67 described species	
Liulaobei, Jiuliqiao, Jinshanzhai, Shijia, Weiji, Gouhou & Jingeryu fms., ~850-820 Ma	(Duan 1982; Wang et al. 1984; Steiner 1994, 1997)
Xiamaling, Changlongshan & Nanfen fms., ~850 Ma	(Duan 1982; Du and Tian 1986)
Wynniatt Fm., ~ 850 Ma	(Hofmann and Rainbird 1994)
Halkal Fm., ~850 Ma	(Maithy and Babu 1996; Sharma and Shukla 2012)
Shihuiding Fm., ~850 Ma	(Zhang et al. 1991; Zhang et al. 1995)
Little Dal Group, 1030 – 780 Ma	(Hofmann 1985)
Late Riphean, Pav'yuga Fm., ~780	(Gnilovskaya et al. 2000)
Kulady Fm, Burksaya 3410, ~800-750	(Nagovitsin et al. 2015)
Cryogenian (720 – 635 Ma): 12 specimens, 7 described species	
Nantuo Fm., 654 – 635 Ma	(Ye et al. 2015)
Ediacaran (635 – 541 Ma): 712 specimens, 70 described species	
Khatyspyt Fm., ~550	(Grazhdankin et al. 2008; Nagovitsin et al. 2015; Rogov et al. 2015; CSGM # 2026; Duda et al. 2016)
Doushantuo Fm., 635 – 551 Ma	(Zhang 1989; Steiner 1994, 1997; Xiao et al. 2002; Zhao et al. 2004; Tang et al. 2006; Wang and Wang 2008; Wang et al. 2011; Wang and Wang 2011; Wang et al. 2014)
Lantian Fm., 635 – 551 Ma	(Steiner 1994; Yuan et al. 1999; Wan et al. 2013)
Perevalok Fm., ~ 558 Ma	(Grazhdankin et al. 2007; Marusin et al. 2011; CSGM # 2025)

Lyamtsa/Lamtsa Fm., > 558 Ma	(Leonov 2007)
Yorga/Erga Fm., ~ 550 Ma	(Leonov 2007)
Dengying Fm. (Shibantan Mb.), 551 – 541 Ma	(Yin and Gao 1995)
Dengying Fm. (Jiucheng Mb.), 551 – 541 Ma	(Steiner 1994, 1997)
Yuhucun Fm., (Jiucheng Mb.), 550 – 541 Ma	(Tang et al. 2007; Tang et al. 2008)
Liuchapo Fm., 551 – 541 Ma	(Steiner 1994)
Guaicurus Fm., 543 – 541 Ma	(Gaucher et al. 2003)
Zuun-Arts Fm., 550 – 541 Ma	(Dornbos et al. 2016)
Deep Spring Fm., ~ 549 Ma	(Rowland and Rodriguez 2014)
Dabis Fm. (Kliphoek Mb.) > 547 Ma	(Leonov et al. 2009)
Kanilov Fm.	(Steiner 1997)
Domo Extremeño Group	(Jensen et al. 2007)
Vingerbreek & Feldschuhhorn fms., 549 – 545 Ma	(Cohen et al. 2009)
Yaryshev Fm., 553 – 551 Ma	(Gnilovskaya et al. 1988)
Nagoryany Fm., ~550 Ma	(Gnilovskaya et al. 1988)
Studenitsa Fm., 545-541 Ma	(Gnilovskaya et al. 1988)
Feropont'ev Fm., ~ 550 Ma	(Gnilovskaya et al. 1988)
Zharnovka Fm., ~ 545	(Gnilovskaya et al. 1988)
Kotlin Fm., ~550 Ma	(Gnilovskaya et al. 1988)
Sokolets Fm., ~ 545	(Gnilovskaya et al. 1988)
Cambrian (541 – 485 Ma): 80 species-level occurrences, 42 described species	
(data from LoDuca et al. 2017)	
Ordovician (485 – 444 Ma): 38 species-level occurrences, 24 described species	
(data from LoDuca et al. 2017)	
Silurian (444 – 419 Ma): 72 species-level occurrences, 46 described species	
(data from LoDuca et al. 2017)	

Table 3.3. Principal morphogroups of noncalcified macroalgae and their relationships to functional-form groups (FFG). *, if branches cylindrical and some > 2 mm in width; **, if leathery; ***, if cortex present. #, *Vendotaenia* was described by different authors as a tubular or ribbonlike organism (e.g. Sun 1986; Cohen et al. 2009). Adopted from LoDuca et al. (2017).

Morphogroup	Form	Characteristics	Examples (Genera)	FFG
1. Tubiform		Simple unbranched cylindrical thalli with an aspect ratio > 2 and a width ≥ 0.1 mm.	*Fuxianospira*, *Sinocylindra*, *Vendotaenia*[#] *Jiuqunaoella*	1
2. Ribbon-like		Simple unbranched ribbon-like thalli with a width ≥ 0.1 mm.	*Mezenia* *Vendotaenia*[#] *Algites*	1
3. Spherical		Simple spherical thalli.	*Chuaria* *Beltanelloides* *Aggregatosphaera*	1
4. Delicately Dichotomously Branched	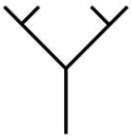	Thalli consisting of cylindrical or ribbon-shaped elements with anisotomous, isotomous, or pseudomonopodial bifurcations; all or most branches < 2 mm in width.	*Marpolia*, *Lenocladium*, *Bosworthia*, *Dalyia*, *Wahpia*, *Waputikia*, *Miaohephyton*, *Elainabella*, *Doushantuophyton*, *Enteromorphites*, *Konglingiphyton* *Eoholynia*	2, 2.5*
5. Coarsely Dichotomously Branched		Thalli consisting of cylindrical or ribbon-shaped elements with anisotomous, isotomous, or pseudomonopodial bifurcations; all or most branches > 2 mm in width.	*Buthotrephis*, *Manitobia*, *Winnepegia*, *Thalassocystis*, *Vialovinia*, *Yeaia*	3, 4**
6. Stoloniform	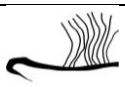	Thalli consisting of a prostrate runner bearing erect branches.	*Parallelphyton*, *Buthograptus*, *Menieria*	2
7. Frondose		Leaf-like thalli consisting of simple upright lanceolate blade-, sheet-, or fan-shaped elements, either singularly or in multiples joined at the base, and with or without internal filaments.	*Fractibeltia*, *Inmostia*, *Leafiophyton*, *Parafunaria*, *Plantulaformis*, *Punctarioposis*, *Enfieldia*, *Flabellophyton*	1
8. Simple Monopodial		Thalli consisting of a central axis bearing secondary elements (laterals) arranged in a radial fashion. Laterals are of simple cylindrical form and do not branch.	*Chaetocladus*, *Medusaegraptus*, *Dowlingia*, *Whiteavesia*, *Westonia*, *Mukschensia*, *Anomalophyton*	2.5

9. Complex Monopodial	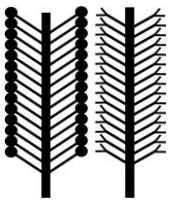	Thallus architecture as in simple monopodial but laterals show branching and/or have complex forms (e.g., forming a cortex).	*Corematocladus, Archaeobatophora, Amia, Kinwowia, Heterocladus, Leveilleites, Inopinatella, Kalania, Estoniocaulis, Mastopora, Diplospirograptus, Palmatophycus,*	2.5, 3***
10. Miscellaneous	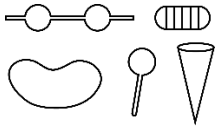	Array of different morphologies, which do not fit in any of above categories: conical forms, reniforms, thalli with transverse annulation, etc. Most of them do not have formal taxonomic names.	*Longfengshania Protoconites*	1

Table 3.4 Results of statistical tests among geochronological bins, with Cryogenian data excluded. P-values with Bonferronni corrections (to account for multiple comparisons) of PERMANOVA and MANOVA tests are shown for pairwise comparison of sum NMDS variances for each geochronological bin. Abbreviations follow those in Table 3.1. Pink-shaded cells have p-values < 0.05 (significant difference between geochronological bins). P-values in bold represent neighborhood comparisons (i.e., P-M, M-T, T-E, E-C, C-O, and O-S), which are considered for the purpose of this study. Thus, there is significant difference in sum NMDS variance in E-T, E-C, and C-O comparisons.

PERMANOVA							
	P	**M**	**T**	**E**	**C**	**O**	**S**
P		**1.00**	0.67	1.00	0.00	0.00	0.00
M			**1.00**	0.06	0.00	0.00	0.00
T				**0.00**	0.01	0.00	0.00
E					**0.01**	0.00	0.00
C						**0.01**	0.01
O							**1.00**
S							
MANOVA							
	P	**M**	**T**	**E**	**C**	**O**	**S**
P		**15.96**	10.94	0.50	0.00	0.00	0.00
M			**17.98**	0.01	0.00	0.00	0.00
T				**0.00**	0.00	0.00	0.00
E					**0.00**	0.00	0.00
C						**0.00**	0.00
O							**3.72**
S							

Table 3.5. Results of statistical tests among Ediacaran assemblages. P-values with Bonferronni corrections (to account for multiple comparisons) of PERMANOVA and MANOVA tests are shown for pairwise comparison of sum NMDS variances for 9 selected Ediacaran assemblages. Abbreviations follow those in Fig. 3.4. Pink-shaded cells have p-values < 0.05 (significant difference between two assemblages). Stars (*) represent Ediacaran assemblages where the sample size is < 10 species/morphotype-level occurrences. P-values in bold indicate cases where PERMANOVA and MANOVA tests are in agreement with each other.

PERMANOVA									
	DG	**DM**	**DS***	**LN**	**PV**	**KH**	**YJ***	**DK***	**LP***
DG		1.00	1.00	0.96	0.00	**0.01**	1.00	1.00	**0.01**
DM			1.00	0.62	**0.02**	**0.00**	0.21	1.00	**0.01**
DS*				**0.02**	**1.00**	1.00	0.00	0.08	**0.01**
LN					**0.00**	**0.00**	1.00	0.61	1.00
PV						0.76	**0.00**	**0.00**	**0.00**
KH							**0.00**	0.10	**0.00**
YJ*								0.00	0.15
DK*									0.05
LP*									
MANOVA									
	DG	**DM**	**DS***	**LN**	**PV**	**KH**	**YJ***	**DK***	**LP***
DG		21.73	2.92	0.19	0.06	**0.00**	3.85	1.28	**0.00**
DM			2.02	0.00	**0.00**	**0.00**	0.13	1.95	**0.00**
DS*				**0.00**	30.77	5.69	0.14	0.36	**0.00**
LN					**0.00**	**0.00**	8.39	0.09	7.19
PV						1.22	**0.00**	**0.04**	**0.00**
KH							**0.00**	0.01	**0.00**
YJ*								0.10	0.23
DK*									0.02
LP*									

Table 3.S1. Results of statistical tests among geochronological bins, with Cryogenian data included. P-values with Bonferronni corrections (to account for multiple comparisons) of PERMANOVA and MANOVA tests are shown for pairwise comparison of sum NMDS variances for each geochronological time bin. Abbreviations follow those in Table 3.1. Pink-shaded cells have p-values < 0.05 (significant difference between two geochronological bins). P-values in bold represent neighborhood comparisons (i.e., P-M, M-T, T-Cr, Cr-E, E-C, C-O, and O-S), which are considered for the purpose of this study. Thus, there is significant difference in sum NMDS variance in Cr-T, Cr-E*, E-C*, and C-O comparisons. Stars mark pairs showing significant difference only in MANOVA test but not in PERMANOVA test.

PERMANOVA								
	P	**M**	**T**	**Cr**	**E**	**C**	**O**	**S**
P		**1.00**	1.00	0.01	1.00	0.00	0.00	0.01
M			**1.00**	0.00	1.00	0.00	0.00	0.00
T				**0.00**	1.00	0.00	0.00	0.00
Cr					**0.08**	0.15	0.13	0.16
E						**0.00**	0.00	0.00
C							**0.31**	0.08
O								**1.00**
S								
MANOVA								
	P	**M**	**T**	**Cr**	**E**	**C**	**O**	**S**
P		**23.78**	17.92	0.04	10.66	0.00	0.00	0.00
M			**17.90**	0.00	4.67	0.00	0.00	0.00
T				**0.00**	2.17	0.00	0.00	0.00
Cr					**0.01***	0.06	0.00	0.00
E						**0.00**	0.00	0.00
C							**0.04***	0.00
O								**10.41**
S								

3.9 Figures and figure captions

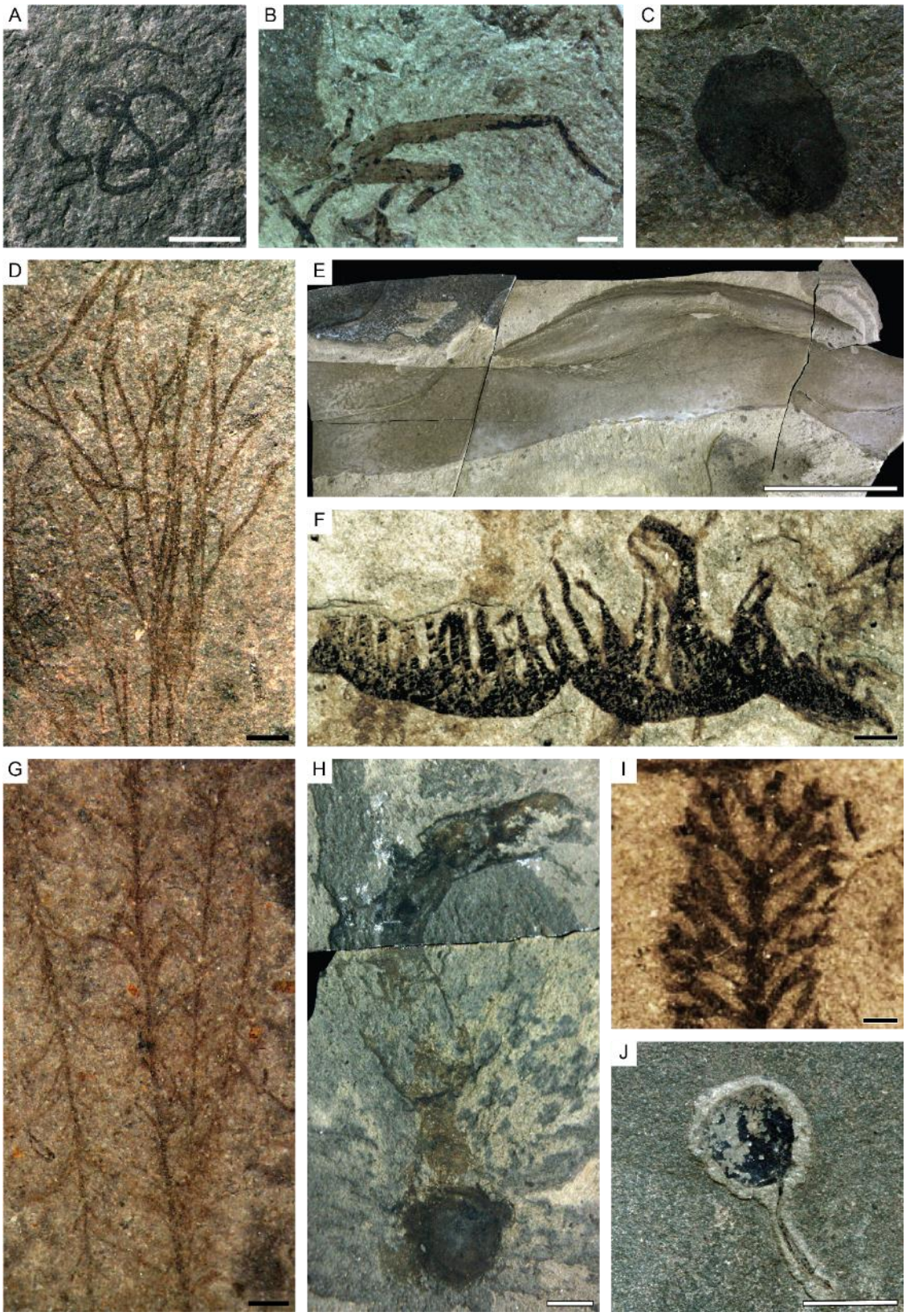

Figure 3.1. Representative fossils of macroalgal morphogroups. (A) Tubular (tubiform) macroalga *Jiuqunaoella simplicis*, late Ediacaran, Khatyspyt Formation, Arctic Siberia, CSGM #2026-20 (Nagovitsin et al. 2015). (B) Ribbon-like fossil, late Ediacaran, Khatyspyt Formation, Arctic Siberia, CSGM #2026-31 (Duda et al. 2016). (C) Spherical *Chuaria*-like macroalga, late Ediacaran, Khatyspyt Formation, Arctic Siberia, CSGM #2026-60. (D) Delicately dichotomously branched form *Doushantuophyton lineare*, late Ediacaran, Miaohe Member of upper Doushantuo Formation, village of Miaohe, Hubei Province, South China, HBM-505 (Xiao et al. 2002). (E) Ribbon-like macroalga *Mezenia sp.*, late Ediacaran, Khatyspyt Formation, Arctic Siberia, CSGM #2026-107. (F) Stoloniform *Parallelphyton*-like macroalga, Cryogenian, Nantuo Formation, the Songluo section, Hubei Province, South China (Ye et al. 2015). (G) Simple monopodially branched macroalga *Anomalophyton zhangzhongyingi*, late Ediacaran, Miaohe Member of upper Doushantuo Formation, village of Miaohe, Hubei Province, South China, HBM-498 (Xiao et al. 2002). (H) Frondose macroalga with differentiated stipe and discoidal holdfast, late Ediacaran, Khatyspyt Formation, Arctic Siberia, CSGM #2026-78. (I) Complex monopodially branched macroalga *Primicorallina trentonensis*, Ordovician, Trenton Group, New York, USA (LoDuca et al 2017). (J) Example of the miscellaneous morphogroup, *Longfengshania* sp. with a spherical body and a stipe or tether, late Ediacaran, Khatyspyt Formation, Arctic Siberia, CSGM #2026-215. Scale bars: 1 mm in D, F, G, I; 10 mm in A–C, H, J; 100 mm in E.

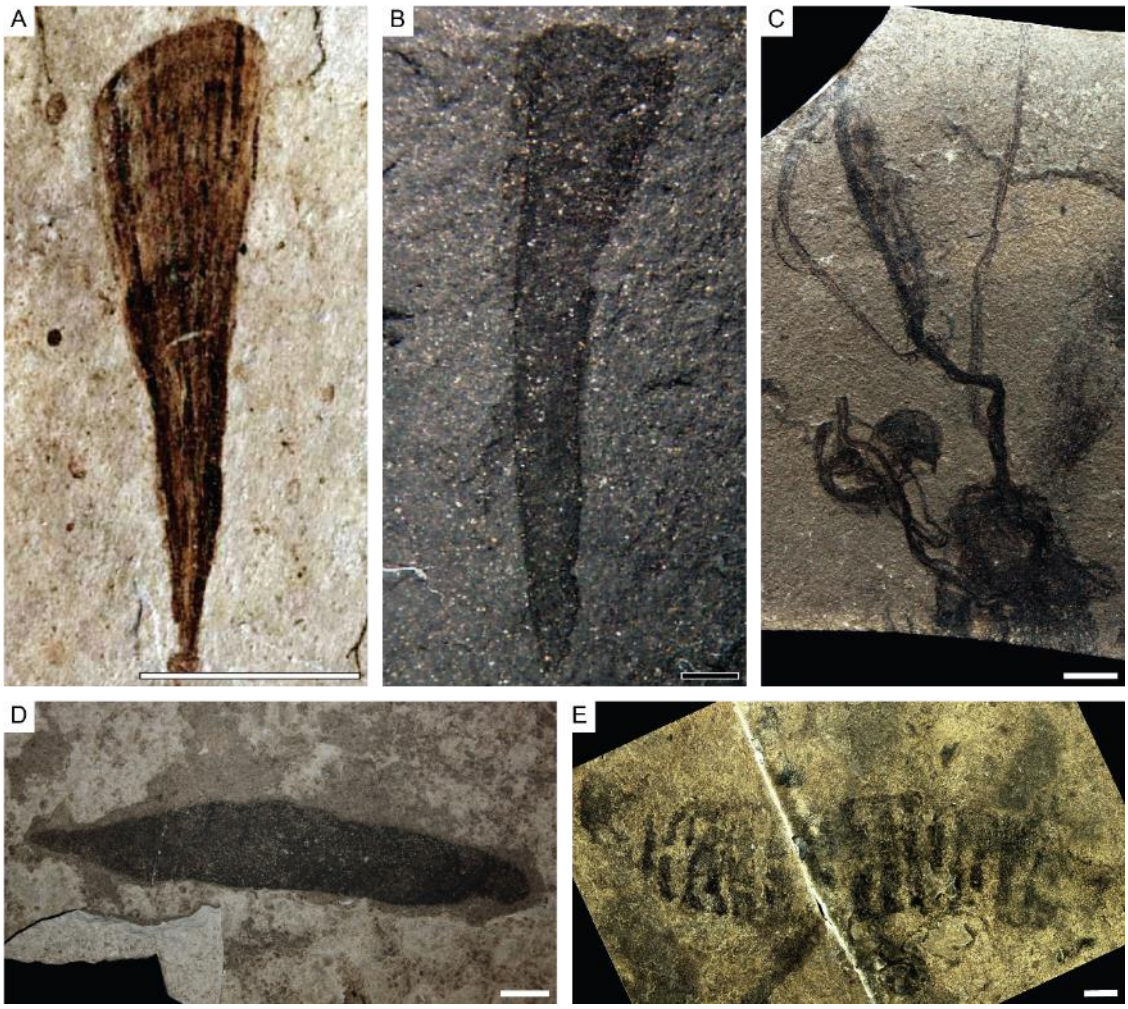

Figure 3.2. Representative fossils of macroalgal morphogroups. (A–C) Examples of the miscellaneous morphogroup, including (A) fan-like fossil *Flabellophyton lantianensis*, late Ediacaran, Lantian Formation, Anhui Province, China (Yuan et al. 2016); (B) conical fossil *Protoconites minor*, late Ediacaran, Miaohe Member of upper Doushantuo Formation, Miaohe village, Hubei Province, South China, MH-0307 (Xiao et al. 2002); and (C) bundled filamentous or cable-like macroalga *Longifuniculum dissolutum*, late Ediacaran, Khatyspyt Formation, Arctic Siberia, CSGM #2026-4. (D) Lanceolate form, late Ediacaran, Khatyspyt Formation, Arctic Siberia, CSGM #2026-54. (E) Tomaculate fossil with transverse annulations, late Ediacaran, Khatyspyt Formation, Arctic Siberia, CSGM #2026-161 (Grazhdankin et al. 2008). Scale bars: 1 mm in B; 10 mm in A, C–E.

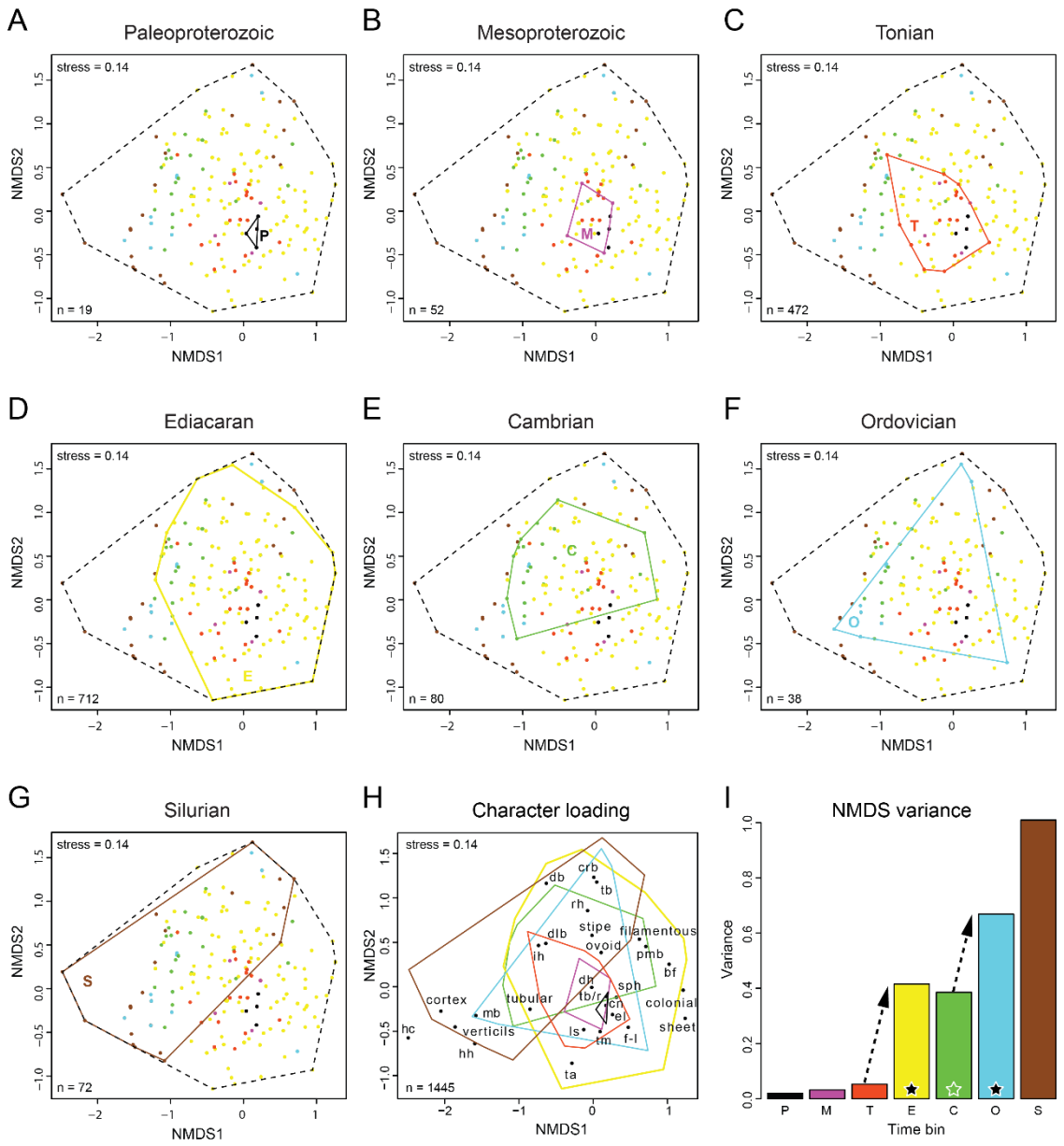

Figure 3.3. NMDS analysis of all macroalgal fossils. (A–G) Scatter plots and convex hulls (polygons in solid line) of realized morphospace in each geochronological bin from the Paleoproterozoic to the Silurian, in comparison with that of all macroalgal fossils in our database (convex hull in dashed line). Morphospace gradually expands from the Paleoproterozoic to the Ediacaran, after which it expands to the bottom left (cortex-forming monopodial branched forms) in the Cambrian–Silurian and to the top right corner (coarsely branched and thick blade forms) in the Ordovician–Silurian. Stress values and n values (number of species-level occurrences for the early Paleozoic bins and number of specimens

for Proterozoic bins) are shown in each panel. (H) Character loading diagram, with convex hulls of all bins. Abbreviations: crb – coarsely branched form; cn – conical form; bf – bundled filaments; db – dichotomously branched form; dlb – delicately branched form; dh – discoidal holdfast; el – ellipsoidal form; f-l – fan-like form; hc – heterocladous form; hh – hook-like holdfast; ih – inferred holdfast; ls – longitudinal striation; mb – monopodially branched form; pmb – pseudomonopodially branched form; rh – rhizoidal holdfast; sph – spherical form; tb – thick blade; tb/r – thin blade or ribbon; tm – tomaculate form; ta – transverse annulation. (I) Sum variances of the first two NMDS dimensions, showing two stepwise increases in the Ediacaran and Ordovician periods. Statistically significant increase or decrease relative to preceding geochronological bin is marked by a solid or empty star, respectively. P – Paleoproterozoic (black), M – Mesoproterozoic (pink), T – Tonian (orange), E – Ediacaran (yellow), C – Cambrian (green), O – Ordovician (brown), S – Silurian (light blue).

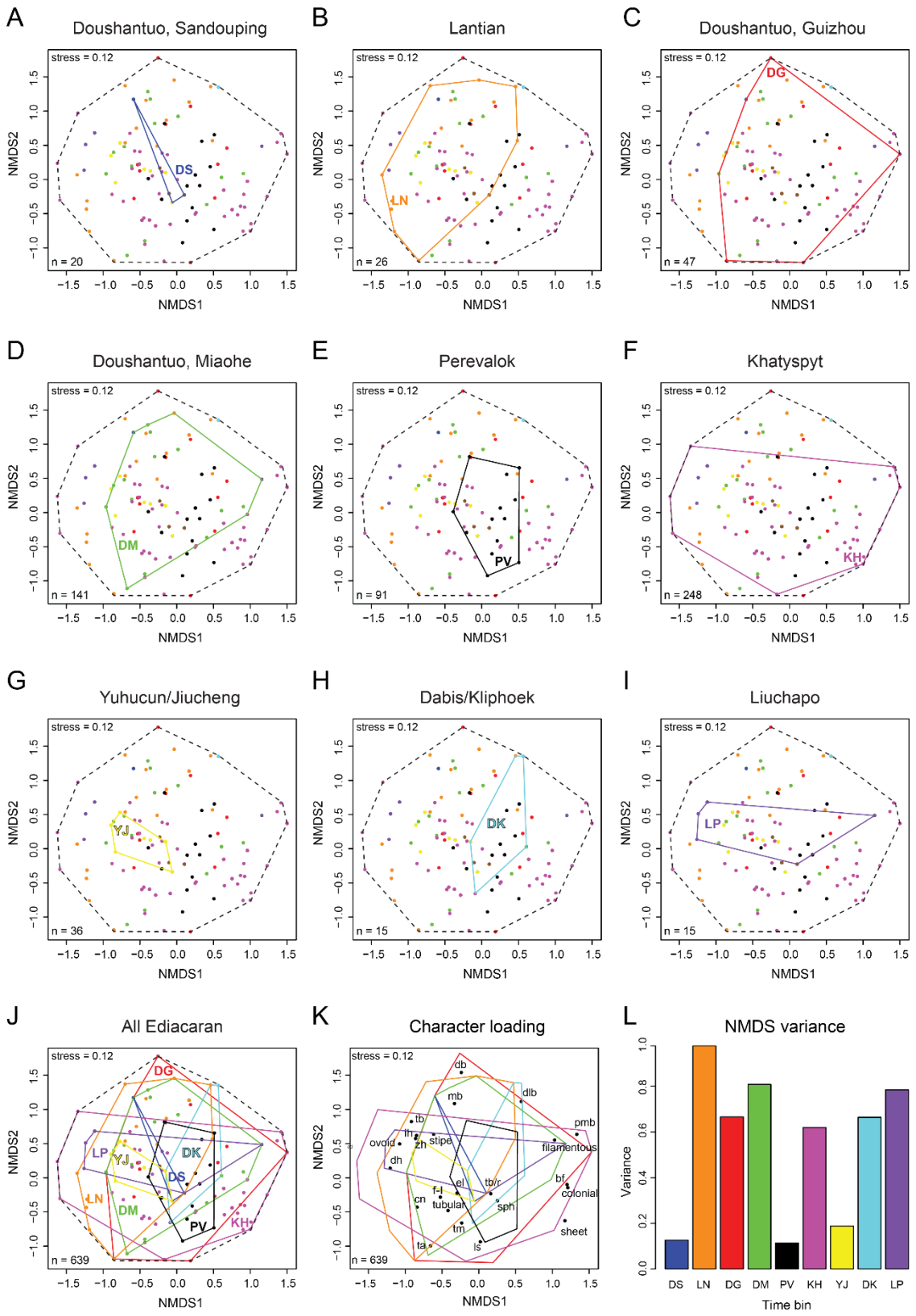

Figure 3.4. NMDS analysis of Ediacaran macroalgal fossils. (A–J) Scatter plots and convex hulls (polygons in solid line) of realized morphospace in nine Ediacaran assemblages in

comparison with that of all Ediacaran macroalgal fossils in our database (convex hulls in dashed line). Stress and n values (number of specimens in each assemblage) are shown in each panel. (K) Character loading diagram, with convex hulls of all Ediacaran assemblages. Abbreviations follow those in Figure 3.3. (L) Sum variances of the first two NMDS dimensions for all nine Ediacaran assemblages. DS – lower Doushantuo Formation, Sandouping, Hubei Province, China (blue); LN – lower Lantian Formation, Anhui Province, China (orange); DG – upper Doushantuo Formation at Wenghui, Guizhou Province, China (red); DM – Miaohe Member of upper Doushantuo Formation, Miaohe village, Hubei province, China (green); PV – Perevalok Formation, Ural Mountains, Russia (black); KH – Khatyspyt Formation, Arctic Siberia (pink); YJ – Jiucheng Member of the Yuhucun Formation, Yunnan Province, China (yellow); DK –Kliphoek Member of the Dabis Formation of the Kuibis Subgroup, Namibia (light blue); LP – Liuchapo Formation, Hunan Province, China (purple).

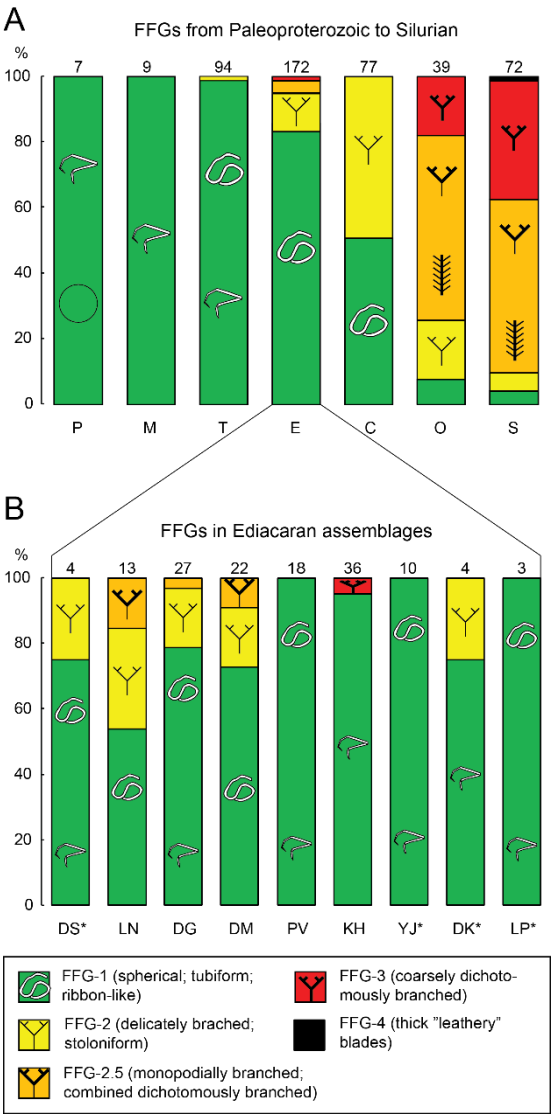

Figure 3.5. Distribution of functional-form groups (FFGs), calculated as percentage of species-level occurrences (see text). (A) Temporal distribution of FFGs from the Paleoproterozoic to the Silurian. Species/morphotype-level richness is marked at the top of each time bin. Abbreviations follow those in Fig. 3.3. (B) Distribution of FFGs among nine Ediacaran assemblages. Species/morphotype-level occurrences are shown at the top of each assemblage. Stars (*) represent Ediacaran assemblages where the sample size is too small (< 10 species-level occurrences). Function-from groups (Littler and Arnold 1982; Steneck and Dethier 1994; LoDuca et al. 2017): 1 (green) – tubiform, ribbon-like, spherical, and miscellaneous morphogroups; 2 (yellow) – delicately dichotomously branched, stoloniform

morphogroups; 2.5 (orange) – delicately dichotomously branched form, in which some of the branches are greater than 2 mm, as well as complex monopodial branched forms; 3 (red) – coarsely dichotomously branched forms or coarsely monopodially branched forms with cortex; 4 (black) – thick (leathery) blades and branches.

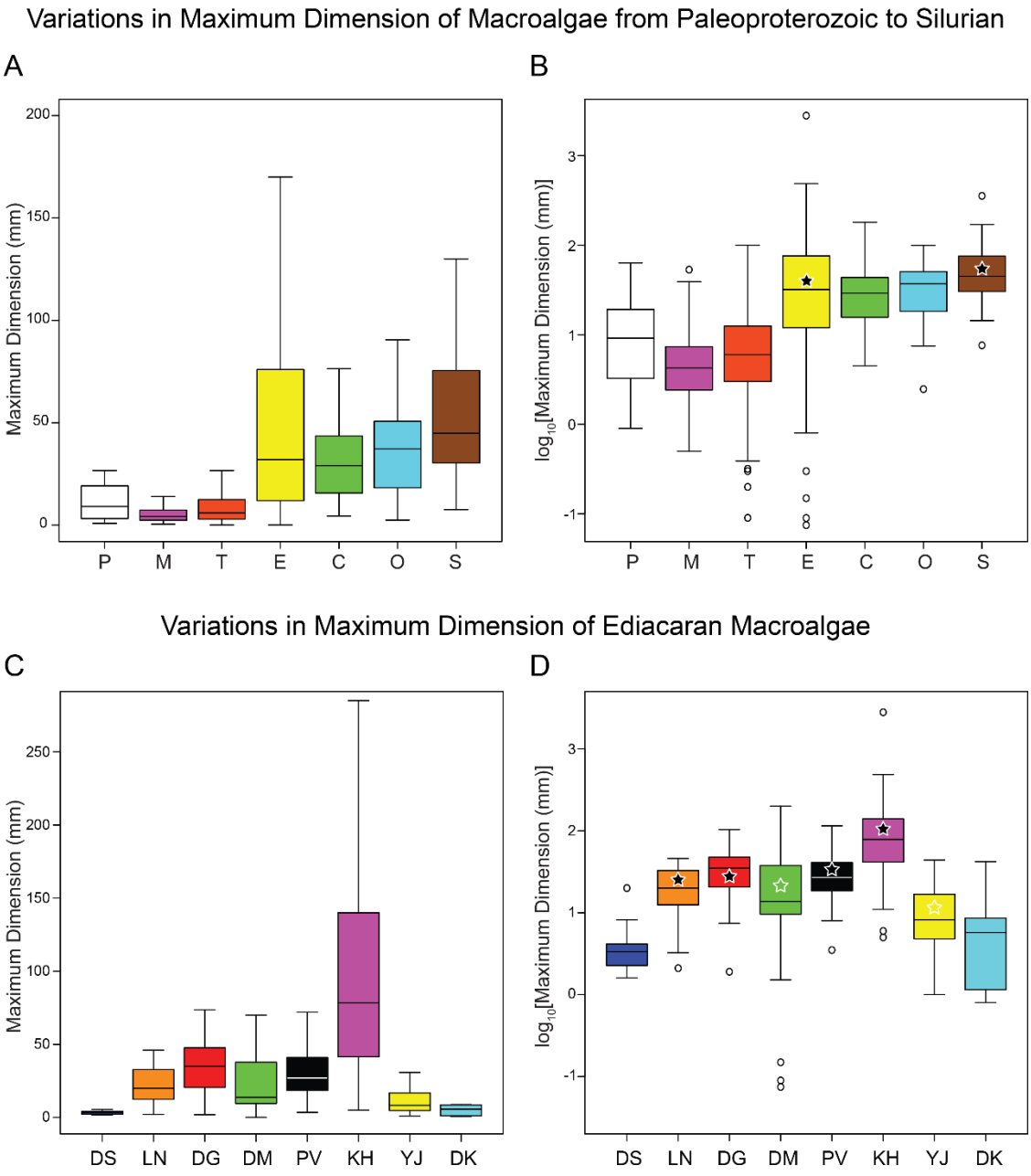

Figure 3.6. Variations in maximum dimension (mm) of macroalgal fossils. (A–B) Paleoproterozoic to Silurian in linear and $\log_{10}$ scales. (C–D) Eight Ediacaran assemblages in linear and $\log_{10}$ scales. The LP assemblage (Liuchapo Formation) is not included because it does not have enough complete samples for measurements. Box-and-whisker plots show the median, lower and upper quartiles, and maximum and minimum values of each geochronological bin. Outliers are shown only in $\log_{10}$ plots. Statistically significant increase

or decrease relative to preceding geochronological bin is marked by a solid or empty star, respectively. Abbreviations follow those in Figures 3.3 and 3.4.

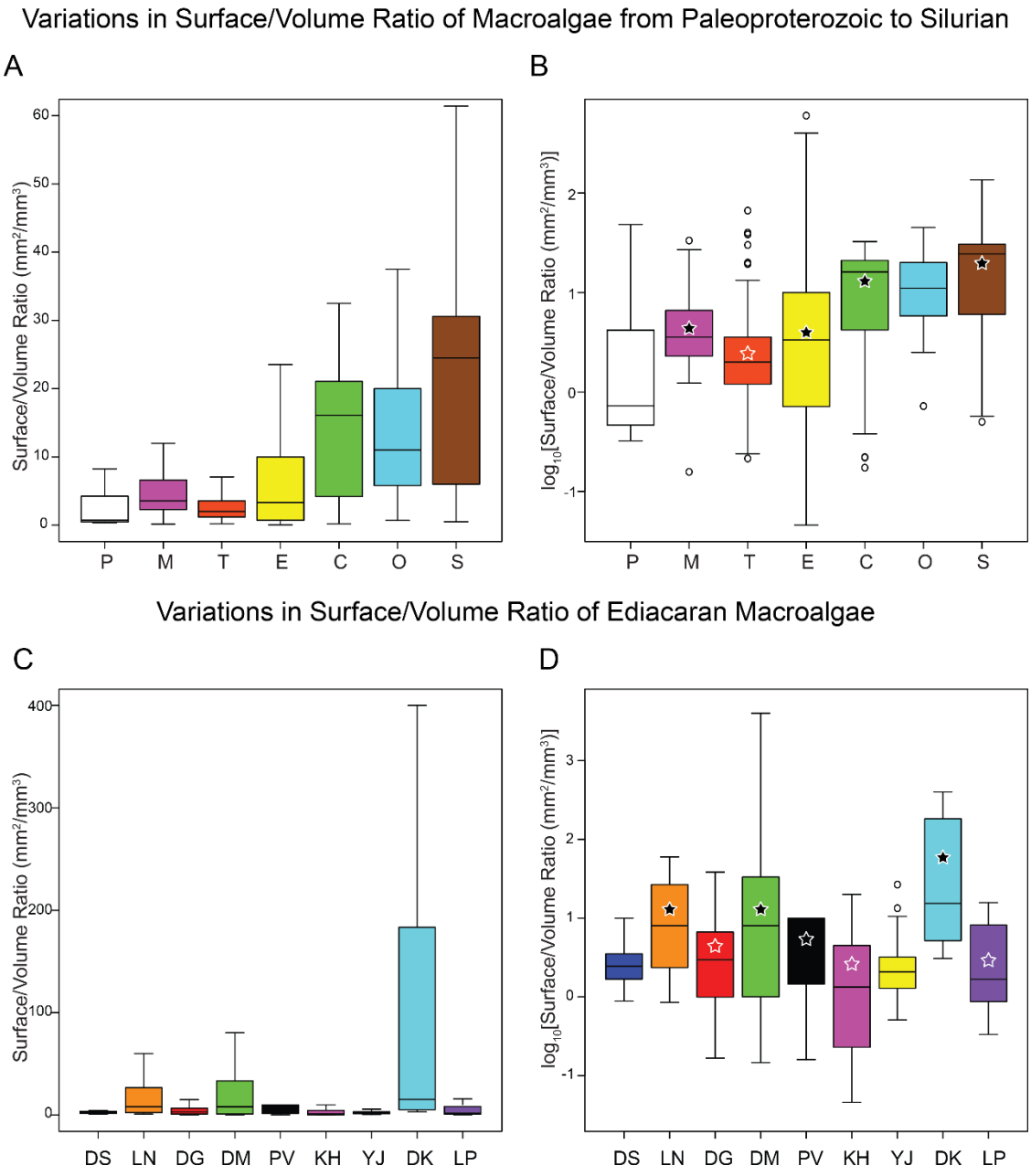

Figure 3.7. Variations in surface/volume ratio (mm^2/mm^3) of macroalgal fossils. (A–B) Paleoproterozoic to Silurian in linear and log_{10} scales. (C–D) Nine Ediacaran macroalgal assemblages in linear and log_{10} scales. Box-and-whisker plots show the median, lower and upper quartiles, and maximum and minimum values of each geochronological bin. Outliers are shown only in log_{10} plots. Plot with Cryogenian data is shown in Figure 3.S1E. Statistically significant increase or decrease relative to preceding geochronological bin is

marked by a solid or empty star, respectively. Abbreviations follow those in Figures 3.3 and 3.4.

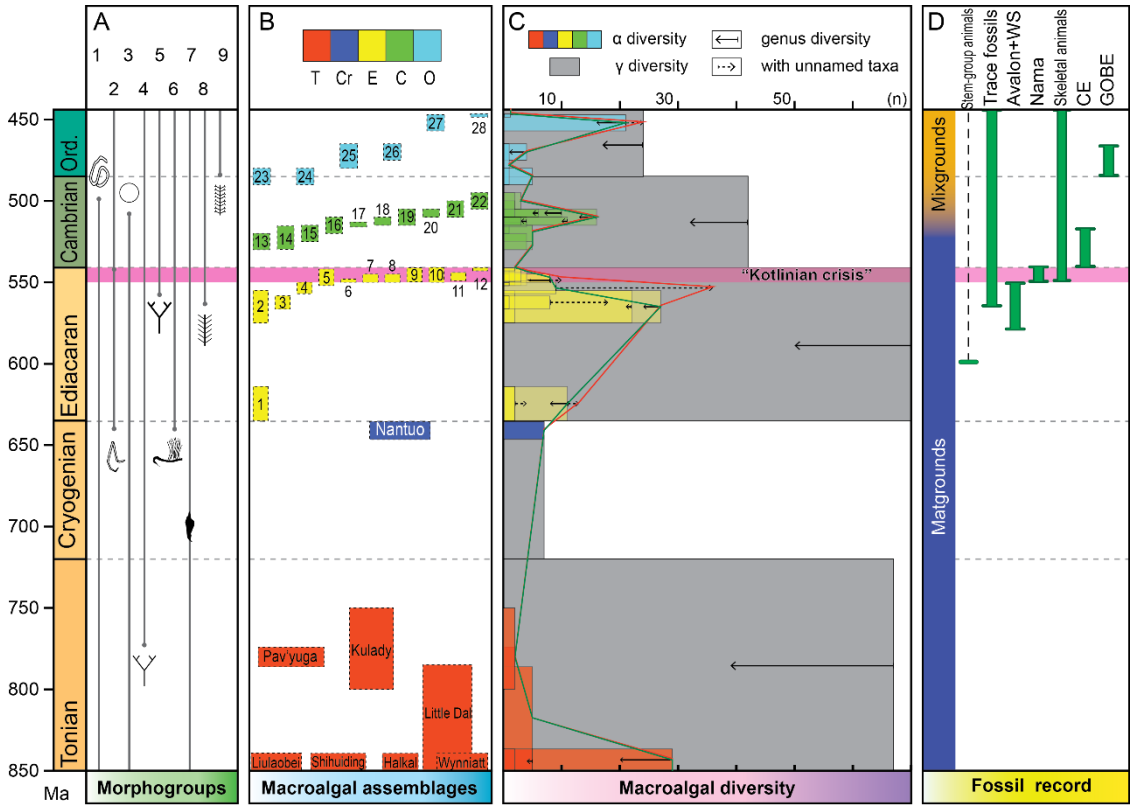

Figure 3.8. Diagram summarizing the major trends of macroalgal evolution during the Neoproterozoic and early Paleozoic, and their relationship with the evolutionary history of Ediacara-type macro-organisms, Ediacaran-Cambrian animals, and major animal evolutionary events. (A) Stratigraphic range of macroalgal morphogroups. Morphogroups are represented by stylized symbols and numbers (Table 2) and their first appearance is shown in grey dots. (B) Tonian–Ordovician macroalgal assemblages in our database. *Tonian*: Liulaobei Fm and its equivalents, China - ~ 850 Ma (Dong et al. 2008); Shihuiding Fm, China - ~ 850 (Xu et al. 2013); Halkal Fm, India – ~ 850 Ma (Maithy and Babu 1996); Wynniatt Fm, Canada – ~ 850 Ma (Thomson et al. 2014); Little Dal Group, Canada – <1030 ~ 779 Ma (Batten et al. 2004); Pav'yuga Fm, Russia – ~780 Ma (Vorob'eva et al. 2006), Kulady Fm, Russia – 800-750 Ma (Nagovitsin et al. 2015). *Cryogenian*: Nantuo Fm, China – 654 ~ 635 Ma (Ye et al. 2015). *Ediacaran*: 1 – lower Doushantuo Fm, Sandouping, Hubei Province (Tang et al. 2006; Wang et al. 2011) and Lantian Fm, Anhui Province, China (Yuan et al. 2011); 2 – upper Doushantuo

Fm, Miaohe village, Hubei Province and Guizhou Province, South China (Condon et al. 2005); 3 – Perevalok Fm, the Urals and Lyamtsa Fm., White Sea, Russia (Grazhdankin et al. 2007); 4 – Khatyspyt Fm, Arctic Siberia, Russia (Nagovitsin et al. 2015; Bykova et al. 2017); 5 – Podolia: Kanilov, Yaryshev, Nagoryany, Studenitsa, Zharnovka fms (Grazhdankin 2014) and European Platform: Kotlin, Feropont'ev, Sokolets fms (Gnilovskaya et al. 1988); 6 – Deep Spring Fm, Nevada, USA (Rowland and Rodriguez 2014); 7 – Erga Fm, White Sea, Russia (Grazhdankin 2014); 8 – Dengying Fm, Hubei Province and Yuhucun Fm, Yunnan Province, China (Tang et al. 2008); 9 – Liuchapo Fm, Hunan Province, China (Chen et al. 2015); 10 – Zuun-Arts Fm, Mongolia (Dornbos et al. 2016); 11 – Dabis Fm, Namibia (Leonov et al. 2009); 12 – Guaicurus Fm, Brazil (Gaucher et al. 2003). *Cambrian*: 13 – Yanjiahe Fm, Hubei Province, China; 14 – Niutitang Fm, Guizhou Province, China; 15 – Sinks Fm, Siberia, Russia; 16 – Paseky Fm, Czech Republic; 17 – Kinzers Fm, PA, USA; 18 – Yu'anshan Fm, Yunnan Province; Balang Fm and Tsinghsutung Fm, Guizhou Province, China; 19 – Kali Fm, Guizhou Province, China; 20 – Tulip Beds, Stephan Fm, Canada; 21 – Huaqiao Fm, Hunan Province, China; 22 – Conasauga Fm, GA and Marjum Fm, UT, USA. *Ordovician*: 23 - Fezuoata Shale, Morocco; 24 – Dol-cyn-Afon, North Wales; 25 – Didymograptus Shale, Finland; 26 – Longmendong and Taoqupo fms, Shaanxi Province, China; 27 – Trenton and Churchill River groups, Manitoba and Ottawa Fm, Ontario, Canada; 28 – Soom Shale Fm, South Africa. Data for Cambrian and Ordovician assemblages are taken from LoDuca et al. (2017). (C) Alpha (in colors) and gamma (in gray) diversity of the macroalgae through time. Each bar represents the number of named species, as published, in each assemblage or geochronological bin. Solid arrows pointing to the left indicate genus-level richness, as published in each assemblage or geochronological bin. Dashed arrows pointing to the right indicate species-level richness as published, plus unnamed taxa as published as well as unpublished morphotypes as evaluated by the authors. Green line depicts

the maximum alpha diversity of described species, and red line shows the maximum alpha diversity of described species plus unnamed or unpublished morphotypes. (D) Major evolutionary events (in green bars, from Schiffbauer et al. 2016), including the earliest stem-group animals (Xiao et al. 2014); stratigraphic range of Ediacara-type macrofossils (Avalon, White Sea, and Nama assemblages), trace fossils of bioturbating animals, and skeletal animals; Cambrian explosion (CE); and Great Ordovician Biodiversification Event (GOBE). Ord – Ordovician; Avalon + WS – Avalon and White Sea assemblages of Ediacara-type fossils; Nama – Nama assemblage of Ediacara-type fossils; CE – Cambrian Explosion; GOBE – Great Ordovician Biodiversification Event Kotlinian crisis event is shown in pink bar.

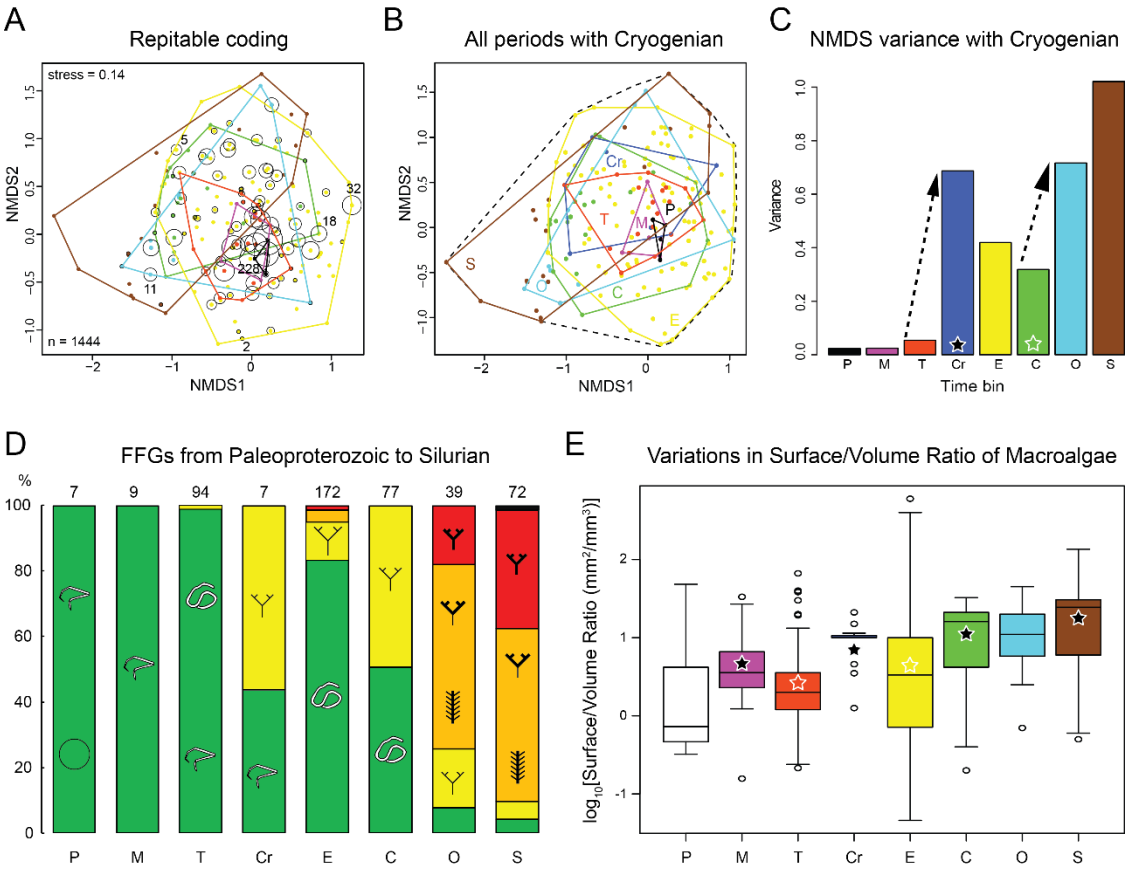

Figure 3.S1. Additional NMDS and FFG analyses of Proterozoic and early Paleozoic macroalgal fossils. (A) Same analysis as shown in Fig. 3.3 (i.e., Cryogenian data are excluded), but with graphical representation of duplicate codings. Because Proterozoic fossils were coded on the basis of specimens (as opposed to species occurrences for early Paleozoic fossils), multiple specimens may share the same coding and are thus plotted at the same point in the NMDS space. The circle surrounding a point is scaled to the $\log_2$ of the number of specimens sharing the same coding. For example, a few circles are marked with numbers to show the number of specimens sharing the same coding. The different coding schemes for Proterozoic vs. early Paleozoic fossils do not affect the size and shape of convex hulls, but do affect the calculation of NMDS variances (i.e., variances of Proterozoic bins, particularly Ediacaran where the level of duplicate coding is high, are artificially reduced relative to early Paleozoic ones). Colors of geochronological bins follow Fig. 3.3. (B–C) NMDS analysis with

Cryogenian data (Ye et al. 2015), illustrating that the sum NMDS variance of the Cryogenian is exaggerated because of the low number of duplicate codings in the Cryogenian relative to other Proterozoic bins. (D) Functional-form groups (FFGs) of Proterozoic and early Paleozoic macroalgae, with Cryogenian data included. Specie/morphotype-level richness is marked at top of each time bin. (E) Surface/volume ratio (mm^2/mm^3) of Proterozoic and early Paleozoic macroalgal fossils, with Cryogenian data included. Box-and-whisker plots show the median, lower and upper quartiles, and maximum and minimum values of each geochronological bin. Circles represent outliers. Statistically significant increase or decrease relative to preceding geochronological bin is marked by a solid or empty star, respectively. Abbreviations follow those in Figure 3.3. Cr – Cryogenian.

3.10 References

Alroy, J., C. R. Marshall, R. K. Bambach, K. Bezusko, M. Foote, F.T.Fürsich, T. A. Hansen, S. M. Holland, L. C. Ivany, D. Jablonski, D. K. Jacobs, D. C. Jones, M. A. Kosnik, S. Lidgard, S. Low, A. I. Miller, P. M. Novack-Gottshall, T. D. Olszewski, M. E. Patzkowsky, D. M. Raup, K. Roy, J. J. J. Sepkoski, M. G. Sommers, P. J. Wagner, and A. Webber. 2001. Effects of sampling standardization on estimates of Phanerozoic marine diversification. Proceedings of the National Academy of Sciences, USA 98(11):6261-6266.

Bambach, R. K. 1993. Seafood through time: Changes in biomass, energetics, and productivity in the marine ecosystem. Paleobiology 19(3):372-379.

Batten, K. L., G. M. Narbonne, and N. P. James. 2004. Paleoenvironments and growth of early Neoproterozoic calcimicrobial reefs: platformal Little Dal Group, northwestern Canada. Precambrian Research 133(3-4):249-269.

Boag, T., S. A. F. Darroch, and M. Laflamme. 2016. Ediacaran distributions in space and time: testing assemblage concepts of earliest macroscopic body fossils. Paleobiology 42:574-594.

Brasier, M. D. 1992. Background to the Cambrian Explosion. Journal of the Geological Society, London 149:585-587.

Brown, J. W., and U. Sorhannus. 2010. A molecular genetic timescale for the diversification of autotrophic stramenopiles (Ochrophyta): substantive underestimation of putative fossil ages. PLoS One 5:e12759.

Bykova, N. V., B. C. Gill, D. Grazhdankin, V. Rogov, and S. Xiao. 2017. A geochemical study of the Ediacaran discoidal fossil *Aspidella* preserved in limestones: Implications for its taphonomy and paleoecology. Geobiology 15:572-587.

Chen, D., X. Zhou, Y. Fu, J. Wang, and D. Yan. 2015. New U-Pb zircon ages of the Ediacaran-Cambrian boundary strata in South China. Terra Nova 27(1):62-68.

Christie, H., K. M. Norderhaug, and S. Fredriksen. 2009. Macrophytes as habitat for fauna. Marine ecology progress series 396:221-233.

Cohen, P. A., A. Bradley, A. H. Knoll, J. P. Grotzinger, S. Jensen, J. Abelson, K. Hand, G. Love, J. Metz, N. McLoughlin, P. Meister, R. Shepard, M. Tice, and J. P. Wilson. 2009. Tubular compression fossils from the Ediacaran Nama Group, Namibia. Journal of Paleontology 83:110-122.

Condon, D., M. Zhu, S. Bowring, W. Wang, A. Yang, and Y. Jin. 2005. U-Pb ages from the Neoproterozoic Doushantuo Formation, China. Science 308:95-98.

Darroch, S. A. F., E. A. Sperling, T. H. Boag, R. A. Racicot, S. J. Mason, A. S. Morgan, S. Tweedt, P. Myrow, D. T. Johnston, D. H. Erwin, and M. Laflamme. 2015. Biotic replacement and mass extinction of the Ediacara biota. Proceedings of the Royal Society B (Biological Sciences) 282:20151003.

Dong, L., S. Xiao, B. Shen, X. Yuan, X. Yan, and Y. Peng. 2008. Restudy of the worm-like carbonaceous compression fossils *Protoarenicola*, *Pararenicola*, and *Sinosabellidites* from early Neoproterozoic successions in North China. Palaeogeography Palaeoclimatology Palaeoecology 258:138-161.

Dornbos, S. Q., T. Oji, A. Kanayama, and S. Gonchigdorj. 2016. A new Burgess Shale-type deposit from the Ediacaran of western Mongolia. Scientific Reports 6:23438.

Du, R., and L. Tian. 1986. The Macroalgal Fossils of the Qingbaikou Period in the Yanshan Range. Hebei Science and Technology Press, Shijiazhuang.

Duan, C. 1982. Late Precambrian algal megafossils *Chuaria* and *Tawuia* in some areas of eastern China. Alcheringa 6:57-68.

Duda, J.-P., V. Thiel, J. Reitner, and D. Grazhdankin. 2016. Openening up a window into ecosystems with Ediacara-type organisms: preservation of molecular fossils in the Khatyspyt Lagerstätte (Arctic Siberia). Paläontologische Zeitschrift 90:659-671.

Gaucher, C., P. C. s. Boggiani, P. Sprechmann, A. N. b. Sial, and T. Fairchild. 2003. Integrated correlation of the Vendian to Cambrian Arroyo del Soldado and Corumba´ Groups (Uruguay and Brazil): palaeogeographic, palaeoclimatic and palaeobiologic implications. Precambrian Research 120:241-278.

Gnilovskaya, M. B., A. A. Istchenko, C. M. Kolesniko, L. V. Korenchuk, and A. P. Udalstov. 1988. Vendotaenids of the East European Platform (in Russian). Nauka, Leningrad.

Gnilovskaya, M. B., A. F. Veis, A. Y. Bekker, V. G. Olovyanishnikov, and M. E. Raaben. 2000. Pre-Ediacarian fauna from Timan (Annelidomorphs of the late Riphean). Stratigraphy and Geological Correlation 8(4):327-352.

Grazhdankin, D. 2014. Patterns of evolution of the Ediacaran soft-bodied biota. Journal of Paleontology 88(2):269-283.

Grazhdankin, D. V., U. Balthasar, K. E. Nagovitsin, and B. B. Kochnev. 2008. Carbonate-hosted Avalon-type fossils in Arctic Siberia. Geology 36:803–806.

Grazhdankin, D. V., K. E. Nagovitsin, and A. V. Maslov. 2007. Late Vendian Miaohe-type ecological assemblage of the East European Platform. Doklady Earth Sciences 417(8):1183-1187.

Han, T.-M., and B. Runnegar. 1992. Megascopic eukaryotic algae from the 2.1 billion-year-old Negaunee Iron-Formation, Michigan. Science 257:232-235.

Hanisak, M. D., M. M. Littler, and D. S. Littler. 1988. Significance of macroalgal polymorphism: Intraspecific tests of the functional-form model. Marine Biology 99(2):157-165.

Hofmann, H. J. 1985. The mid-Proterozoic Little Dal macrobiota, Mackenzie Mountains, north-west Canada. Palaeontology 28:331-354.

Hofmann, H. J. 1994. Proterozoic carbonaceous compressions ("metaphytes" and "worms"). Pp. 342-357. *In* S. Bengtson, ed. Early Life on Earth. Columbia University Press, New York.

Hofmann, H. J., and R. H. Rainbird. 1994. Carbonaceous megafossils from the Neoproterozoic Shaler Supergroup of Arctic Canada. Palaeontology 37(4):721-731.

Huntley, J. W., S. Xiao, and M. Kowalewski. 2006. On the morphological history of Proterozoic and Cambrian acritarchs. Pp. 23-56. *In* S. Xiao, and A. J. Kaufman, eds. Neoproterozoic Geobiology and Paleobiology. Springer, Dordrecht, the Netherlands.

Jensen, S., T. Palacios, and M. Marti Mus. 2007. A brief review of the fossil record of the Ediacaran Cambrian transition in the area of Montes de Toledo Guadalupe, Spain. Geological Society, London, Special Publication 286:223-235.

Kimura, H., R. Matsumoto, Y. Kakuwa, B. Hamdi, and H. Zibaseresht. 1997. The Vendian-Cambrian $d^{13}C$ record, north Iran: Evidence for overturning the ocean before the Cambrian Explosion. Earth and Planetary Science Letters 147:E1-E7.

Knoll, A. H., and M. A. Nowak. 2017. The timetable of evolution. Science Advnaces 3:e1603076.

Kolesnikov, A. V., V. V. Marusin, K. E. Nagovitsin, A. V. Maslov, and D. V. Grazhdankin. 2015. Ediacaran biota in the aftermath of the Kotlinian crisis: Asha Group of the South Urals. Precambrian Research 263:59-78.

Kowalewski, M., and K. W. Flessa. 1996. Improving with age: The fossil record of lingulide brachiopods and the nature of taphonomic megabiases. Geology 24:977–980.

Kumar, S. 1995. Megafossils from the Mesoproterozoic Rohtas Formation (the Vindhyan Supergroup), Katni area, central India. Precambrian Research 72:171-184.

Kumar, S. 2001. Mesoproterozoic megafossil *Chuaria–Tawuia* association may represent parts of a multicellular plant, Vindhyan Supergroup, Central India. Precambrian Research 106:187-211.

Laflamme, M., S. A. F. Darroch, S. M. Tweedt, K. J. Peterson, and D. H. Erwin. 2013. The end of the Ediacara biota: Extinction, biotic replacement, or Cheshire Cat? Gondwana Research 23:558-573.

Leonov, M. V. 2007. Comparative taphonomy of Vendian genera *Beltanelloides* and *Nemiana*: taxonomy and lifestyle. Geological Society, London, Special Publications 286(259-267).

Leonov, M. V., M. A. Fedonkin, P. Vickers-Rich, A. Y. Ivantsov, and P. Trusler. 2009. Discovery of the first macroscopic algal assemblage in the Terminal Proterozoic of Namibia, southwest Africa. Communications of the Geological Survey of Namibia 14:87-93.

Littler, M. M., and K. E. Arnold. 1982. Primary productivity of marine macroalgal functional-form groups from southwestern North America. Journal of Phycology 18:307-311.

Littler, M. M., and D. S. Littler. 1980. The evolution of thallus form and survival strategies in benthic marine macroalgae: Field and laboratory tests of a functional form model. The American Naturalist 116(1):25-44.

LoDuca, S. T., N. Bykova, M. Wu, S. Xiao, and Y. Zhao. 2017. Seaweed morphology and ecology during the great animal diversification events of the early Paleozoic: A tale of two floras. Geobiology 15(4):588-616.

Maithy, P. K., and R. Babu. 1996. Carbonaceous macrofossils and organic-walled microfossils from the Halkal Formation, Bhima Group, Karnataka, with remarks on age. The Palaeobotanist 45:1-6.

Marusin, V. V., D. V. Grazhdankin, and A. V. Maslov. 2011. Redkino Stage in evolution of Vendian macrophytes. Doklady Earth Sciences 436(2):197-202.

Meyer, M., S. Xiao, B. C. Gill, J. D. Schiffbauer, Z. Chen, C. Zhou, and X. Yuan. 2014. Interactions between Ediacaran animals and microbial mats: insights from *Lamonte trevallis*, a new trace fossil from the Dengying Formation of South China. Palaeogeography Palaeoclimatology Palaeoecology 396:62-74.

Muscente, A. D., J. D. Schiffbauer, J. Broce, M. Laflamme, K. O'Donnell, T. H. Boag, M. Meyer, A. D. Hawkins, J. W. Huntley, M. McNamara, L. A. MacKenzie, G. D. Stanley Jr., N. W. Hinman, M. H. Hofmann, and S. Xiao. 2017. Exceptionally preserved fossil assemblages through geologic time and space. Gondwana Research 48:164-188.

Nagovitsin, K. E., V. I. Rogov, V. V. Marusin, G. A. Karlova, A. V. Kolesnikov, N. V. Bykova, and D. V. Grazhdankin. 2015. Revised Neoproterozoic and Terreneuvian stratigraphy of the Lena-Anabar Basin and north-western slope of the Olenek Uplift, Siberian Platform. Precambrian Research 270:226-245.

Nielsen, S. L., and K. Sand-Jensen. 1990. Allometric scaling of maximal photosynthetic growth rate to surface/volume ratio. Limnology and Oceanography 35(1):177-181.

Oksanen, J., F. G. Blanchet, R. Kindt, P. Legendre, P. R. Minchin, R. B. O'Hara, G. L. Simpson, P. Solymos, M. H. H. Stevens, and H. Wagner. 2016. vegan: Community Ecology Package. R package version 2.3-4. https://CRAN.R-project.org/package=vegan.

Padilla, D. K., and B. J. Allen. 2000. Paradigm lost: Reconsidering functional form and group hypotheses in marine ecology. Journal of Experimental Marine Biology and Ecology 250:207-221.

Parfrey, L. W., D. J. G. Lahr, A. H. Knoll, and L. A. Katz. 2011. Estimating the timing of early eukaryotic diversification with multigene molecular clocks. Proceedings of the National Academy of Sciences of the United States of America 108:13624–13629.

Penny, A. M., R. A. Wood, A. Curtis, F. Bowyer, R. Tostevin, and K.-H. Hoffmann. 2014. Ediacaran metazoan reefs from the Nama Group, Namibia. Science 344:1504-1506.

Rogov, V. I., G. A. Karlova, V. V. Marusin, B. B. Kochnev, K. E. Nagovitsin, and D. V. Grazhdankin. 2015. Duration of the first biozone in the Siberian hypostratotype of the Vendian. Russian Geology and Geophysics 56:573-583.

Rowland, S. M., and M. G. Rodriguez. 2014. A multicellular alga with exceptional preservation from the Ediacaran of Nevada. Journal of Paleontology 88(2):263-268.

Schiffbauer, J. D., J. W. Huntley, O. N. G. R., S. A. F. Darroch, M. Laflamme, and Y. Cai. 2016. The latest Ediacaran wormworld fauna: setting the ecological stage for the Cambrian explosion. GSA Today 26(11):4-11.

Schiffman, S. S., M. L. Reynolds, and F. W. Young. 1981. Introduction to Multidimensional Scaling: Theory, Methods and Applications. Academic Press, New York.

Schneider, D. A., M. E. Bickford, W. F. Cannon, K. J. Schulz, and M. A. Hamilton. 2002. Age of volcanic rocks and syndepositional iron formations, Marquette Range Supergroup: Implications for the tectonic setting of Paleoproterozoic iron formations of the Lake Superior region. Canadian Journal of Earth Sciences 39(6):999-1012.

Schröder, S., and J. P. Grotzinger. 2007. Evidence for anoxia at the Ediacaran-Cambrian boundary: the record of redox-sensitive trace elements and rare earth elements in Oman. Journal of the Geological Society, London 164:175-187.

Sharma, M., and Y. Shukla. 2009. Taxonomy and affinity of Early Mesoproterozoic megascopic helically coiled and related fossils from the Rohtas Formation, the Vindhyan Supergroup, India. Precambrian Research 193:105–122.

Sharma, M., and Y. Shukla. 2012. Megascopic carbonaceous compression fossils from the Neoproterozoic Bhima Basin, Karnataka, South India. Geological Society of London Special Publications 366:277-293.

Silberfeld, T., J. W. Leigh, H. Verbruggen, C. Cruaud, B. de Reviers, and F. Rousseau. 2010. A multi-locus time-calibrated phylogeny of the brown algae (Heterokonta, Ochrophyta, Phaeophyceae): Investigating the evolutionary nature of the ‘‘brown algal crown radiation". Molecular Phylogenetics and Evolution 56:659-674.

Smith, E. F., L. L. Nelson, M. A. Strange, A. E. Eyster, S. M. Rowland, D. P. Schrag, and F. A. Macdonald. 2016. The end of the Ediacaran: Two new exceptionally preserved body fossil assemblages from Mount Dunfee, Nevada, USA. Geology 44:911-914.

Sperling, E. A., C. J. Wolock, A. S. Morgan, B. C. Gill, M. Kunzmann, G. P. Halverson, F. A. Macdonald, A. H. Knoll, and D. T. Johnston. 2015. Statistical analysis of iron geochemical data suggests limited late Proterozoic oxygenation. Nature 523(7561):451-454.

Stanley, S. M. 1973. An ecological theory for the sudden origin of multicellular life in the late Precambrian. Proceedings of the National Academy of Sciences, USA 70:1486-1489.

Steiner, M. 1994. Die neoproterozoischen Megaalgen Südchinas. Berliner geowissenschaftliche Abhandlungen (E) 15:1-146.

Steiner, M. 1997. *Chuaria circularis* Walcott 1899 -- "megasphaeromorph acritarch" or prokaryotic colony? Acta Universitatis Carolinae Geologica 40:645-665.

Steneck, R. S., and M. M. Dethier. 1994. A functional-group approach to the structure of algal-dominated communities. Oikos 69(3):476-498.

Sun, W. 1986. Late Precambrian pennatulids (sea pens) from the eastern Yangtze Gorge, China: *Paracharnia* gen. nov. Precambrian Research 31:361-375.

Tang, F., X. Song, C. Yin, P. Liu, S. M. Awramik, Z. Wang, and L. Gao. 2007. Discoveries of new Longfengshaniaceae from the uppermost Ediacaran in eastern Yunnan, South China and the significance. Frontier of Earth Science in China 1:142-149.

Tang, F., C. Yin, P. Liu, L. Gao, and W. Zhang. 2008. A new diverse macrofossil Lagerstätte from the uppermost Ediacaran of southwestern China. Acta Geologica Sinica 82:1095-1103.

Tang, F., C. Yin, Y. Liu, Z. Wang, and L. Gao. 2006. Discovery of macroscopic carbonaceous compression fossils from the Doushantuo Formation in eastern Yangtze Gorges. Chinese Science Bulletin 50:2632-2637.

Tang, Q., K. Pang, X. Yuan, and S. Xiao. 2017. Electron microscopy reveals evidence for simple multicellularity in the Proterozoic fossil *Chuaria*. Geology 45(1):75-78.

Tarhan, L. G., M. L. Droser, N. J. Planavsky, and D. T. Johnston. 2015. Protracted development of bioturbation through the early Palaeozoic Era. Nature Geoscience 8:865-869.

Thomson, D., R. H. Rainbird, and G. Dix. 2014. Architecture of Neoproterozoic intracratonic carbonate ramp succession: Wynniatt Formation, Amundsen Basin, Arctic Canada. Sedimentary Geolody 299:1190138.

Vorob'eva, N. G., V. N. Sergeev, and M. A. Semikhatov. 2006. Unique lower Vendian Kel'tma microbiota, Timan ridge: New evidence for the paleontological essence and global significance of the Vendian system. Doklady Earth Sciences 410:1038-1043.

Walter, M. R., R. Du, and R. J. Horodyski. 1990. Coiled carbonaceous megafossils from the middle Proterozoic of Jixian (Tianjin) and Montana. American Journal of Science 290-A:133-148.

Wan, B., X. Yuan, Z. Chen, C. Guan, K. Pang, Q. Tang, and X. Rao. 2013. Quantitative analysis of *Flabellophyton* from the Ediacaran Lantian biota, South China: application

of geometric morphometrics in Precambrian fossil research. Acta Geologica Sinica 87(4):905-915.

Wan, B., X. Yuan, Z. Chen, C. Guan, K. Pang, Q. Tang, and S. Xiao. 2016. Systematic description of putative animal fossils from the early Ediacaran Lantian Formation of South China. Palaeontology 59(4):515-532.

Wang, G., S. Zhang, S. Li, Y. Yan, S. Dou, and D. Fang. 1984. Research on the Upper Precambrian of Northern Jiangsu and Anhui Provinces. Anhui Press of Science and Technology, Hefei, Anhui.

Wang, Y., H. Chen, X. Wang, and Y. Huang. 2011. Evolution of the Ediacaran Doushantuoian Meta-Paleo-Community in Northeast Guizhou, South China. Acta Geologica Sinica 85(3):533-543.

Wang, Y., and X. Wang. 2008. Macroalgal holdfasts and their interaction with environments from the Neoproterozoic Doushantuo Formation in Guizhou, South China. Frontiers of Biology in China 3(1):113-122.

Wang, Y., and X. Wang. 2011. New observations on *Cucullus* Steiner from the Neoproterozoic Doushantuo Formation of Guizhou, South China. Lethaia 44:275-286.

Wang, Y., Y. Wang, W. Du, and X. Wang. 2014. The correlation between macroscopic algae and metazoans in the Ediacaran: a case study on the Wenghui biota in northeastern Guizhou, South China. Australian Journal of Earth Sciences: An International Geoscience Journal of the Geological Society of Australia 61(7):967-977.

Xiao, S., and L. Dong. 2006. On the morphological and ecological history of Proterozoic macroalgae. Pp. 57-90. *In* S. Xiao, and A. J. Kaufman, eds. Neoproterozoic Geobiology and Paleobiology. Springer, Dordrecht, the Netherlands.

Xiao, S., and M. Laflamme. 2009. On the eve of animal radiation: Phylogeny, ecology and evolution of the Ediacara biota. Trends in Ecology & Evolution 24:31-40.

Xiao, S., A. D. Muscente, L. Chen, C. Zhou, J. D. Schiffbauer, A. D. Wood, N. F. Polys, and X. Yuan. 2014. The Weng'an biota and the Ediacaran radiation of multicellular eukaryotes. National Science Review 1(4):498-520.

Xiao, S., G. M. Narbonne, C. Zhou, M. Laflamme, D. Grazhdankin, M. Moczydłowska-Vidal, and H. Cui. 2016. Towards an Ediacaran time scale: problems, protocols and prospects. Episodes 39(4):540-555.

Xiao, S., X. Yuan, M. Steiner, and A. H. Knoll. 2002. Macroscopic carbonaceous compressions in a terminal Proterozoic shale: A systematic reassessment of the Miaohe biota, South China. Journal of Paleontology 76:347-376.

Xu, D., Z. Wang, J. Cai, C. Wu, N. Bakun-Czubarow, L. Wang, H. Chen, M. J. Baker, and M. A. Kusiak. 2013. Geological characteristics and metallogenesis of the Shilu Fe-ore deposit in Hainan Province, South China. Ore Geology Reviews 53:318-342.

Ye, Q., J. Tong, S. Xiao, S. Zhu, Z. An, L. Tian, and J. Hu. 2015. The survival of benthic macroscopic phototrophs on a Neoproterozoic snowball Earth. Geology 43(6):507-510.

Yin, C., and L. Gao. 1995. Microfossils from the Shibantan Member of the Dengying Formation in the Yangtze Gorges, western Hubei. Geological Review 41:197-204.

Yuan, X., Z. Chen, S. Xiao, C. Zhou, and H. Hua. 2011. An early Ediacaran assemblage of macroscopic and morphologically differentiated eukaryotes. Nature 470:390-393.

Yuan, X., J. Li, and R. Cao. 1999. A diverse metaphyte assemblage from the Neoproterozoic black shales of South China. Lethaia 32:143-155.

Yuan, X., B. Wan, C. Guan, Z. Chen, C. Zhou, S. Xiao, W. Wang, K. Pang, Q. Tang, and H. Hua. 2016. The Lantian Biota. Shanghai Science and Technology Press, Shanghai.

Zhang, R., S. Feng, G. Ma, G. Xu, and D. Yan. 1991. Late Precambrian macroscopic fossil algae from Hainan Island. Acta Palaeontologica Sinica 30(1):115-125.

Zhang, R., H. Yao, and D. Yan. 1995. Study on systematic position of *Tawuia* in Shilu Group in Hainan Island and depositional environment. Palaeoworld 6:1-14.

Zhang, Y. 1989. Multicellular thallophytes with differentiated tissues from late Proterozoic phosphate rocks of South China. Lethaia 22:113-132.

Zhao, Y. L., M. Chen, J. Peng, M. Y. Yu, M. H. He, Y. Wang, R. J. Yang, P. L. Wang, and Z. H. Zhang. 2004. Discovery of a Miaohe-type Biota from the Neoproterozoic Doushantuo formation in Jiangkou County, Guizhou Province, China. Chinese Science Bulletin 49(20):2224-2226.

Zhu, S., and H. Chen. 1995. Megascopic multicellular organisms from the 1700-million-year-old Tuanshanzi Formation in the Jixian area, North China. Science 270:620-622.

Zhu, S., S. Sun, X. Huang, Y. He, G. Zhu, L. Sun, and K. Zhang. 2000. Discovery of carbonaceous compressions and their multicellular tissues from the Changzhougou Formation (1800 Ma) in the Yanshan Range, North China. Chinese Science Bulletin 45(9):841-846.

Zhu, S., M. Zhu, A. H. Knoll, Z. Yin, F. Zhao, S. Sun, Y. Qu, M. Shi, and H. Liu. 2016a. Decimetre-scale multicellular eukaryotes from the 1.56-billion-year-old Gaoyuzhuang Formation in North China. Nature Communications 2016(7):DOI: 10.1038/ncomms11500.

Zhu, S., M. Zhu, A. H. Knoll, Z. Yin, F. S. Zhao, Shufen, Y. Qu, M. Shi, and H. Liu. 2016b. Decimetre-scale multicellular eukaryotes from the 1.56-billion-year-old Gaoyuzhuang Formation in North China. Nature Communications 2016(7):DOI: 10.1038/ncomms11500.

CHAPTER 4

Closing thoughts on the paleoecology and taphonomy of Ediacaran macrofossils

N. BYKOVA

Department of Geosciences, Virginia Tech, Blacksburg, VA 24061, USA

4.1 Conclusions

The chapters of this original research in this dissertation demonstrate innovative approaches and methods for studying the paleoecology and taphonomy of Ediacaran macrofossils. In chapter 2, I explored geochemical tools to resolve taphonomic and paleoecological questions of Ediacara-like fossils for the first time. In chapter 3, statistical methods were used in combination with functional-form group approach to reveal morphological and ecological trends in macroalgal evolution during the Proterozoic and early Paleozoic. These methods and approaches offer new opportunities to test major paleobiologic and geobiologic hypotheses, thus improving our understanding of the history of the biosphere and the Earth system. The following paragraphs summarize the main conclusions from these two research projects.

Chapter 2 – published as "A geochemical study of the Ediacaran discoidal fossil *Aspidella* preserved in limestones: Implications for its taphonomy and paleoecology" in *Geobiology* (Bykova et al. 2017) – describes the results of the geochemical analyses of the first-described Ediacaran taxon *Aspidella*, which is considered as a holdfast of the unknown benthic organism (Gehling et al. 2000; Tarhan et al. 2015). This study was possible because of the unique fossil preservation in the carbonates of the Khatyspyt Formation. Using an array of geochemical data, including organic carbon isotopes ($\delta^{13}C_{org}$), carbonate carbon isotopes ($\delta^{13}C_{carb}$), carbonate oxygen isotopes ($\delta^{18}O_{carb}$), pyrite sulfur isotopes ($\delta^{34}S_{pyr}$), and iron speciation data, I was able to contribute to the understanding of the taphonomy and paleoecology of *Aspidella*. Based on our results, *Aspidella* was reconstructed as a benthic organism anchored in the sediment while alive. After death, early diagenetic cementation of the holdfast of *Aspidella* led to its remarkable three-dimensional preservation. Our data indicate that *Aspidella* did not host and derive significant amount of its biomass from microbial symbionts such as methanogens, methylotrophs, or sulfide-oxidizing bacteria

(Bykova et al. 2017). As for redox conditions of water column in which *Aspidella* lived, iron speciation yielded equivocal results. However, the combination of geochemical data (Cui et al. 2016; Duda et al. 2016) and field observations suggests that *Aspidella* was an opportunistic organism that capitalized upon intermittent oxic intervals in Ediacaran oceans that were characterized by rapid redox fluctuations.

Chapter 3 – Inspired by Grazhdankin et al.'s (2008) discovery of abundant macroalgal community from the Khatyspyt Formation, I developed a study to analyze the big-picture evolutionary pattern of Proterozoic and Paleozoic macroalgae. This research is built on previous study by Xiao and Dong (2006), who explored the morphological and evolutional trends in macroalgae in Proterozoic, using the non-parametric multidimensional scaling (NMDS) analysis. For my investigation, the original database of Xiao and Dong (2006) was significantly expanded (from 578 entries in previous study to 1458 entries of macroalgal fossils in this study), which allowed a detailed analysis of Ediacaran assemblages to gain insights into macroalgal evolution in this critical time period of Earth history. Moreover, data from early Paleozoic macroalgae were added and separately analyzed (LoDuca et al. 2017). A comprehensive analysis of Proterozoic and early Paleozoic macroalgal fossils revealed an overall increase in morphospace range, functional-form group representation, maximum dimension, and surface area to volume ratio. This expansion, however, is not monotonous and involves two stepwise increases in the Ediacaran and Ordovician periods. Also, we found that there is no Cambrian explosion of macroalgae; indeed, if anything, there is a slight decline in macroalgal morphospace range in the Cambrian Period (LoDuca et al. 2017). A detailed analysis of Ediacaran macroalgal assemblages shows that older Ediacaran assemblages (635 – 550 Ma) demonstrate greater taxonomic diversity, morphospace range, and maximum size (proxy for canopy height) than younger ones (550-540 Ma). Thus, the evolutionary pattern of

Ediacaran macroalgae echoes that of Ediacara-like organisms, both experiencing an extinction event during the last ~10 Ma of Ediacaran Period.

4.2 References

Bykova, N., B. C. Gill, D. Grazhdankin, V. Rogov, and S. Xiao. 2017. A geochemical study of the Ediacaran discoidal fossil *Aspidella* preserved in limestones: implications for its taphonomy and paleoecology. Geobiology 15(4):572-587.

Cui, H., D. V. Grazhdankin, S. Xiao, A. J. Kaufman, S. Peek, V. I. Rogov, N. V. Bykova, N. Sievers, and X.-M. Liu. 2016. The effect of ocean redox conditions on the distribution of early metazoans: Evidence from the terminal Ediacaran Khatyspyt Formation in Arctic Siberia. Palaeogeography, Plaeoclimatology, Palaeoecology 461:122-139.

Duda, J.-P., V. Thiel, J. Reitner, and D. Grazhdankin. 2016. Openening up a window into ecosystems with Ediacara-type organisms: preservation of molecular fossils in the Khatyspyt Lagerstätte (Arctic Siberia). Paläontologische Zeitschrift 90:659-671.

Gehling, J. G., G. M. Narbonne, and M. M. Anderson. 2000. The first named Ediacaran body fossil, *Aspidella terranovica*. Palaeontology 43(3):427-456.

Grazhdankin, D. V., U. Balthasar, K. E. Nagovitsin, and B. B. Kochnev. 2008. Carbonate-hosted Avalon-type fossils in Arctic Siberia. Geology 36:803–806.

LoDuca, S. T., N. Bykova, M. Wu, S. Xiao, and Y. Zhao. 2017. Seaweed morphology and ecology during the great animal diversification events of the early Paleozoic: A tale of two floras. Geobiology 15(4):588-616.

Tarhan, L. G., M. L. Droser, J. G. Gehling, and M. P. Dzaugis. 2015. Taphonomy and morphology of the Ediacara form genus *Aspidella*. Precambrian Research 257:124-136.

Xiao, S., and L. Dong. 2006. On the morphological and ecological history of Proterozoic macroalgae. Pp. 57-90. *In* S. Xiao, and A. J. Kaufman, eds. Neoproterozoic Geobiology and Paleobiology. Springer, Dordrecht, the Netherlands.